THE STELLAR CONTENT OF M82

Thesis by

Robert West O'Connell

In Partial Fulfillment of the Requirements

For the Degree of

Doctor of Philosophy

California Institute of Technology

Pasadena, California

1970

(Submitted May 13, 1970)

ACKNOWLEDGEMENTS

I am very grateful to Wallace Sargent and J. B. Oke for supervising this research and for supplying encouragement and advice when needed. Dr. Sargent also obtained several excellent spectra of M82 for me. Special thanks go to Dr. Oke for his generous offer of the 200" observing time required to complete the M82 observations.

I appreciate Hyron Spinrad's interest and encouragement throughout the entire course of this project and the loan of his own extensive photoelectric data in advance of publication.

I especially wish to thank Allan Sandage for several valuable and particularly stimulating conversations regarding this problem and for the opportunity to study his beautiful series of direct plates of M82.

Thanks also go to Sidney van den Bergh for several interesting conversations and the loan of his remarkable direct and spectroscopic plates of M82.

During the uncertain early stages of this research, I benefited from conversations regarding mainly its observational feasibility with Maarten Schmidt, Guido Münch, Rudy Schild, and, especially, Art Vaughn.

I wish to thank Jerry Kristian for advice and encouragement of a more general nature.

Several conversations with Jesse Greenstein were enjoyable and stimulating.

I am grateful to Richard Sramek for a number of discussions regarding the radio structure of M82.

For other conversations I wish to thank Dennis Baker, John Faulkner, Jim Gunn, Doug Keeley, Barry Lasker, Donald Lynden-Bell, Al Moffet, Val Oinas, Pat Osmer, Manuel Peimbert,

Bruce Peterson, Jeff Scargle, Michael Scholz, Seth Shostak, Alan Solinger, and Natarajan Visvanathan.

J. B. Oke, Bruce Peterson, Fritz Bartlett, and Ed Seltzer provided needed computer programs and/or programming assistance.

In addition to those already mentioned, plates were loaned to me by Chris Anderson, Chip Arp, Guido Münch, and Jeff Scargle.

I thank the Observing Committee for a disproportionate amount of 60" and 100" observing time and the gallant Mt. Wilson night assistants--Henry Schaefer, Ray and Mario Jacques, and John Adkins--for making it as profitable and comfortable as possible. Gene Hancock provided amusing anecdotes on cloudy nights. I am grateful for the additional help of Judy Cohen, Greg Shields and, especially, Eric Persson with some of the observations. Chris and Kurt Anderson gave me an introduction to the instruments.

Finally, I wish to express my appreciation to Halton Arp for his continual interest and encouragement and for providing me a first, albeit turbulent, encounter with extragalactic research.

For financial support I am indebted to the National Science Foundation for Pre-Doctoral Fellowships and the California Institute for a Van Maanen Fellowship and a research assistantship.

ABSTRACT

The stellar contents of two regions on the peculiar galaxy M82 are investigated by spectral synthesis. One of the regions is identified as the nucleus of the galaxy on the basis of its surface brightness and inferred mass density; the other is spectrally representative of the disk of M82. Narrow-band spectrophotometry for both regions can be satisfactorily interpreted in terms of ordinary kinds of stars and dust prevalent in the solar neighborhood if 10^3 $M_\odot$ of dust is mixed with the stars in the nucleus. There is no evidence for stellar abundance anomalies or the presence of significant amounts of non-stellar radiation except for gaseous emission between 3400 and 11000 Å. Approximately 50% of the observed Na I λ5892 absorption feature originates in the interstellar medium of M82. The deduced main sequence luminosity functions for both regions resemble that for the galactic disk in the solar vicinity except that an excess of massive stars ($M_V < -3$) exists in the nucleus and a deficiency, in the disk. Sufficient numbers of hot stars are present in the nucleus to maintain the observed level of nuclear interstellar ionization. The absence of massive stars in the disk is corroborated by photographic and spectroscopic evidence and may be the result of a suppression of star formation by a nuclear disturbance. The mass density inferred from the synthesis for the small disk region observed is much higher than found in typical late-type galaxies.

The results of extensive absorption feature index photometry of common galactic stars are also described.

TABLE OF CONTENTS

I INTRODUCTION TO THE PROBLEM OF M82

A Introduction

M82 is one of the most unusual bright galaxies. Its numerous peculiar aspects have been discussed in a large body of literature, most of which deals with the interpretation of the radiation from the galaxy's unique filamentary system, its apparent explosive ejection, and its relationship to the central radio source (3C 231) (Lynds and Sandage 1963; Burbidge, Burbidge, and Rubin 1964; Elvius 1963, 1969; Sandage and Miller 1964; Solinger 1969a,b,c; Sandage and Visvanathan 1969; Wray and Heckathorn 1969; Solinger 1969a summarizes all previous work.)[1] However, apart from these exotic phenomena, M82 is clearly atypical of bright nearby galaxies. Particularly notable are its complex dust network and the sharp contrast between its lack of resolution and high color index (equivalent to a late G star) on one hand and its very early absorption-line spectral type (A5, the earliest type listed by Humason, Mayall and Sandage 1956) on the other.

This latter puzzle has prompted much speculation

---

[1]Burbidge, Burbidge and Rubin (1964) and Lynds and Sandage (1963) will be denoted BBR and LS, respectively, below.

regarding the stellar content of M82, including suggestions that the galaxy is dominated by Population II stars (Markarian 1963b) or that the Balmer lines are produced in an interstellar medium excited by ultraviolet synchrotron radiation (Gurzadian 1963). To further explore this problem, we have undertaken a spectrophotoelectric analysis of the stellar content of M82.

The remainder of this chapter is devoted to inferences concerning the stellar content of M82 and the nature of its nucleus which can be drawn from direct photographs, spectra, and filter photometry. (Most of the direct plates discussed here were taken with the 200" telescope by A. R. Sandage and kindly lent to the author.) The observational program is outlined in Part IC, and its results are described in Parts II and III.

B Properties of M82

General characteristics of M82

Relevant physical parameters for M82 are presented in Table I. Their values are calculated assuming M82 to be a member of the M81 group with a distance modulus as determined for NGC 2403 by Tammann and Sandage (1968). Unless noted, all other calculations in the paper likewise assume this modulus. The suggestion (BBR) that M82 is in fact at a significantly greater distance is discussed below. The intrinsic photometric data given in Table I includes no

TABLE I

PHYSICAL PROPERTIES OF M82

Hubble classification: Irr II (1)
Distance modulus: 27.5 (2)
Distance: 3.2 Mpc
Systemic velocity: v_r = +410 km/sec relative to local group (13)
Angular scale: 1" = 15.4 psc; 1' = 920 psc

Dimensions:
to m_{pg} = $26^m/\square$" isophote, 13.4' x 8.5' (3) (12.3 x 7.8 kpc)
to m_{pg} = $22^m/\square$" isophote, 6.1' x 1.7' (4) (5.7 x 1.6 kpc)
Axial ratio (m_{pg} = $22^m/\square$" isophote): 0.28

Integrated photometry to m_{pg} = $26^m/\square$" isophote: (3)

m_{pg} = 9.20
m_{pv} = 8.39
CI = 0.81
equivalent (B-V) = 0.95 transformation from (5)

UBV photometry of central 138": (6)

V = 9.27
B-V = 0.91
U-B = 0.39

Absolute luminosities to m_{pg} = $26^m/\square$" isophote:

M_{pg} = -18.3 L_{pg} = 2.8×10^9 $L_{pg}(\odot)$
M_V = -19.1 L_V = 3.5×10^9 $L_V(\odot)$

Mass:[1] 1.0×10^{10} $M_\odot$ (7)
$M_{H\ I}$: 1.7×10^9 $M_\odot$ (8)
H I surface density: 2.9×10^{-3} gm/cm^2 (9)
Mass to light ratio: $M/L_V = 4\ (M/L_V)_\odot$

1. The position of the dynamical center of M82 is disputed by various observers with a subsequent variation in its total mass derived from the same rotation curve (12) by a factor of 2. (See 7, 8, 10, 11.) The mass value quoted assumes the dynamical center to be near the bright H II region SW of the central lane after (7). It is a Keplerian estimate for the mass internal to r = 2.3 kpc.

Table I (continued)

3C 231

Spectrum

ν (MHz)	$F_\nu \times 10^{26}$ (W m^{-2} Hz^{-1})	
178	14.0	(14)
610	10.7	(15)
1425	8.1	(16)
2695	5.6	(17)
5000	3.9	(18)

Spectral index (19)

ν (MHz)	α
300	-0.17
3000	-0.57

Spatial distribution: simple gaussian elliptical structure. At least 90% of the flux at 610 MHz is contained in a gaussian component with a half-power diameter of 0.7' (15).

Half-power diameter (20)

ν (MHz)	PA 65°	PA 155°
408	0.85'	0.67'
1407	0.58'	0.33'

Infra-red source: possibly variable

Spectrum (21)

λ (μ)	$F_\nu \times 10^{26}$ (W m^{-2} Hz^{-1})
1.25	1.6 ± .1
2.2	2.3 ± .1
3.4	2.3 ± .1
5.0	8.4 ± 1.
10.2	26. ± 1.
22.	81. ± 16.

References

1 Sandage 1961
2 Tammann and Sandage 1968
3 Holmberg 1958
4 Markaryan 1963
5 Johnson 1955
6 de Vaucouleurs 1959
7 BBR
8 Volders and Hogbom 1961
9 Epstein 1964
10 Elvius 1964

Table I (continued)

11 Duflot 1965
12 Mayall 1960
13 Humason, Mayall and Sandage 1956
14 Conway et. al. 1963
15 R. Sramek, private communication
16 Fomalont 1968
17 Kellerman et. al. 1969
18 Pauliny-Toth and Kellerman 1968
19 Dent and Haddock 1966
20 MacDonald et. al. 1968
21 Kleinmann and Low 1970

correction for internal dust absorption; this may be as large as 3.5^{m} at 5500 Å in the bright central regions.

Less than one per cent (de Vaucouleurs 1962) of the bright galaxies possess features sufficiently similar to M82's to be grouped under the revised Hubble classification Irr II of which M82 is the prototype (Sandage 1961). However, the Irr II galaxies probably do not represent a class with similar intrinsic physical properties, in contrast to the other Hubble classes. Many Irr II's, for example, do not have early-type spectra.

It is usually suggested (Morgan and Mayall 1959; van den Bergh 1969) that M82 is an edge-on Irr I or Sc galaxy, obscured and reddened by an overlying dust network, which is possibly associated with the disturbance in its nucleus. Indeed, most of M82's properties are intermediate between those of Irr I and Sc galaxies, as Table II indicates. Correcting its (B-V) to that of an Sc galaxy according to the standard Whitford (1958) interstellar extinction law would place M82 among the brightest Sc galaxies.

One of the fundamental characteristics of nearby Sc and Irr galaxies is their high resolution into stars, clusters and H II regions (Sandage 1961). In the next section, we examine the resolution of M82 and show that the form of the luminosity function for massive stars in M82 is clearly different from that in normal late-type systems. Therefore, M82 cannot be regarded as a normal galaxy with an anomalous

TABLE II

COMPARISON OF M82 AND NORMAL LATE-TYPE GALAXIES

	Mean Sc	Mean Irr I	M82[e]	References
Spectral type	F0-F5	A5-F0	A5	1
Major axis (kpc) to $26^m pg/\square''$ isophote	24.0	10.6	12.3	2
Axial ratio[a]	0.2	0.2	0.28	2
Integrated M_V[b]	-20.0	-17.4	-19.1	2
Integrated (B-V)[b,c]	0.32	0.23	0.95	2
Mass[d] ($M_\odot$)	6×10^{10}	8×10^9	1×10^{10}	3
$M_{H\ I} / M_{tot}$[d]	0.08	0.17	0.17	3
H I surface density (10^{-3} g cm^{-2})	1.7	3.3	2.9	3
$(M/L_{pg})/(M/L_{pg})_\odot$[b,d]	7	9	5	3

Notes

a. Sc and Irr I values are intrinsic axial ratios. M82 value is apparent.
b. Photometry is integrated to the $m_{pg} = 26^m/\square''$ isophote. For Sc and Irr I, photometry is corrected for mean effects of internal absorption. See Section 4 of (2).
c. (B-V) is calculated from CI by the relation given by Johnson (1955).
d. Total masses of Sc and Irr I galaxies are estimated from 21 cm rotation curves.
e. Data from Table I.

References for Table II

1. Morgan and Mayall 1957

2. Holmberg 1964

3. Epstein 1964. "Ir" column in Epstein's Table VI includes Irr II. Only Irr I's are included here.

amount of dust. In this respect, other Irr II galaxies with early-type spectra (e.g. NGC 520 and 3077) are probably similar to M82.

Resolution of M82

i) Clusters

The absence in M82 of resolution into large star clouds, which in normal late-type galaxies range downward from 500 parsecs in diameter (30" at M82) and $M_V = -11$, is dramatized by comparison to NGC 2403 (Hubble type Sc), another member of the M81 group (cf. photographs reproduced in the Hubble Atlas, Tammann and Sandage 1968, and Plate 1). It is highly improbable that all such stellar groupings are selectively obscured by dust in M82: bright star clouds are not strongly correlated with large obscuring clouds in normal late-type galaxies. They are easily visible in edge-on galaxies particularly because the largest associations usually occur at their peripheries. The distance modulus of M82 would have to be larger than 33 in order that typical large associations like H and χ Persei be invisible on photographs such as those in Plate 1. This possibility is ruled out in the subsequent discussion. Hence, it must be presumed that such objects are absent in M82.

ii) H II regions

The conspicuous H II regions normally associated with spiral structure in late-type galaxies also appear to be absent in M82. Based on the strong correlation between the

PLATE 1: Three 200" Photographs of M82

All prints have the same scale and orientation.

1a) 103a-O emulsion + WG2 filter ($\lambda\lambda$3800-5000); 20 minute exposure (Sandage). The print has been dodged to show the complex central structure. Numerous starlike images are visible on this plate and on 1b. Labeled examples are mentioned in the text.

1b) 103a-E emulsion + RG1 filter ($\lambda\lambda$6100-6700); 60 minute exposure (Sandage). The ejected Hα filaments are visible in the center of the galaxy. Note the absence of compact Hα regions in the disk of M82. Object 4 is clearly diffuse on the original plate.

1c) 1N emulsion + GG13 + Wr89B filters ($\lambda\lambda$7000-9000); 30 minute exposure (van den Bergh). Note the large contrast between the nuclear regions and the disk at 8000 $\mathring{A}$. The bright region 15" W of region A is barely visible in Plate 1a as an arclike feature with several stellar images superposed. The pair of starlike objects 30" W of the nucleus is discussed in Part I B. The companion image to BD $+70^{\circ}$ 587 (the brightest star in the field) is produced by a beam splitter and is 5^{m} fainter than the primary image.

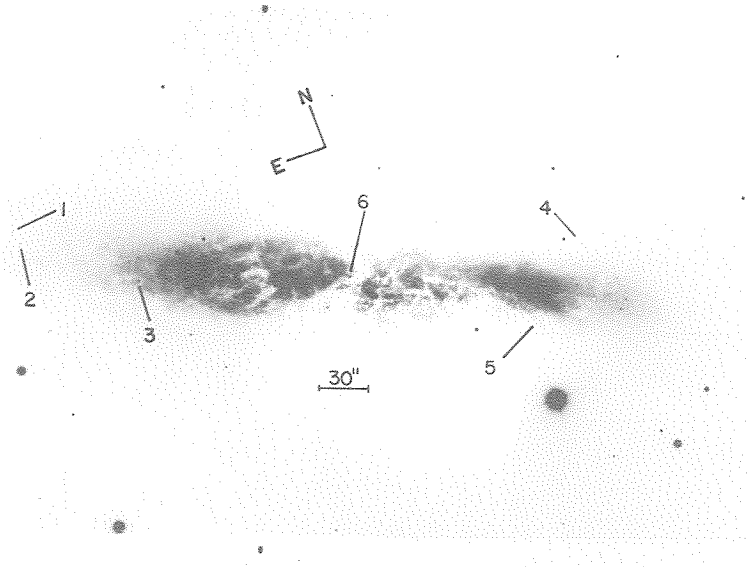

1a

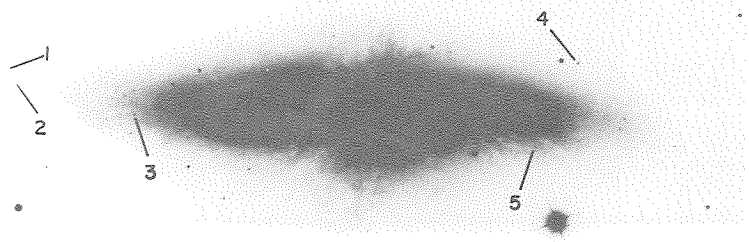

1b

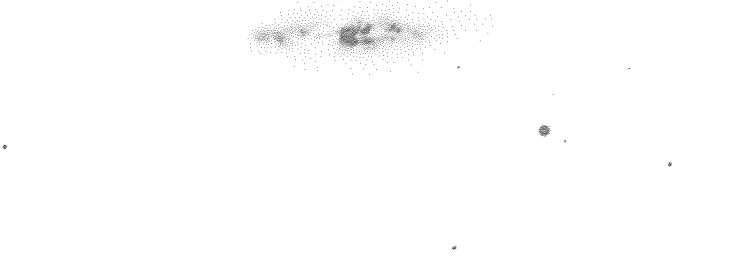

1c

PLATE 1

number of H II regions and the neutral hydrogen content in such galaxies found by Hodge (1967) and Gougenheim (1969), one would expect M82 to contain some 30-40 H II regions (with typical diameters of 50 parsecs and luminosities $M_V \approx -8$). H II regions are usually well distributed across the images of late-type galaxies, extending as far as the $26^m/\square$ " isophote in Irr I galaxies (Hodge 1969a,b). However, the available Hα interference filter photographs (LS, Courtes et. al. 1965) clearly show that, apart from the intense H II cloud associated with the filamentary structure SW of the central dust lane, no obvious H II regions exist on the surface of the galaxy. (The nuclear knots, referred to as region "A" below, and possibly some of the other knotty structures underlying the H II fan are H II regions but are not the typical sort of emission regions under discussion here. See the remarks below.) Very faint [O II] λ3727 emission is visible over much of the main body of M82 on deep plates taken by Mayall. However, two deep spectra by Sargent sampling regions of the main body 600 parsecs long (north-south) on opposite sides of the nucleus at a radius of 1.4 kpc show no trace of Hα emission. The diffuse background of line emission in M82 is definitely fainter than is found in normal late-type galaxies (Burbidge and Burbidge 1962; Mayall 1958). Comparison of Mayall's (1960) absorption line rotation curve and the 21 cm velocity profile of Volders and Hogbom (1961) shows that considerable

amounts of H I exist away from the disturbed H II region in M82. (This assumes that the bulk of the H I is not itself involved in the exploding filaments, whose average velocity when weighted by brightness is probably close to the centroid of the 21 cm profile. The mass of the filaments would have to be increased to 10^8-10^9 $M_\odot$ if a significant fraction of the 21 cm radiation originates in them.) Hence, the absence of H II regions must be attributed to a scarcity of strongly ionizing stars (i.e. stars brighter than $M_V \approx -4$) rather than of interstellar gas.

(Hα emission in the bright fanlike cloud at the base of the filamentary structure may be traced for a total of 110" [1.7 kpc] along the major axis of M82 [BBR, Duflot 1965]. It extends 40" NE of the central knots but is much weaker than to the SW.

Knowledge of the ratio of line to continuous emission in the filaments is important for their interpretation [Solinger 1969a,c; Sandage and Visvanathan 1969]. Unfortunately, the spatial distribution of line emission in the filaments is difficult to establish from the [primarily photographic] studies available. In particular, it is not known if line emission extends farther than 3 kpc from the major axis. Hydrogen emission has been detected spectrographically and photoelectrically at distances of 1.5 kpc from the major axis [BBR, Elvius 1963] and with interference filter photographs, at 3 kpc [LS]. Comparison of various

plates taken by Sandage of the filamentary structure within 2 kpc of the major axis indicates that large variations in the ratio of Hα to continuum emission are present and that the filaments display more fine structure in Hα than in the continuum. However, it does not appear that the lines and continuum radiation originate in two entirely distinct sets of filaments, as in the Crab Nebula. Several structures with strong Hα emission are also clearly present on plates taken in the wavelength interval 5000-6200 Å, where line emission in the M82 filaments is minimal.)

iii) Resolved starlike objects

On the other hand, the spatial density of individual faint starlike objects[1] is clearly higher on and near the surface of M82 than in the adjacent field; most of these objects are presumably associated with M82. Approximately 50 are visible to B = 22. Examples are indicated on Plates 1a and 1b. The objects are fairly evenly distributed along the fainter portions of the main body and apart from a possible group just SW of the central lane show no tendency to group together. The density excess over the field apparently extends up to about 80" from the major axis. A number of the objects (e.g. those labeled 1 and 4) are definitely nonstellar; however, it is difficult to judge the

---

[1]These objects are to be distinguished from the clearly extended knotty features discussed below.

diffuseness of most against the galaxy background. They exhibit a large range in color: 1 and 2 are blue; 3, 4, and 5 are red. The (B-V) of the reddest objects is probably larger than 1.5^m. Those objects bright enough to be visible on the available Hα interference filter plates show no Hα enhancement. Only a few of the objects are brighter than B = 19. Estimates based on Sandage's plates place the B magnitudes of the brightest objects (e.g. number 6) between 18 and 19 and hence their $M_B \approx -9$, assuming a distance modulus of 27.5. This is similar to the absolute magnitudes of the brightest supergiant stars found in normal late-type galaxies (Sandage 1962).

In view of the diffuseness of some of these objects and the fact that they are not clustered like the supergiants observed in other galaxies, the most plausible interpretation is that most are compact star clusters such as those found in the Magellanic Clouds (Bok 1966), M33 (Hiltner 1960) or NGC 2403 (Tammann and Sandage 1968). Such clusters have mean diameters around 25 parsecs, $M_V \gtrapprox -10$ and intrinsic (B-V)'s ranging from 0.0 to 1.0. Those objects associated with M82 with larger color indices may be either reddened or foreground stars. (Tammann and Sandage note that stars with colors up to (B-V) = 1.9 are common in galactic polar fields.)

Even if the majority of the nondiffuse resolved objects in M82 were supergiants, it is clear from their paucity that

the luminosity function for bright stars in M82 is different from that in ordinary late-type galaxies. Less than 40 images possibly identifiable with supergiants are visible to B = 22 on the surface of M82. One may estimate from Tammann and Sandage (1968) that approximately 1500 recognizable stars may be found on the surface of NGC 2403 to B = 21.5 (i.e. $M_B \approx -6$). Since the intrinsic luminosity of M82 is probably larger than NGC 2403's, it is evident that if we assume the form of M82's luminosity function is similar to NGC 2403's, only a few percent of the total number of supergiants expected are visible. Possible obscuration of supergiants by dust cannot wholly explain the situation: in view of the general distribution of dust over the surface of the galaxy, the ratio of the number of resolved stars to the apparent total luminosity is likely to be little changed by dust.

iv) Notable resolved objects

Several of the starlike objects are particularly interesting:

Number 4, for example, is clearly diffuse and yet has a (B-V) $\gtrsim$ 1.5. The color has been estimated from the Palomar Sky Survey plates so is unlikely to be influenced by any possible variability of the object. No star cluster or galaxy is known with so red an intrinsic color. The object is unlikely to be highly reddened since it lies off the main body and along that edge of M82 least influenced by

absorption.

On a 200" 1-N plate lent to us by van den Bergh two almost-stellar features separated by 4" and lying approximately 30" SW of the central lane along the major axis are very bright at 8000 Å (see Plate 1c). The fainter of the two is far redder than the brighter, being invisible on O plates. It is not possible to judge whether the two features are actually stellar since both are superposed on a diffuse background. However, very short exposure plates by Sandage show that the brighter feature at least contains a starlike image (and has the highest surface brightness of any region on the galaxy). The energy distribution of the brighter feature determined by Lasker photometry (see Appendix A) is similar to that found in other neighboring bright regions, but contamination by the background is probably significant. Estimates based on van den Bergh's plates indicate that the fainter object brightens by over 2^m between 6500 and 8200 Å. The relative colors and magnitudes of the two objects do not rule out the possibility that they are a pair of foreground M dwarfs.

v) Discussion

The deficiency of resolved stars and H II regions in M82 prompted the suggestion (BBR) that it is significantly more distant than the M81 group. The high velocity of M82 (+190 km/sec) relative to the mean for the remainder of the group lends some weight to this proposal. Any substantial

increase in distance modulus, of course, implies that the brighter of the observed starlike objects are definitely not individual stars since no stars brighter than $M_V \approx -10$ are known (Sandage 1962). If we presume that the luminosity function of M82 is similar to that of NGC 2403 or NGC 6822 (Kayser 1967), then the smallest modulus at which fewer than about 50 stars will be resolved to B = 22 is m-M = 31. At this distance, M82 would be one of the largest and brightest galaxies known, have a neutral hydrogen-to-total-mass ratio near unity, and additionally fall 800 km/sec short of the velocity predicted by the Hubble relation--hardly a credible set of circumstances.

The implication of the evidence in this section is therefore that a deficiency of stars brighter than $M_V \approx -5$ exists in M82 relative to normal late-type galaxies. Correspondingly, stellar formation rates per unit mass in M82 for stars more massive than 15 $M_\odot$ must have been smaller over the past 10^7 years than in typical Sc and Irr I galaxies.

Distribution of dust, color and spectral type

M82's remarkable dust network covers the entire face of the galaxy with only the NW edge showing little absorption. Dense patches are visible 3 kpc from the nucleus along the major axis and up to 600 parsecs from the major axis along the minor axis. (It should be noted that dust is rather inconspicuous in Irr I galaxies.) The dust clearly extends into the brighter filamentary structures north of the

galaxy. It is possible that the filaments contain a relatively large amount of dust inasmuch as the most chaotic absorption and apparently largest reddening occur directly beneath the H II cloud SW of the nucleus. Fine structure in the dust lanes is visible down to the seeing limit on the best plates (about 15 parsecs).

As Morgan and Mayall (1959) first suggested, the large color variation across M82 (easily visible in color photographs such as those by Ables and Christy 1966) is undoubtedly primarily governed by internal interstellar extinction and not variations of stellar content. In fact, the variation of spectral type (first reported by BBR) on the surface of M82 is in the opposite sense to the color gradient. Spectra taken by Sargent indicate that the spectral type is clearly later farther from the nuclear region, with especially the G band and Mg I λ5175 triplet becoming more conspicuous in the outer regions. Regions A and B (a guide to labeled regions on M82 is given in Figure 1) show spectral types, based on Ca II K, Ca II H + Hε , and Hδ , between A5 and A7; whereas the fainter parts of the main body (regions E and F) have types between F0 and F5.

Surface photometry reported by Elvius (1963) and Markaryan (1963a) shows that (B-V) declines fairly systematically by over $.5^{m}$ outward from the center along both the major and minor axes. The color index on the major axis does not fall to a value appropriate to the spectral type

FIGURE 1

Identification of photometered regions on M82. Compare to Plate 1. The energy distributions labeled E, F, G, and H plotted in Figure 3 are averages for the several locations indicated here.

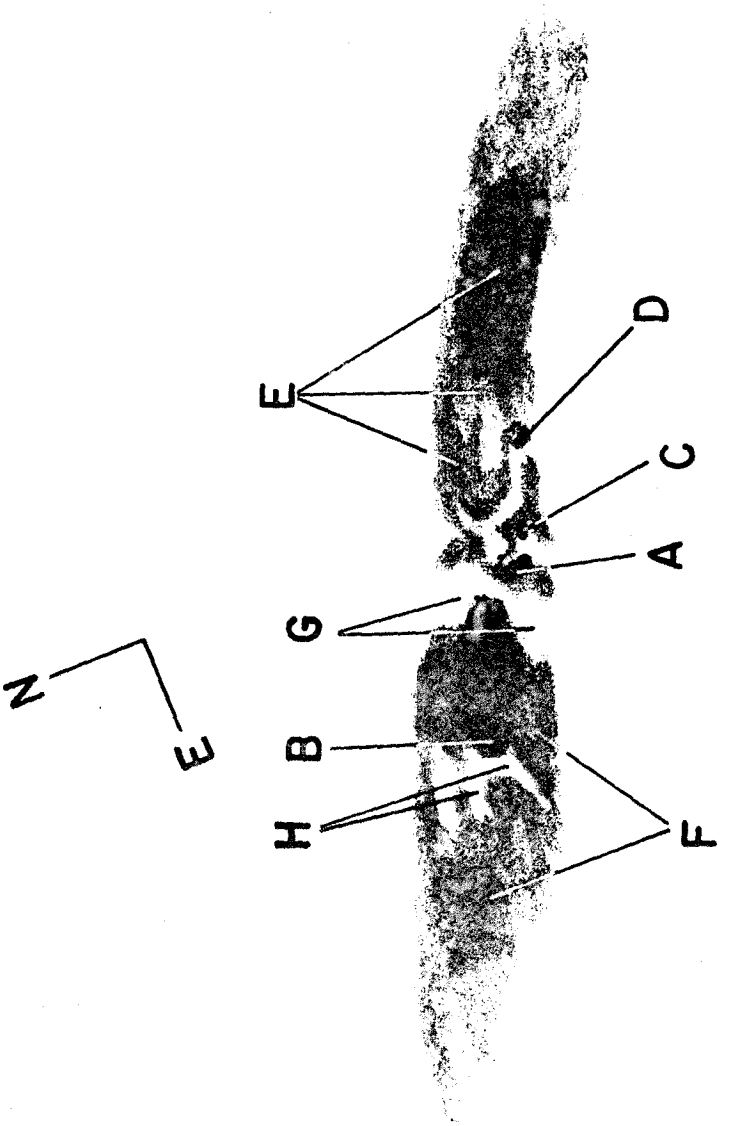
E
D
C
A
G
N
E
B
H
F

until r = 3.3 kpc.

Lasker interference filter photometry undertaken in this program (see Appendix A) of M82 and other objects is presented in Figures 2 and 3. Table III lists pertinent data on the objects observed; all observations are of the nuclei unless otherwise noted.

Note that the slope of the energy distribution of M82A above 6000 Å is larger than observed in any other galaxy, including NGC 5195, which is likely to be highly reddened. Region C is similar to A, and both show the presence of [S II] λλ6716 and 6731 in the λ6784 filter. Although similar to A and C below 6000 Å, D is fainter above 6000 Å. The energy distributions of dust lanes G and H are similar to A and C longward of 6000 Å, suggesting that dust is responsible for the large near infra-red fluxes from A and C.

The energy distributions of the remaining regions are not unlike the nuclei of M51 and M101. The fact that these nuclei have a significantly later spectral type than regions B, E, and F is indicative of the presence of reddening throughout the entire body of M82. That these regions all have similar energy distributions suggests that the bulk of the main body of M82 has fairly uniform properties.

From Lasker photometry we find that the total absorption of the strong central lane is about 2 magnitudes at 5500 Å. A rough estimate of the total mass of dust visible

TABLE III

INTERFERENCE FILTER OBSERVATIONS

NGC	Hubble Type	Aperture Diameter (" arc)	Number of Observations	Notes
3031	Sb	12.7	2	M81
3077	Irr II	19.9	2	in M81 group
5194	Sc	12.7	2	M51
5194	Spiral Arm	19.9	1	aperture center 100"N, 90"E of nucleus
5195	Irr II	12.7	2	companion to M51; heavy dust lanes.
5457	Sc	19.9	1	M101
3034	Irr II			M82; See Figure 1 for identification of labeled regions.
A		8.0	3	nuclear region
B		8.0	4	
C		8.0	1	knot near A
D		8.0	2	
E		19.9	4	
F		19.9	3	
G		12.7	2	central dust lane
H		8.0,12.7	2	dust lanes adjacent to B

FIGURE 2

Energy distributions from Lasker filter photometry normalized at 6067 Å for five galaxies and the nucleus of M82. Observations are of the galactic nuclei unless noted. Table III summarizes further information on this photometry. Probable errors are 0.05^{m} except for the 3474 Å point.

1. NGC 5194 spiral arm region
2. NGC 3077
3. NGC 5457
4. NGC 5194 nucleus
5. NGC 3031
6. NGC 5195

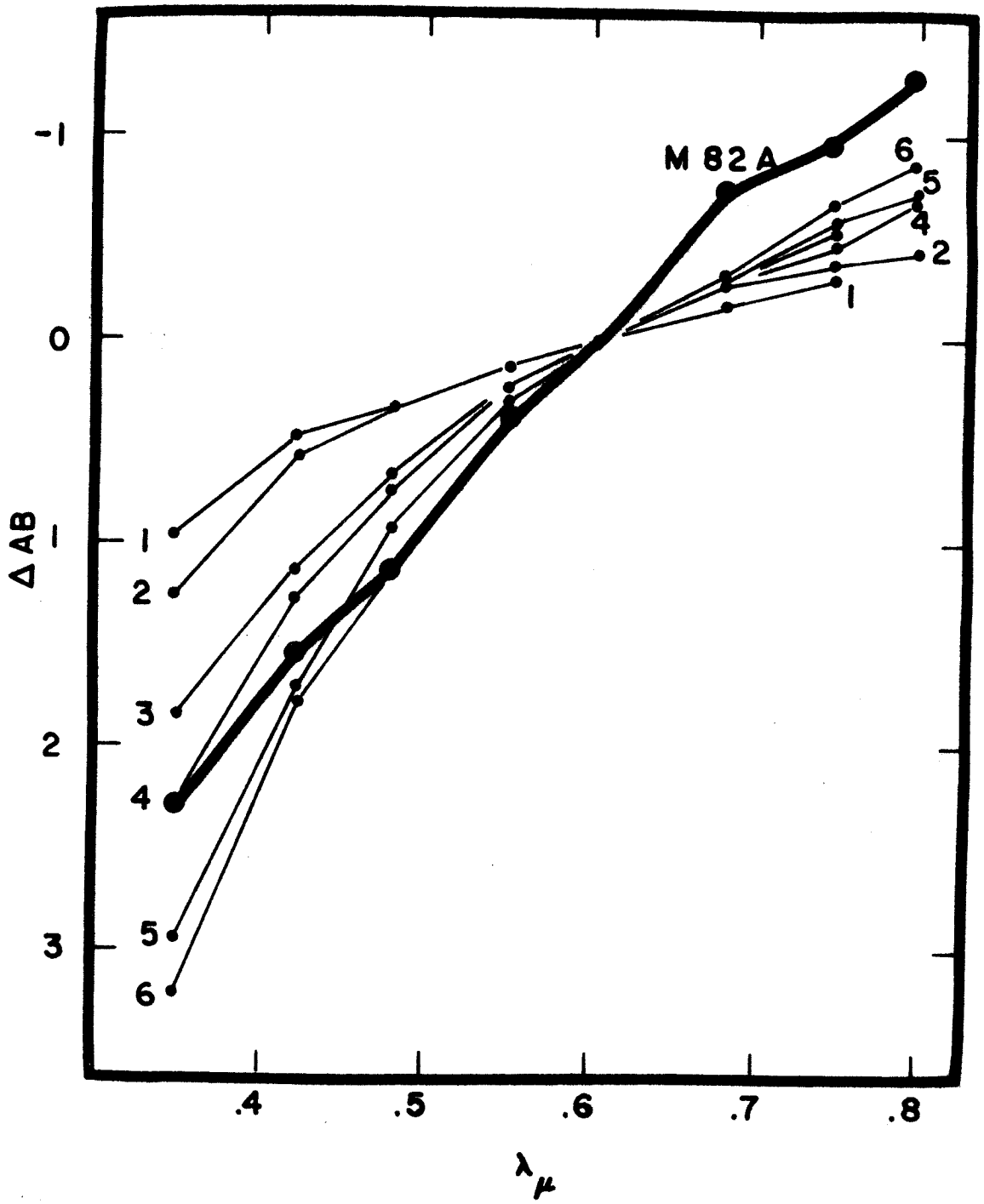
M 82 A
6
5
4
2
1
1
2
3
4
5
6
-1
0
1
2
3
ΔAB
.4
.5
.6
.7
.8
λμ

FIGURE 3

Lasker energy distributions for various regions on M82. Regions B, E and F are representative of the disk. Regions A and C are of high surface brightness and are in the general nuclear vicinity of the galaxy. Regions A, C and D lie beneath the filamentary Hα cloud visible on Plate 1b. G and H are dust lanes. Probable errors are 0.05^{m} except for the λ3474 point.

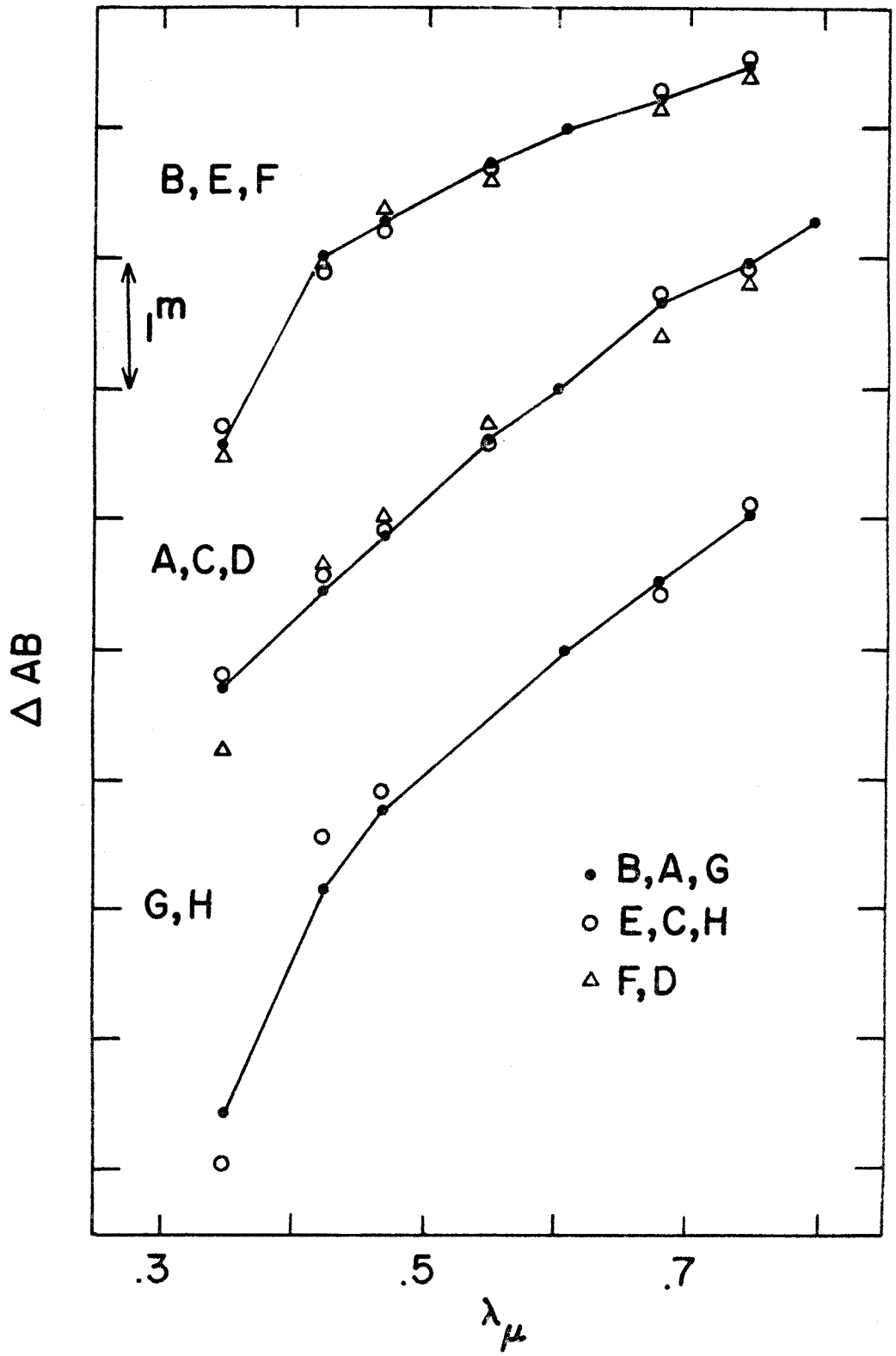
B, E, F
1m
A, C, D
G, H
• B, A, G
○ E, C, H
△ F, D
Δ AB
.3
.5
.7
λμ

on M82 (assuming spherical grains with radii and mass densities of $r = .05\ \mu$ and $\rho = 1\ gm/cm^3$) is 10^4-$10^5\ M_\odot$.

Given the chaotic distribution of dust in M82 and particularly its large dispersion perpendicular to the major axis, it is doubtful that the Hubble criterion for the near side as applied by LS is valid. In fact, from the lack of absorption along the NW edge, one might deduce that the SE edge is the near side, in direct contradiction to the orientation suggested by LS. It remains reasonable, however, to presume that the filaments are expanding away from the nucleus rather than contracting.

In the above discussion, we have implicitly assumed that the contrast between M82's color index and spectral type is entirely a product of internal interstellar extinction and not of more esoteric mechanisms (e.g. such as suggested by Markaryan 1963a). The analysis of Part III will justify this assumption.

Nuclear regions

As noted by Raff (1969) and Solinger (1969b) the bright central regions of M82 are highly complex (cf. BBR, the Hubble Atlas and Plate 1). Knotty structures with diameters of 30-40 parsecs are visible on both sides of the central dust lane and are clearly irregularities in the distribution of luminous material rather than the result of patchy dust absorption. They are reminiscent of the knotlike H II regions found in some late-type galaxies (e.g. NGC 55,

de Vaucouleurs 1961a; and NGC 4631, de Vaucouleurs 1963). The most conspicuous feature SW of the lane--three contiguous knots forming a 10"x3" structure, denoted "A" in Figure 1--lying immediately adjacent to the central lane has been taken to be the dynamical center of M82 by BBR and Mayall (1960) and the nucleus by Peimbert and Spinrad (1969) and by Bertola et. al. (1969). Although spectra (LS, BBR, van den Bergh 1969) clearly show that region A emits line radiation in excess of the overlying filamentary emission as well as a strong stellar continuum, it is not known whether or not the other features in the area are also H II regions. Sandage's H α interference filter photographs indicate that several of the knotty structures superposed on the central dust lane are not H II regions. Markaryan (1963a) reports finding three Hα knots SW of the lane; however, these are possibly only the three knots comprising region A.

Region A is clearly an exceptional feature. In almost all position angles, its enhanced emission lines show no departure from the peculiar velocity field in the adjacent filaments (BBR); hence, it is probable that region A is physically linked to the filaments and their explosive ejection. Short exposure photographs show that A has the highest surface brightness of any area on M82 with the exception of the red starlike feature described above. Spectrophotometry of A (see Part III) with a 7" aperture yields a surface brightness of 17.0 V magnitudes/□ ", which is to be compared

to 15.7 $m_V/\square''$ reported by Sandage et. al. (1969) for a 7.6" aperture observation of the nucleus of M81. The indicated absolute magnitude for A is about $M_V = -14.5$, brighter than any single common stellar agglomeration except superassociations (Ambartsumian 1963), which generally have diameters of 500 parsecs, and galactic nuclei. Its volume emissivity is about 200 $L_V(\odot)/psc^3$; for a region of radius 38 parsecs at the nucleus of M81, the corresponding figure is 430 $L_V(\odot)/psc^3$ (from Sandage et. al. 1969). (The surface brightness at 5500 Å of the region labeled B in Figure 1 when measured through a 7" diaphragm is almost identical to that of A; but presumably the light originates in a much larger volume.) The volume emissivities of the nuclei of M31 and M32 average 6000 $L_V(\odot)/psc^3$ (Lallemand et. al. 1960; Walker 1962). Note that no corrections for dust absorption have been made to the M82 photometry and may increase the luminosity of region A at 5500 Å by a factor of 40.

Photoelectric observations by Kleinmann and Low (1969) located a compact far infra-red source coincident with region A whose spectrum between 5 and 22 microns resembles that of the Seyfert galaxy NGC 1068 but which has a total luminosity fifteen times smaller. Furthermore, the center of 3C 231 (MacDonald et. al. 1968) lies within a few arc seconds of the center of region A.

In view of this discussion, it seems reasonable to identify region A with the nucleus of M82. However,

Solinger (1969a), whose electron scattering model for the polarized continuum of the filaments requires a compact high-luminosity source of radiation, suggested that M82 contains a Seyfert nucleus obscured by dust clouds. He did not consider region A to be a likely nucleus because it does not show the line broadening characteristic of Seyfert nuclei (van den Bergh 1969; Bertola et. al. 1969).

Several attempts to locate a hidden nucleus photographically in the near infra-red have been made (van den Bergh 1969; Bertola et. al. 1969; Raff 1969) and indicate that region A and some of the surrounding knotty structures are considerably brighter relative to the remainder of the galaxy at 1 μ than at 5000 Å. However, no new nuclear feature has been discovered. A recalculation by Solinger (1969b) of the predicted position of the Seyfert nucleus (defined by the center of symmetry of polarization vectors in the filaments) makes it coincident with region A.

Altogether, it seems most probable that region A itself is the nucleus and center of activity in M82, although the possibility that a Seyfert nucleus lies hidden on the line of sight behind it cannot be excluded at present.

Resume

To summarize the results of this section:

a) In integrated properties apart from color, M82 is intermediate between Sc and Irr I galaxies.

b) However, the paucity of resolved stars and H II

regions on M82 indicates that the luminosity function for stars brighter than $M_V \approx -5$ is depressed relative to that for normal Sc or Irr I systems.

c) The color distribution on M82 is primarily governed by dust, which permeates the entire galaxy but, from the general trend in color index found by Markaryan (1963a), is more important toward the central regions. The actual gradient of stellar content, as determined from spectral types, is small and in the opposite sense to that encountered in typical Sc galaxies.

d) Region A is probably the source of the unusual activity in M82. It has an energy distribution from 3500-8000 Å very unlike that found in other galactic nuclei, probably primarily due to heavy dust obscuration.

C Outline of the Observational Program

In the remainder of this paper, we explore the stellar contents of regions A and B on M82 with the technique of spectral synthesis employed fairly successfully by Spinrad (1966) and Spinrad and Taylor (1970) on the nuclei of elliptical and spiral galaxies. The object of this method is to reproduce narrow band spectro-photoelectric observations of a composite spectrum with a plausible mixture of individual stellar spectra. Spectral data is taken over as long a wavelength baseline as is feasible and includes a number of strong absorption features which are sensitive to stellar

luminosity and temperature. Previous synthesis studies employing intermediate-band photometry include those of Wood (1966), Tull (1963) and McClure and van den Bergh (1968).

M82 presents a problem somewhat removed from the galaxies studied in detail up to the present, which are mainly "k-nuclei" objects--that is, their nuclear spectral type in the blue is approximately K0 or later (see Morgan and Mayall 1957; Morgan 1958, 1959a, 1959b; and Morgan and Osterbrock 1969). Only one previous study (the de Vaucouleurs' 1960 photographic study of the Large Magellanic Cloud) has been attempted of a galaxy with an early spectral type (denoted "EST" below). Additionally complicating is the presence of large reddening, emission lines, and possible nonstellar radiation in M82. In particular, one anticipates that the additional degrees of freedom introduced by unknown amounts of total extinction and possible variations in the form of the reddening law will make the synthesis far less tractable. Emphasis must be placed on spectral feature indices which are essentially independent of the reddening law.

Stellar spectrophotometry suitable for application to EST galaxies is not available; hence, a major part of the observing program here is devoted to a survey of bright nearby stars. The results of this survey and a discussion of the photometric indices used to study composite spectra

are given in Chapter II. The results of M82 photometry and its interpretation comprise Chapter III.

II STELLAR INDEX PHOTOMETRY

This chapter discusses the stellar survey and the spectral indices which are formed to facilitate the intercomparison of stellar and galaxy spectra. Tables and figures pertaining to the survey have been grouped in Appendix B.

A Stellar Survey

The stellar survey was intended to provide a compilation of basic spectrophotometric data on representative types of stars in the solar neighborhood. Similar kinds of surveys are under way by Spinrad and Taylor (1969, 1970) and de Vaucouleurs (Tinsley 1967). In this program, emphasis was placed on stellar types prevalent in young stellar groups and hence likely to be important in galaxies with early-type spectra. For various reasons the coverage of types was not as thorough as desirable. In particular, no A-K supergiants were included nor was a sufficient number of B stars, considering the rapid variation of spectral feature strengths among them. Likewise,

observational limitations prevented the inclusion of a globular cluster, and an adequate survey of individual metal-poor stars would have been prohibitively time consuming in view of their faintness and the large range of metal abundance involved. Hence, only a few Pop II stars were included to test the effects of metal abundance on the spectral indices. A sample of "super metal rich" (denoted "SMR" below) stars, which are apparently important in k-nuclei (Spinrad 1966; Spinrad and Taylor 1969, 1970; McClure and van den Bergh 1968; McClure 1969), was also included.

Stars for the survey were selected at random from a variety of sources. Primary, but not universal, criteria were that they be classified on the MK system, that they be bright (usually $m_V \leq 6^m$) and that they be in a favorable observing position. Major sources included Hoffleit 1964; Johnson and Morgan 1953; Roman 1952 (G-K III and IV); Whiteoak 1967 and Jones 1966 (K-M V); Eggen 1960 (G-K IV); and Hiltner 1956 (O-B). Two M supergiants in H and χ Persei were included on the basis of Wildey's (1964) reddening determination for them. A list of SMR stars was provided by Spinrad (private communication). Two Population II giants

were taken from Wallerstein et. al. (1963). Wherever possible, preference was given to stars with abundance determinations (Cayrel and Cayrel de Strobel 1966). A list of all stars observed according to spectral type is given in Table BI.

The bandpass sequence employed in the survey is given in Table IV. Details on observing technique and the selection of bandpasses may be found in Appendix A. As indicated there, the average accuracy of the stellar data is 3%.

Interstellar reddening was removed from the completed scans according to the Whitford (1958) extinction law. Color excesses were determined from apparent B-V colors tabulated in any of the reliable lists above or in Blanco et. al. (1968); intrinsic colors were taken from Johnson (1966a). Several of the sources gave color excesses which were adopted. Late-type giants were assumed to be unreddened at the suggestion of Johnson (1966a).

The unreddened scans were normalized at 5050 Å and continuum and feature indices formed. Relative fluxes per unit frequency rather than magnitudes were used throughout. As explained in Part II B a given feature index is directly

TABLE IV

SCANNER BANDPASS SEQUENCE

$\Delta\lambda$ = 20 Å		$\Delta\lambda$ = 30 Å	
λ(Å)	Feature	λ(Å)	Feature
3448	continuum	5050	continuum
3570	continuum	5175	Mg I (+MgH)
3620	continuum	5300	continuum
3784	continuum	5820	continuum
3798	H 10	5892	Na I (+TiO)
3815	continuum (+He I)		
3835	H 9	6100	continuum
3860	continuum	6180	TiO λ6160
3910	continuum	6370	continuum
3933	Ca II		
		7050	continuum (+TiO)
4015	continuum	7100	TiO $\lambda\lambda$7054,7088
4101	Hδ	7400	continuum
4200	CN λ4216		
4270	continuum	8050	continuum
4305	CH λ4314	8190	Na I
4400	continuum	8400	continuum
4430	interstellar	8542	Ca II
4500	continuum	8800	continuum
		8880	TiO $\lambda\lambda$8860,8868
5050	continuum		
5175	Mg I (+MgH)	9190	CN $\lambda\lambda$9174,9198
5300	continuum	9950	continuum
		10400	continuum
		10800	continuum

related to the equivalent width of total absorption within the feature bandpass relative to the "continuum" linearly interpolated from the two sidebands. The feature indices are highly insensitive to reddening. A complete discussion of the stellar indices is given below.

The stars were divided into groups, listed in Table BI, of uniform spectral properties primarily on the basis of their MK spectral classification. It was clear, however, as indicated in Part II B and also discussed by Spinrad and Taylor (1969), that for K and M stars the MK classification is not always a good criterion of temperature (or, in this survey, the V/R temperature index). Hence, the later type stars were grouped according to their V/R index. The final groupings were adjusted such that the mean energy distribution for each had as small a standard deviation as possible. Several stars whose V/R fell between two groups and outside reasonable bounds for either were not included since undesirable distortions of the group spectra were apt to occur where only partial scans were available.

SMR giants were grouped separately inasmuch as their spectral indices differed significantly from other giants of the same temperature. Index enhancement in the few SMR

dwarfs observed was not large enough to warrent a similar separation. The B stars were divided into three groups because of the strong dependence of their Balmer line strengths and Balmer jumps on temperature. Although observations for only five B stars are available, all are of high quality.

The energy distributions of all stars in each group were averaged with equal weights. The average standard deviation for most groups is less than 3% and is primarily a reflection of the range in temperature within each group. The standard deviations are normally much smaller than the differences in energy distributions between adjacent groups. Table BII lists all group mean flux data. No data was obtained for M dwarfs shortward of 3900 Å. This is not a serious omission because the contribution of M dwarf light to early-type composite spectra in the ultraviolet is probably negligible.

A given group mean energy distribution does not necessarily approximate the mean of a complete sample of stars in the solar neighborhood with the appropriate MK spectral type: the samples in this program are too small, and for later types the cosmic dispersion is too large for

this to be the case. This is especially true of the subgiants, which possess a large cosmic dispersion of feature strengths but for which there are only two or three examples per spectral type group. The influence of possible "super metal richness" on the MK luminosity classification for subgiants additionally complicates matters.

Direct observations in certain spectral regions were not available for several groups of stars. For use in the synthesis, artificial energy distributions to cover these regions had to be created. The most serious omission in terms of the synthesis of early spectral type galaxies was the region shortward of 5050 Å for G5-9 V stars. An artificial energy distribution was produced by superposing the blue spectra for the G0-4 V and K0-2 V groups with those weights which yielded the best fit to the G5-9 V data longward of 5050 Å. The resulting spectrum is probably quite close to what would actually be observed and is entirely adequate for the purpose of synthesis. The feature indices produced fall exactly on the dwarf index-temperature correlations.

Less reliable artificial distributions were evolved for M3-4 V stars between 4000 and 5050 Å and for M5-6 V

between 4000 and 10800 Å. In both cases the artificial data was taken from scans kindly provided by Spinrad. Unfortunately, he uses a different wavelength sequence than the present program and 15 Å resolution below 5360 Å. However, by comparing Spinrad's scans to ours wherever possible, a receipe for conversion to our system was devised. The λ5175 Mg I and λ8542 Ca II indices were calculated from the correlations between our indices and Spinrad's discussed in Part IIB.

This data may be regarded as only schematically representative of late M V energy distributions but is probably adequate for use in the present program.

B Spectral Indices; Results of the Survey

Definition and interpretation of indices

Two kinds of spectral indices are used in this program: continuum and feature indices. The continuum indices are simply ratios of the mean fluxes per unit frequency in two different wavelength regions. The mean flux in each region is taken to be the average of the fluxes in two representative non-feature bandpasses. These two bandpasses are listed in Table V for each spectral region of interest. The

TABLE V

SPECTRAL INDICES

Feature Indices

Index Name and Feature Bandpass	Bandwidth (Å)	Feature	Sidebands
H 3798	20	H 10	λλ3784,3815
H 3835	20	H 9	λλ3815,3860
CaK 3933	20	Ca II λ3933	λλ3910,4015
H 4101	20	H δ	λλ4015,4270
CN 4200	20	CN λ4216	λλ4015,4270
G 4305	20	CH λ4314	λλ4270,4400
IS 4430	20	Interstellar λ4430	λλ4400,4500
MgI 5175	30	Mg I λλ5167,5173,5184	λλ5050,5300
NaD 5892	30	Na I λλ5890,5896	λλ5820,6100
TiO 6180	30	TiO λ6159	λλ6100,6370
TiO 7100	30	TiO λλ7054,7088	λλ7050,7400
NaI 8190	30	Na I λλ8183,8195	λλ8050,8400
CaII 8542	30	Ca II λ8542	λλ8400,8800
TiO 8880	30	TiO λλ8860,8868	λλ8800,9190
CN 9190	30	CN λλ9174,9198	λλ8800,9950

Continuum Indices

Spectral Region	Bandpasses
U	λλ3570,3620
B	λλ4270,4400
V	λλ5300,5820
R	λλ7050,7400
I	λλ8400,8800
J	λλ10400,10800

notation for each of the five continuum indices tabulated for each stellar type in Table B III directly indicates the spectral regions involved and the sense of the ratio.

Feature strengths in stellar and galaxy spectra are measured in the following way: for each spectral feature, two nearby continuum sidebands (at λ_1 and λ_3) bracketing the feature wavelength (λ_2) are selected. A "continuum" flux per unit wavelength at λ_2 is found by linear interpolation of the sideband fluxes. The feature index is then defined as the ratio of the observed flux per unit wavelength at λ_2 to the interpolated flux. That is...

$$I = \frac{f_2/\lambda_2^2}{f_1/\lambda_1^2 + \{(\lambda_2 - \lambda_1)/(\lambda_3 - \lambda_1)\}(f_3/\lambda_3^2 - f_1/\lambda_1^2)}$$

where $f_i = \frac{10^{-.4AB_i}}{10^{-.4AB_{5050}}}$ (AB magnitudes are defined by $AB_i = -2.5 \log F_i - 48.55$ where F_i is the observed extra-atmospheric flux at λ_i in ergs sec^{-1} cm^{-2} Hz^{-1}.) Table V lists all feature bandpasses and associated sidebands in the program. The indices calculated for the mean group spectra are tabulated in Table B III.

If the two sidebands are free of blanketing and if the linear interpolation accurately represents the continuum at λ_2, then the total equivalent width of absorption in the feature bandpass is $W = \Delta\lambda(1-I)$ Å, where $\Delta\lambda$ is the bandwidth used to observe λ_2. (The quantity $(1-I)\times 100$ is referred to as the blocking fraction.) Even if these two conditions are satisfied, W does not necessarily equal the equivalent width of the feature of interest for two reasons. In the first place, the feature itself may be broader than the bandpass used to observe it, as in the case of molecular bands or the hydrogen lines in A stars. More commonly, there is background blanketing in the feature bandpass. Therefore, the absolute value, I, of an index does not bear any invariant relation to the feature itself. For instance, the complete absence of a given feature is not necessarily indicated only by an index of 1.0. However, for those temperature and luminosity domains where a particular feature significantly influences a bandpass, changes in the index may be assumed to be directly related to changes in the feature's strength. The problem of deriving feature equivalent widths from index photometry for small ranges of stellar temperature and luminosity has been more fully

discussed by Spinrad and Taylor (1969) and Taylor (1970). Photographic equivalent width data for a number of the features measured here has been compiled by Tinsley (1967).

Background line blanketing

Quite often, the behavior of an index is influenced by differential line blanketing between the feature bandpass and sidebands. Generally, sidebands were chosen as the nearest regions to a feature which offer minimal blanketing in those stars where the feature is strongest. In some cases, one sideband is used in conjunction with two features and was therefore located midway between them.

It is not possible below 5000 Å to select sidebands which contain less than, say, 3% blanketing for stars of all types. However, in the infra-red beyond 8000 Å, appropriate choice of bandpasses can limit background blanketing to about 1 Å in almost all stars earlier than M4.

In stars earlier than F0, most sidebands are almost free of blanketing. In early B stars helium lines are present in a number of bandpasses. Their influence is probably greatest on λλ3819, 4015, 5892, and 7050; but their effect is not severe. Apart from the Paschen lines,

bandpasses longward of 7400 Å are essentially free of blanketing.

For stars of middle type (F0-K0) blanketing is appreciable in all regions below 7000 Å. In bandpasses below 4000 Å, it averages about 8 Å. Particularly heavy blanketing due to iron and magnesium lines and CN bands occurs in λλ3835 and 3860. Blanketing averages about 4 Å between 4000 and 5000 Å. Fe I λ4271, which reaches about 2 Å equivalent width in middle K stars, appears in λ4270 in G stars. Between 5000 and 7000 Å, mean blanketing is 2 Å with no particularly strong features occuring in sidebands. Again, redward of 7000 Å, blanketing is less than 1 Å in all bandpasses.

Stars later than K0 suffer heavy blanketing for all points below 5000 Å. In M stars λ5050 becomes particularly heavily blanketed, and all bandpasses between 5000 and 7000 Å suffer some TiO absorption. TiO blanketing is worst for λλ5175, 5820 and 5892. λ5175 is also affected by MgH λ5211. λ7050 contains the TiO λ7054 bandhead but is still useful as a sideband for λ7100. In stars later than about M5, strong TiO bands influence λλ8050, 8190 and 8542. λ8050 is additionally blanketed by VO. However, λλ8400,

8800 and 9190 remain relatively clear. λ9190 is used as a sideband for λ8880 even though it includes a CN feature since the feature is generally weak or absent in stars with strong TiO λ8860 (Wing et. al., 1967).

Reddening effects

Because each feature index is formed by comparing the observed flux in the feature bandpass to a pseudo-continuum flux evaluated at the same wavelength, the effects of interstellar extinction are minimized. The smaller the wavelength interval between the sidebands, the greater is the insensitivity of the index to reddening. Sample calculations on a typical spectrum indicate that most indices change by less than .01 for a change of E(B-V) from 0.0 to 2.0. As expected, the largest change (.027) occurs for I_{9190}, which also involves the largest wavelength interval. Almost all indices are lowered in value (i.e. the apparent feature strengths increase) by increased reddening.

Continuum indices are, of course, far more sensitive to reddening but are not particularly useful in dealing with highly composite galaxy spectra anyway. It is possible to form reddening-independent continuum indices similar to

"Q" (Becker 1963) from any three bandpasses if a reddening law is assumed.

Index--temperature, luminosity correlations

A complete listing of both continuum and feature indices for all stellar groups used in the synthesis is given in Table B III. It should be noted that certain of the entries in the table do not represent direct observations (see Part II A). Figures B1-B16 display the dependence of the various indices on temperature and luminosity. The abscissa in most figures is the continuum index V/R, which is used here as a temperature parameter. The V/R and feature indices are discussed in detail below. Comments on the dispersion in index strength are based on plots of individual objects. In addition to two Population II giants, which are included in the group data, HD 161817 and μ Cas are plotted as examples of metal deficient objects. Index data for the latter two objects is given in Table B IV.

V/R: Any of the continuum indices apart from U/B can be used as temperature parameters. Infra-red indices are preferred because they are generally freer of blanketing.

V/R is employed here because V/I is sensitive to the calibration difficulties encountered at 8800 Å and V/J is often uncertain due to low counting rates in the 10000 Å region. Apart from differential blanketing effects, V/R should be a monotonic function of temperature.

A plot of V/R against MK spectral type for all objects in the program where both are available is given in Figure B1. For types earlier than G0 the scatter is small. Later types display a large scatter in V/R at a given spectral type and also a luminosity separation corresponding to the well known fact that giants at a given spectral type are cooler than dwarfs. This separation is destroyed in M stars by differential blanketing effects. The scatter in V/R is a reflection of luminosity variations, possible errors in spectral type due to metal abundance differences (Spinrad and Taylor, 1969), and the fact that MK criteria in later type stars are not reliable temperature indicators (Cayrel and Jugaku, 1963).

V/R is very similar to the index T defined by Spinrad and Taylor (1969). For those stars in common with Spinrad and Taylor and earlier than M2, a plot of V/R against 1/T gives a tight linear correlation with an average scatter

from the mean of less than .02 in V/R at a fixed 1/T. The correlation for stars later than M2 indicates that V/R is more affected by blanketing in the λ5820 bandpass than by the presence of the TiO λ7054 bandhead in the λ7050 bandpass. CN bands in the 7000 Å region discussed by Spinrad and Taylor may also influence V/R. However, since no attempt is made here to infer stellar temperatures from V/R, no corrections for these various blanketing effects have been made.

The influence of blanketing on V/R is also indicated by comparing the locus of stars to that of black bodies plotted in Figure B1. The dwarf temperature scales given by Johnson (1966a) are used for the black bodies. The influence of Paschen continuous absorption on the R region is evident between B5 and F0. Similarly, strong blanketing in the V band for stars cooler than about K7 depresses the index relative to a black body.

The hydrogen lines (Figures B2, B3, and B5): The temperature and luminosity behavior of the Balmer lines is well established (e.g. Aller, 1960). As expected, all three Balmer indices reach a minimum at about A0 and

increase approximately symmetrically from it on either side. Since Hδ is broader than the bandpass used to observe it, its maximum indicated equivalent width is less than given by Tinsley (1967). The effect of He I λ3819 in early B stars on the λ3815 sideband for I_{3798} and I_{3835} is not large.

B supergiants are well separated from dwarfs in all three indices; however, B giants show separation only in Hδ, which reflects the greater sensitivity of the earlier Balmer lines to luminosity. In G stars, strong background blanketing appears in all indices, particularly I_{3835}. The dispersion in I_{3835} in later types is probably the result of both variable metallic line blanketing in λ3835 and fluctuations in CN λ3883 strength. (CN λ3883 influences the λ3860 sideband of H9.) Both kinds of effects have been observed by Spinrad and Taylor (1969) in these stars. Notice that SMR K stars have significantly stronger λ4101 indices than other stars. This local blanketing excess is also indicated in the differential blanketing diagrams for SMR stars given by Spinrad and Taylor.

CaK 3933 (Figure B4): The K line is one of the resonance lines of Ca II. Its behavior in stellar spectra is fairly

well studied (e.g. Barbier et. al., 1941), and it is an excellent temperature indicator for types A5-K0.

Apart from interstellar calcium lines occuring in some distant O and B stars, the K index first begins to fall at about A3 and continues a striking decrease through K0. The range in I_{3933} for a given luminosity class at constant V/R is about 8%. Luminosity separation begins at about K2, cooler dwarfs showing much weaker lines than giants. Note that SMR stars show no index enhancement in contrast to their behavior in CN, Mg I and Na I. The scatter in index strength for early M dwarfs is large (about 10% from the mean) probably mainly as a result of observational uncertainty. Late type giants show very small scatter. M supergiants do not separate from giants. Metal poor giants have weak lines for their temperature, but the effect is not as striking as for several of the other indices (especially I_{4200} and I_{5175}). The K line strength indicated for HD 161817 is only about half that expected from the determination by Burbidge and Burbidge (1956), but there is no obvious explanation for the discrepancy.

The observed K line behavior parallels that expected from the variation of the ground state population of Ca II

(c.f. Aller 1960). In dwarfs the population increases to a maximum at about K5 and decreases thereafter. The observed blocking fraction maximum here is somewhat earlier, at K2. However, temperature scales are somewhat uncertain for these types. By M2 the index has risen to its value at F5, as expected from the similar ground state population in the two cases. In giants and supergiants the population continues to increase through M3. The giant K index changes little in this region, probably due to heavy background blanketing.

CN 4200 (Figure B6): The blue CN band (bandhead 4216 Å) is a well-known luminosity-sensitive feature in K stars (see Keenan 1963; Griffin and Redman 1960; and McClure and van den Bergh 1968). In addition, CN shows a large cosmic dispersion within a given luminosity and temperature domain which Spinrad and Taylor (1969) conjecture is linked to variations in nitrogen abundance.

In stars earlier than about G5, the index remains constant at about 1.0 with a very small dispersion (2%). For types cooler than G5, giants and dwarfs are dramatically spearated. Dwarfs remain at or above an index of 1.0.

(The index is larger than unity owing to blanketing in the λ4270 sideband.) Giants reach a maximum blocking fraction of about 20% at K5. The dispersion in CN strength for "normal" giants is small (about 5% range). However, "SMR" giants, which are selected partly on the basis of their CN strengths, clearly possess stronger CN than normal giants. Note the virtual absence of CN in the two Population II giants. Subgiants fall between dwarfs and giants, except for the one SMR subgiant for which blue observations are available. This star has even stronger CN than normal giants. The blocking fraction begins to decrease again at M0 III. Note that M supergiants show stronger CN than giants.

The general behavior of I_{4200} agrees with that expected from the dissociation equilibria in dwarf and giant atmospheres given by Aller (1963, p. 130). The maximum abundance of CN calculated in dwarfs is an order of magnitude smaller than in giants, and the peak in giants occurs at K5. However, calculated molecular abundances are highly sensitive to the composition assumed.

There is a good correlation between I_{4200} and the CN measures of Griffin and Redman (1960) and McClure and

van den Bergh (1968) for all stars in common. Scatter in both cases is about 3% from the mean.

G 4305 (Figure B7): The G band is a blend of CH (bandhead 4314 Å) and atomic lines which is characteristic of G stars. Previous studies include those of Griffin and Redman (1960) and Spinrad and Taylor (1969). A number of studies (see Strömgren, 1963) have also been made of the "G break" in the continuum between about 4400 and 4250 Å, which is partly the result of CH blanketing.

Index depression begins at about A0. Although the atomic component of the G blend appears about A2 (Morgan, Keenan and Kellman, 1943), most of the absorption in the index earlier than about F0 probably originates in the blue wing of Hγ. Thereafter, the blocking fraction in all types of stars increases steadily to a maximum of 30% at K0. The range of scatter at constant V/R averages less than 5% for all types through K0. SMR stars show no index enhancement. In cooler stars, luminosity separation occurs, dwarfs showing smaller blocking fractions than giants. No straightforward interpretation for this separation is possible in view of the complexity of the blend itself and

the importance of sideband blanketing. Note that the Population II giants do not show as much weakening of I_{4305} as of I_{4200}.

Correlations between I_{4305} and other G band measures are not particularly good primarily because other surveys use different resolution and sidebands.

IS 4430 (Figure B8): The λ4430 diffuse interstellar feature is a band about 50 Å wide whose source has not yet been successfully identified despite considerable attention in the literature. Extensive photoelectric observations of λ4430 have been made by Stoeckly and Dressler (1964) and by Wampler (1966). Both investigations found a correlation between λ4430 strength and color excess which, however, possessed a great deal of scatter. A similar correlation is shown in Figure B8, in which the difference between I_{4430} for reddened stars and the mean I_{4430} for unreddened stars of types B0-G5 is plotted against E(B-V). Unfortunately, only a handful of reddened stars were observed in this program. The error bars at E(B-V) = 0.0 indicate the range in I_{4430} for unreddened stars of types B0-G5. Differential blanketing does not appear to influence I_{4430}

until about G5, and in stars hotter than this the index remains constant with a standard deviation of less than .01. However, I_{4430} does not show a positive blocking fraction in unreddened stars until K3. Blocking fractions in reddened stars are always positive.

MgI 5175 (Figure B9): The feature bandpass for this index includes all three lines ($\lambda\lambda$5183.6, 5172.7 and 5167.3) of the "b" triplet originating from the metastable 2.7 eV level of Mg I. The b triplet is a well-known luminosity sensitive feature (Fitch and Morgan 1951), and extensive photoelectric measures are available (Deeming 1960), Price 1966, Wood 1969, Spinrad and Taylor 1969).

According to the equivalent widths given by Tinsley (1967), I_{5175} should begin to show the effects of MgI between A5 and F0. There is some index depression earlier than this, possibly due to a local blanketing excess created by iron lines. The blocking fraction in dwarfs rapidly increases between F0 and G0, reaches and maintains a maximum of 35% between K0 and K5, and decreases thereafter. In giants the increase is steady from G5 to about M5; however, the giant blocking fraction is always smaller

than the dwarf until M0 III. The greatest luminosity separation (a blocking fraction difference of 20%) occurs at K2. Dwarfs show small scatter (a maximum range of 6%) about the mean relation. The dispersion is higher in giants and subgiants, which show a range of over 10%. The late G and early K subgiants are not well separated from the giants both because the small subgiant group observed does not properly sample this large intrinsic dispersion and because the dispersion itself is not entirely due to surface gravity effects (Spinrad and Taylor, 1969). Again, SMR stars show significantly larger blocking fractions than their normal counterparts. Note the extreme weakness of Mg I in the two Population II giants. (It should be remembered here that the line strength behavior for these two stars is not necessarily representative of all metal poor stars. For example, Price (1966) has noted large variations in the ratio of Mg I to D line strength among these stars.)

Blanketing of λ5175 by MgH λ5211 begins at about K5 and by TiO λ5167, about M2 III (Ohman, 1936). The behavior of the index in cooler stars is therefore not entirely determined by the strength of Mg I.

The temperature dependence of Mg I in dwarfs roughly corresponds to that expected from variations in the population of the 2.7 eV level given by Aller (1963, p. 122). The strong luminosity dependence of Mg I, however, is not explainable as a simple ionization effect (Deeming, 1960; Price, 1966) and is possible related to stratification in the line-forming layer of giants.

NaD 5892 (Figure B10): This index measures both resonance lines ($\lambda\lambda$5890.0 and 5895.9) of Na I, which serve as temperature and luminosity discriminants among late type stars (Thackeray, 1949; Spinrad, 1962). Previous photoelectric observations include those of Griffin (1961), Price (1966), Wood (1969) and Spinrad and Taylor (1969).

The behavior of I_{5892} is rather similar to that of I_{5175} except that no minimum in the index occurs for either dwarfs or giants. He I λ5876 depresses the index in early B stars. Possible interstellar D line contributions in early-type reddened stars cannot be distinguished from He I. D line blocking starts to appear at about G5 and increases steadily with decreasing temperature. The blocking fraction in giants remains about 10% smaller than in dwarfs for all temperatures. At a given V/R both dwarfs

and giants show a scatter whose range is about 8%. SMR giants show strong Na I enhancement; two SMR dwarfs possess a positive but much weaker enhancement (also present in Mg I) and have been included with normal dwarfs in the K0-K2 V group. Even though the D lines are sensitive to surface gravity, "normal" subgiants and giants appear mixed in the diagram due to the large cosmic dispersion of which the SMR stars are extreme examples. Again, Population II giants possess very small blocking fractions.

Blanketing of λ5892 by TiO λ5861 is present in stars cooler than about M2 III. The λ5820 sideband also suffers blanketing from TiO λ5814. However, the luminosity separation, presumably primarily caused by Na I, is maintained through M5. M supergiants do not separate from M giants.

The correlation between I_{5892} and both Spinrad and Taylor's (1969) and Price's (1966) D line indices is quite good, showing an average scatter about the mean of 2% in both cases. I_{5892} behaves with temperature and luminosity qualitatively as predicted from a simple curve of growth theory by Price (1966).

The TiO indices (Figures B11, B12 and B15): I_{6180}, I_{7100}, and I_{8880} measure TiO bands with heads at, respectively, λ6159, λλ7054 and 7088, and λλ8860 and 8868. They are well-known temperature sensitive features in M stars (Ohman, 1936; Sharpless, 1956). Their large temperature sensitivity allows one to take advantage of the relatively small temperature difference between M giants and dwarfs of the same spectral class and to use them in assigning luminosity classes. However, the bands do not appear to be highly sensitive directly to surface gravity at a given temperature.

I_{6180} and I_{7100} behave similarly, both beginning a decrease at about K2-3 which continues steadily throughout all cooler types. I_{6180} does not show a luminosity separation; but I_{7100} does, giants consistently having a larger blocking fraction than dwarfs at a given temperature. This difference in behavior is probably the result of differential sideband blanketing.

TiO λλ8860 and 8868 make a dramatic appearance at about M5; the blocking fraction increases very rapidly with decreasing temperature. The influence of Paschen line aborption on I_{8880} is evident in B and A stars. Some of

the scatter of the index in G and K stars is produced by variable CN absorption in the λ9190 sideband for the index.

NaI 8190 (Figure B13): The feature bandpass includes all three lines (λ8183.3 and two at λ8194.8) of the triplet originating on the 2.1 eV level of Na I, which is the upper level of the D resonance lines. The triplet is known to be luminosity sensitive in M stars (Sharpless, 1956; Whitford, 1966) and is the weakest feature included in this program. Spinrad and Taylor (1969) have also observed this triplet.

The general behavior if I_{8190} is qualitatively similar to that of I_{5892}. Throughout types A0 to G0, the index shows extremely small dispersion, having an average range of less than 3%. The dispersion abruptly increases to about 5% at G5 with two K subgiants having indices smaller than the average by .1. Luminosity separation does not occur, however, until K5, where giants and dwarfs begin a blocking fraction separation of 5%, which is maintained through M3. The range in index for giants averages about 4% and for dwarfs, about 6%. M supergiants are not distinguishable from giants. At M5 III, strong TiO and VO

blanketing begins in the λ8050 sideband and causes a drastic increase in the index. M6 dwarfs are apparently still hot enough that the blanketing is not important.

Since early-type stars show very small index dispersion, the larger dispersion observed in G-K stars of comparable brightness is probably intrinsic. The scatter in M dwarfs is mainly observational error.

CaII 8542 (Figure B14): The λ8542 line is the central and strongest member of a triplet originating from the metastable 1.69 eV level of CaII. The upper level of the transition is also the upper level of the λ3968 resonance line.

The behavior of λ8542 is qualitatively similar to that of the K line. The increase in line strength expected between A0 and F0 is masked by Paschen line absorption. The dramatic strengthening between F0 and K0 observed for the K line does not occur. Rather, the index maintains approximately a constant strength for all stellar types until about K5. This difference is expected since the population of the 1.69 eV level changes less than that of the ground state by a factor of 4 in this temperature range

(assuming thermal equilibrium). The observed increase in line strength between A5 and K0 is approximately as expected. Note again that as in the case of I_{3933}, SMR stars show no index enhancement.

The 1.69 eV population begins to drop in dwarfs at about K0; in giants the population is maintained about constant through M3. The resultant luminosity separation is clearly present in the index beyond K5. Note that M supergiants show a slight strengthening relative to giants. The great depression of the index appearing about M5 III is produced by the TiO λ8430 band which obliterates Ca II λ8542 in cooler stars.

Observations of another member of the triplet, λ8662, have been reported by Spinrad and Taylor (1969) and correlate reasonably well with I_{8542}.

CN 9190 (Figure B16): The feature bandpass includes two bands from the red CN system with heads at λλ9198 and 9174. Spinrad and Taylor (1969) have also made measures of these features.

The behavior of I_{9190} is, as expected, similar to that of I_{4200} although the red bands are a good deal

weaker. Some scatter is introduced in A stars by variable Paschen line absorption. As with I_{8190}, intrinsic dispersion apparently increases in G and K stars. Luminosity separation occurs at about G5 and reaches a maximum at about K3. SMR stars do not show as striking a blocking fraction excess as they do in I_{4200}. M supergiants are well separated from M giants.

The average scatter about the mean correlation between I_{9190} and the corresponding index given by Spinrad and Taylor (1969) is 3%.

Applications of the indices

It is evident from this discussion that one can almost unambiguously assign a given star to one of the spectral type groups above by use of the various feature indices regardless of reddening. The Balmer lines, K line, G band, and TiO indices may be used as temperature discriminants, while the CN bands, Mg I triplet, Na I lines and Ca II triplet may be used as luminosity indicators. Uncertainty arises only for separation of luminosity classes III-V earlier than $G2_{\Lambda}$ and classes III and IV in the G-K star region of large cosmic dispersion.

For use in composite spectra, one might note that the presence of features at λλ4200, 4430 or 8880 unambiguously indicate the presence of G-M III+ stars, interstellar reddening (if K3+ light is not important at 4400 Å), and M6+ giants, respectively. I_{9190} is useful as an indicator of M supergiants. Since it is present over a wide range of stellar temperature and luminosity, the Ca II λ8542 feature may be used as a discriminant against non-stellar radiation in the near infra-red. It is also the best index of the M giant-to-dwarf ratio.

A high resolution search in quasi-stellar objects and Seyfert nuclei for any of the absorption features studied here would be of use in establishing limits to the stellar contents of such objects. However, the strongest features likely--the K and D lines--may also attain considerable strengths in a disturbed interstellar medium.

With regard to the "super metal-rich" phenomenon, our results confirm those of Spinrad and Taylor (1969) that stars showing enhancement in CN, the D lines or Mg I show little or no enhancement in the G band or either Ca II index. The phenomenon is also reflected in the larger-than-observational dispersion in I_{8190} and I_{9190}.

III SPECTRAL SYNTHESIS FOR M82

In Chapter III we employ the stellar data of Chapter II to analyze spectrophotometry of M82 A and B. We show that it is possible to quantitatively interpret the spectrum of M82 without assuming properties for the dust or stars not common to the solar vicinity and without invoking nonstellar sources of radiation other than hydrogen recombination radiation.

In the first three sections of Chapter III we discuss the quality of the galaxy photometry, compare results for M82 A and B, and develop an approach to the problem of interstellar extinction in M82. The next section describes conditions placed on our population models and the fitting criteria for successful models. The remainder of the chapter discusses the synthesis for each region and its implications.

A Scanner Observations of M82

Observations of M82 A and B with the bandpass sequence of Table IV have been obtained with the 60" and 200"

spectrophotometers. Details of the observations and reduction are given in Appendix A. The adopted energy distributions normalized at 5050 Å are presented in Table VI and Figure 4 and represent the average of all usable MCSP and (between 5050 and 6370 Å only) 60" data. The probable errors listed in parentheses either are the standard deviation of repeated observations or are estimated from the signal-to-noise ratio and uncertainties in the various reduction procedures described in Appendix A. The apparent magnitudes of M82 A and B at 5050 Å and 5500 Å are those obtained by the MCSP on May 20, 1969 with a 7" diameter entrance aperture.

The adopted energy distributions may be compared to previous M82 photometry by Wood (1966), Johnson (1966b) and Peimbert and Spinrad (1970). The first two of these studies are not strictly comparable to ours, as they used 35-51" entrance apertures and intermediate to low spectral resolution. Their agreement with our continua, however, is generally good. Both fall within about 5% of M82 B in the blue and between A and B in the red, in accordance with the relative contributions of regions

TABLE VI

OBSERVED ENERGY DISTRIBUTIONS FOR M82

λ(Å)	Δ AB	
	M82 A	M82 B
3448	1.96 (.04)	1.93 (.04)
3570	1.77 (.04)	1.78 (.04)
3620	1.67 (.04)	1.73 (.04)
3784	1.39 (.04)	1.09 (.04)
3798	1.36 (.04)	1.16 (.04)
3815	1.31 (.04)	0.93 (.04)
3835	1.47 (.04)	1.24 (.04)
3860	1.23 (.04)	0.81 (.04)
3910	1.15 (.04)	0.76 (.04)
3933	1.31 (.04)	0 92 (.04)
4015	1.01 (.04)	0.65 (.04)
4101	0.89 (.04)	0.95 (.03)
4200	0.77 (.04)	0.47 (.03)
4270	0.73 (.04)	0.47 (.03)
4305	0.81 (.04)	0.53 (.03)
4400	0.63 (04)	0.39 (.03)
4430	0.61 (.04)	0.38 (.03)
4500	0.50 (.04)	0 29 (.03)
5050	0.0 (.04)	0.0 (.03)
5175	-0.05 (.04)	-0.03 (.03)
5300	-0.23 (.04)	-0.15 (.03)
5820	-0.87 (.03)	-0.47 (.02)
5892	-0.67 (.03)	-0.31 (.02)
6100	-1.03 (.03)	-0.59 (.02)
6180	-0.99 (.03)	-0.55 (.02)
6370	-1.18 (.03)	-0.68 (.03)
7050	-1.57 (.04)	-0.83 (.04)
7100	-1.55 (.04)	-0.81 (.04)
7400	-1.75 (.04)	-0.87 (.04)
8050	-2.00 (.05)	-0.89 (.05)
8190	-2.06 (.05)	-0.96 (.05)
8400	-2.13 (.05)	-0.96 (.05)
8542	-2.14 (.05)	-0.81 (.05)
8800	-2.35 (.05)	-1.04 (.05)
8880	-2.39 (.05)	-1.02 (.05)
9190	-2.51 (.05)	-1.12 (.06)
9950	-2.80 (.05)	-1.24 (.06)
10400	-3.03 (.06)	-1.26 (.06)
10800	-3.23 (.06)	-1.32 (.06)
AB_{5050}	13.46 (.04)	13.34 (.04)
AB_{5500}	12.99 (.04)	13.05 (.04)

FIGURE 4

The observed energy distributions from Table VI for M82 A and B normalized at 5050 Å. The strength of the λ8542 feature is highly uncertain.

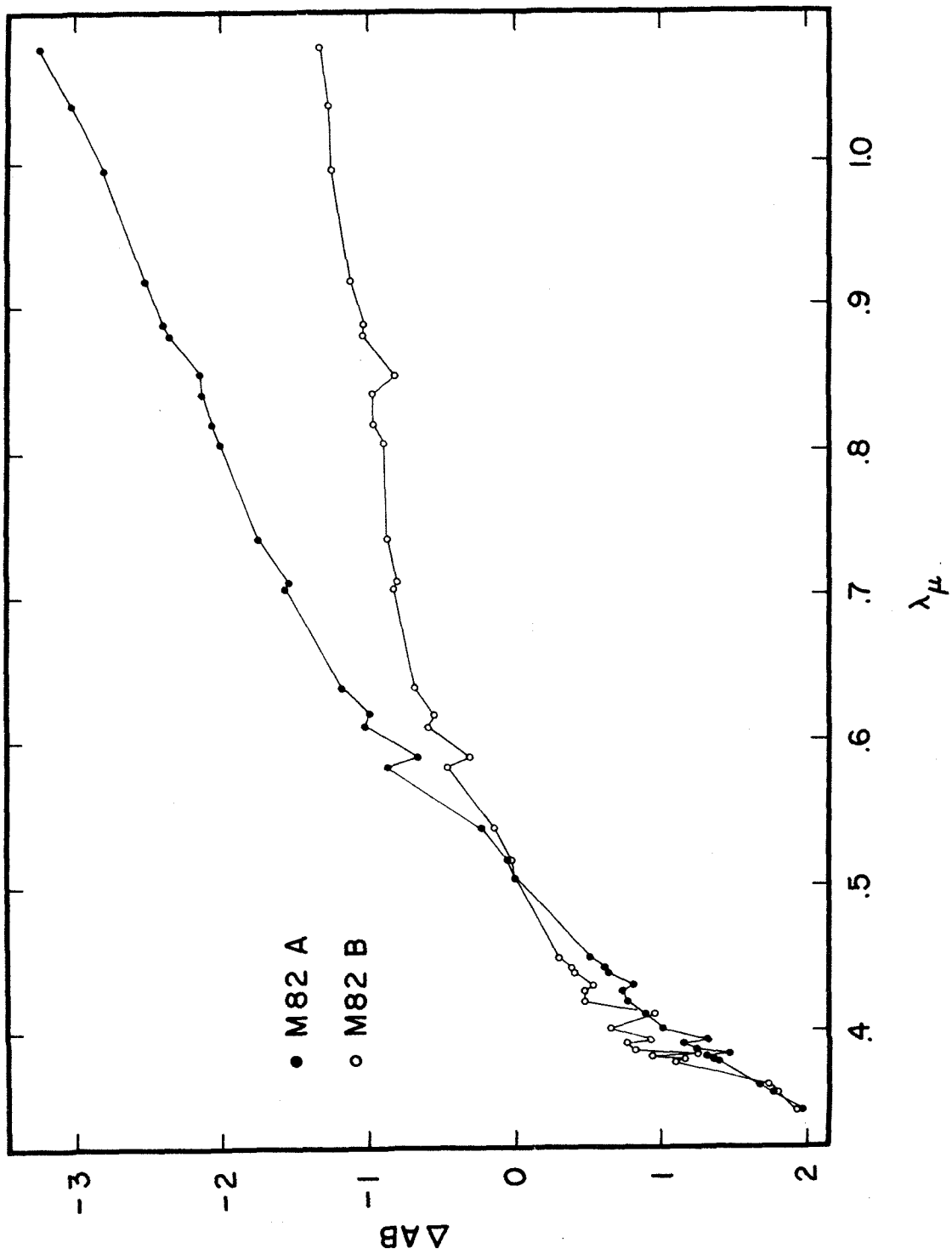
M82 A
M82 B
ΔAB
λμ
-3
-2
-1
0
1
2
.4
.5
.6
.7
.8
.9
1.0

similar to A and B expected in a large aperture centered on the galaxy.

Peimbert and Spinrad's scanner observations of two regions similar to ours generally agree with our data to within a few percent. However, their energy distribution for the "nucleus," when normalized at 5050 Å, falls about $.15^m$ brighter than ours for region A between 3900 and 4500 Å. This discrepancy is most likely the result of a slight difference in aperture centering in the highly complex nuclear region. Peimbert and Spinrad centered their 10" aperture such that the Hα flux was maximized, while we visually centered the brightest part of region A. It should be noted that the two independent MCSP observations of M82 A agreed to $.05^m$ with one another and also with the mean of the lower quality 60" data and Lasker photometry in this wavelength interval. Apparently, appreciable color variations occur on a scale of about 15" of arc within the nuclear region of the galaxy.

Data relevant to the effective spectral resolution of the M82 scans is given in Table VII. MCSP absorption line measures for all features longward of 5000 Å were made with

TABLE VII

M82 SPECTROPHOTOMETRY

Instrument	Aperture "arc	Diameter $Å_2$	Wavelength Interval (Å)	Exit Slot (Å)	Order
60" Cassegrain Scanner	12	14	5050-6370	30	1
200" MCSP	7	17	3400-5800	20	2
			5800-11000	40	1

bandwidths differing from those in the stellar survey. Corrections to the standard bandwidths were determined by correlating the 20 Å Mg I measures (obtained in the second order for most stars) and additional 40 Å measures of the remaining features for a selection of 11 stars with the 30 Å observations of the same objects. Corrections as large as 5% were required. The flux at the D lines (5892 Å) in M82 A was further corrected for contamination from He I λ5876 in emission. The He I intensity was estimated both from the observations of Peimbert and Spinrad (1970) and from 200" image tube spectra. Its contribution to the mean λ5892 measurement was calculated from assumed spectral response profiles for the two scanners to be 1 Å equivalent width. No other corrections were made for emission lines.

Compared to stellar scans, all atomic absorption features in the galaxy scans suffer dilution by the adjacent continuum due to the degraded spectral resolution inherent in slitless spectrophotometry of extended objects. The dilution increases with the ratio of entrance aperture diameter (projected on the exit plane) to the exit slot and with the distance of the absorption feature from the

center of the bandpass. Accordingly, the Mg I and Na I triplets, which include lines more than 5 Å from the center of the bandpass, are the features most susceptible to dilution here. For example, the 60" scanner, when operated with a 30 Å exit slot and a 12 second-of-arc entrance aperture uniformly illuminated with a solar-type spectrum, would produce a blocking fraction for Mg I only 60% of that obtained for a point image. The broad Balmer lines are similarly affected; it is possible that the flux at 4101 Å in M82 has been overestimated by as much as 7% .

Unfortunately, it is not possible to make accurate corrections for the dilution because it is a function of the unknown spectral and spatial distribution of light. Hence, for the purposes of synthesis, all atomic features will be assumed to be somewhat stronger than observed. The Mg I and Na I triplets are given particularly low weight. H10 observations have been discarded altogether because they are highly bandwidth-sensitive due to blending of adjacent hydrogen line wings. Dilution for molecular features cannot be estimated but is not expected to be larger than observational uncertainty.

B M82 Spectral Indices

Line indices formed from the galaxy data of Table VI are given in Table VIII. The probable error of the indices is 4-5%.

Of the features longward of 8000 Å, only Ca II λ8542 was positively detected; but its index value and those for the other infra-red features were too uncertain to include in the synthesis. This results in a palpable handicap to interpretation of the spectrum (cf. Part III E). An upper limit to the strength of the Na I λ8190, TiO λ8880 and CN λ9190 features is about 2 Å equivalent width.

As expected, the value of I_{5175} is too large for the apparent trend indicated by I_{4305}, I_{5892} and I_{6180} (compare the M82 values to Figures B7, B10, and B11). A value $I_{5175} \lesssim .90$ would be more appropriate. The fact that $I_{7100} > I_{6180}$, when the converse is expected because cool stars will contribute more light at 7100 Å than at 6180 Å, is not alarming in view of the errors involved. The Balmer lines in M82 A are filled by emission; recovery of the absorption line strengths is discussed in Part III F. Comparison of the indices and B/V flux ratios for A and B

TABLE VIII

GALAXY SPECTRAL INDICES

Index	M82 A	M82 B	LMC	Galactic Disk	M31
H 3835	---	0.71	0.80	0.73	0.78
CaK 3933	0.84	0.84	0.88	0.79	0.58
H 4101	---	0.72	0.64	0.77	0.96
CN 4200	1.03	1.05		0.98	0.98
G 4305	0.91	0.93	0.87	0.88	0.81
IS 4430	0.98	0.98		1.01	1.01
MgI 5175	0.94	0.96		0.87	0.77
NaD 5892	0.80	0.84		0.91	0.75
TiO 6180	0.92	0.94		0.96	0.86
TiO 7100	0.96	0.98		0.96	0.84
NaI 8190	---	---		0.98	0.95
CaII 8542	---	---		0.92	0.93
TiO 8880	---	---		1.02	1.01
CN 9190	---	---		0.95	1.00
U/B	0.38	0.30		0.41	0.28
B/V	0.31	0.50		0.59	0.32
V/R	0.37	0.61		0.71	0.42
V/I	0.22	0.53		0.61	0.27
V/J	0.10	0.41		0.54	0.21

to those for galactic stars (Table B III) indicates that both A and B are significantly reddened.

Note that all the indices for A and B agree with .02 with the exception of the Na D lines, which are probably stronger in A. The index agreement is better than that expected from the estimated observational uncertainty. Hence, no strong gradient of metal content, such as probably exists in the nuclear regions of k-nuclei galaxies (McClure 1969), is found in M82. However, the CN λ4216 feature, which best exhibits the gradient, is not present; and an accurate CN 9190 observation is not available.

The similarity of spectral indices for A and B also indicates that the principal contributors to light between 3900 and 7400 Å are similar in the two regions. Hence, roughly speaking, the stellar content for spectral types A0 and M0 is almost identical in the two regions, and no nonstellar source of radiation present in the nucleus but not in the disk makes more than about a 20% contribution to the total flux anywhere in this wavelength interval.

Inasmuch as region A lies in a region of heavy obscuration, the enhancement of the nuclear D lines (approximately 1 Å equivalent width) might be attributed

to interstellar Na I in M82. Under galactic conditions, one would expect a corresponding enhancement of Ca II K of only about .25 Å (Routly and Spitzer 1952), which would not be observable. The importance of interstellar absorption is M82 is considered further below. Contributions to the M82 K and D line strengths from the interstellar medium of our galaxy would be no more than .2 and .7 Å EW, respectively (Münch 1968).

The interstellar λ4430 feature shows a marginally positive blocking fraction in both A and B. This cannot be considered a positive detection of the feature, however, particularly because it is not enhanced in A. The reddening differential between A and B would suggest a difference in I_{4430} of roughly .03, according to Figure B 8. Extragalactic λ4430 has been detected so far only in bright stars of the Magellanic Clouds (Hutchings 1964).

Table VIII also contains index values computed from equivalent widths observed by the de Vaucouleurs (1960) for a region of the bar of the Large Magellanic Cloud, values for a composite spectrum of the Population I component of the solar neighborhood, and those for the synthesis of the nucleus of M31 given by Spinrad (1966).

The latter two spectra employ the data of Chapter II. The solar neighborhood model was taken from the spectral-luminosity distribution given by Allen (1964, p. 239) and converted to surface densities on the galactic plane by weighting each stellar type by the z(.1)'s tabulated by Blaauw (1965). Subdwarfs, white dwarfs and A-K supergiants are not included; the globular cluster is neglected in M31. The effects of these omissions on the indices is probably not large.

Allowing for the fact (cf. Part II B) that actual measures of equivalent widths will almost always be larger than those calculated from photometrically measured blocking fractions (especially if EW $\gtrsim$ 5 Å), one finds that M82 and the Large Cloud are fairly similar except that the Cloud has weaker K and H9 features. This is consistent with the excess of stars hotter than B5 in the Cloud relative to M82 suggested by the presence of He I λ3820 in the Cloud (de Vaucouleurs and de Vaucouleurs 1960) and its absence in spectra of M82 (e.g. Mayall 1960). One might note that the absence of CN λ4200 in the Cloud is not consistent with the relatively large contribution of

luminous K and M stars at 4200 Å in the population model deduced by the de Vaucouleurs.

On the other hand, M82 has an earlier spectrum between 3800 and 5000 Å than does the solar neighborhood. In particular, G-K III light, indicated by CN 4200, is not as important in M82 as in the solar vicinity. The D lines and TiO λ6180, however, are stronger in M82.

Indices for the M31 synthesis are included to dramatize the difference between all of the above objects and a typical k-nucleus.

C The Continuous Energy Distribution and the Reddening Law

The energy distributions of regions A and B are remarkably different, as the Lasker photometry indicated (see Part I B). A has a much smaller Balmer jump and is 2^m brighter at 10800 Å than B when normalized at 5050 Å.

Inasmuch as no large difference in stellar content between A and B is evident in the 3900-7400 Å region, it is reasonable to attribute the discrepancy here to interstellar extinction within M82. In Figure 5 we compare the extinction curve obtained from the energy distributions of A and B (curve "M") to that predicted by the Whitford (1958)

FIGURE 5

Extinction curve for the nuclear region of M82 compared to the Whitford law. Curve M is obtained by assuming that the intrinsic energy distribution of region A is the observed distribution for region B. If all extinction in both regions occurs in overlying dust clouds composed of similar grains, this is the same as assuming the intrinsic energy distributions of both regions are identical. W is the Whitford law. Curve X is explained in the text. Normalization for all curves is E(B-V) = 1.0.

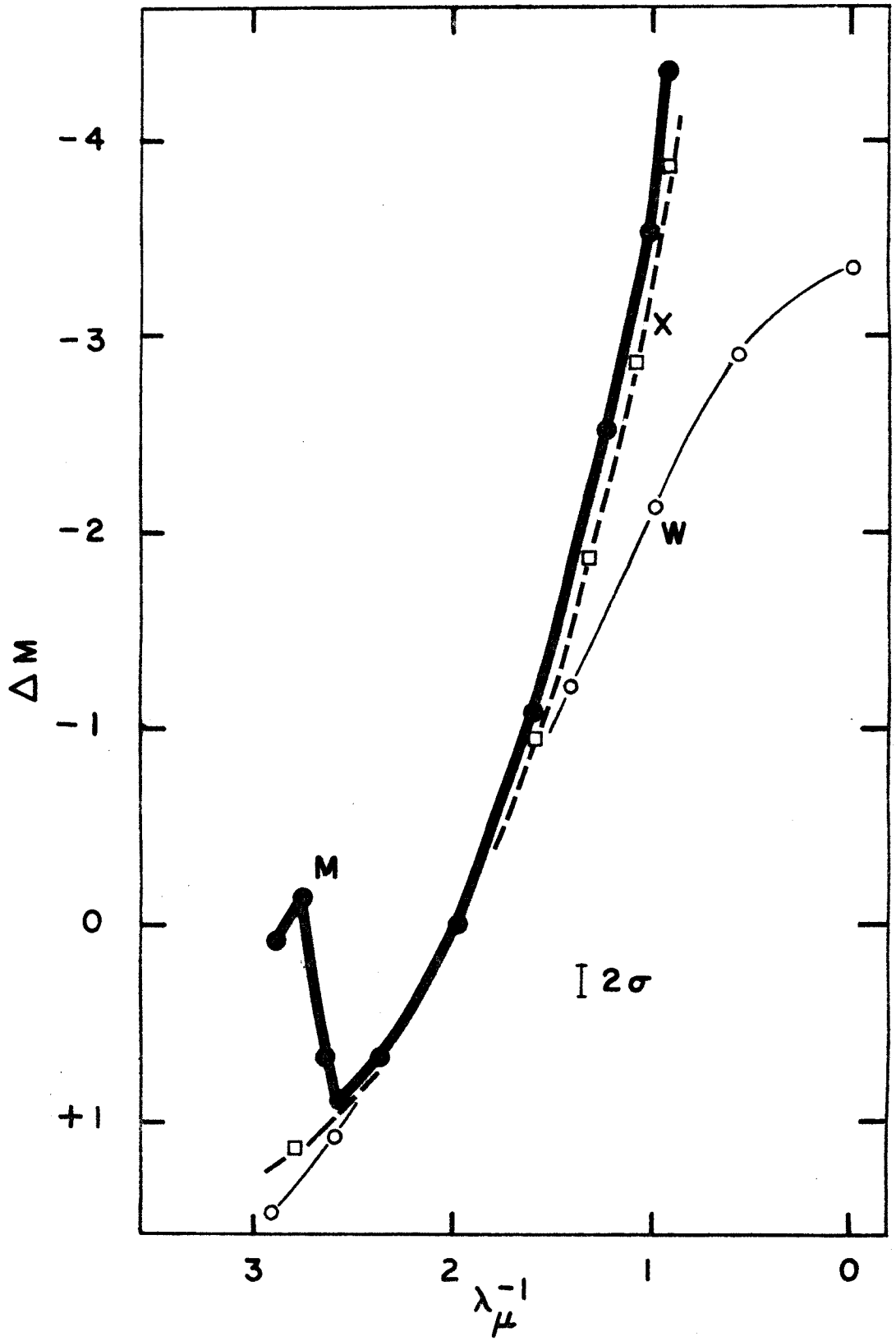
-4
-3
-2
-1
0
+1
ΔM
3
2
1
0
λ_μ^{-1}
M
X
W
I 2σ

law if the two regions have intrinsically similar energy distributions but suffer differential reddening from overlying dust clouds ("W"). Between 3900 and 6000 Å, M and W agree within observational uncertainty; however, outside of these limits, region A emits radiation in excess of that predicted by W. We attribute the ultra-violet excess to a combination of an additional source of high-temperature radiation and (for $\lambda \leq 3646$ Å) Balmer recombination continuum in region A. Note that this excess begins above 3800 Å and therefore cannot originate in Balmer continuum alone. On the other hand, the analysis of Part III F will show that the infra-red excess cannot entirely be produced by additional cool stars, thermal re-radiation from dust or other nonstellar radiation and must be explained primarily by interstellar extinction.

Extinction curves similarly at variance with W above 6000 Å are found from Lasker photometry in dust lanes G and H, where the effects presumably result entirely from interstellar extinction (see Figure 6). These curves are obtained by comparing G and H to region B, which is probably representative of the average galactic background in M82.

FIGURE 6

Lasker photometry extinction curves obtained for dust lanes G and H by comparison to region B. W is the Whitford law. Normalization is E(λ4698) - E(λ6067) = 1.0. The λ3474 point on curve G is highly uncertain. Relative to W, the near infra-red behavior of G and H is similar to that of curve M in Figure 5.

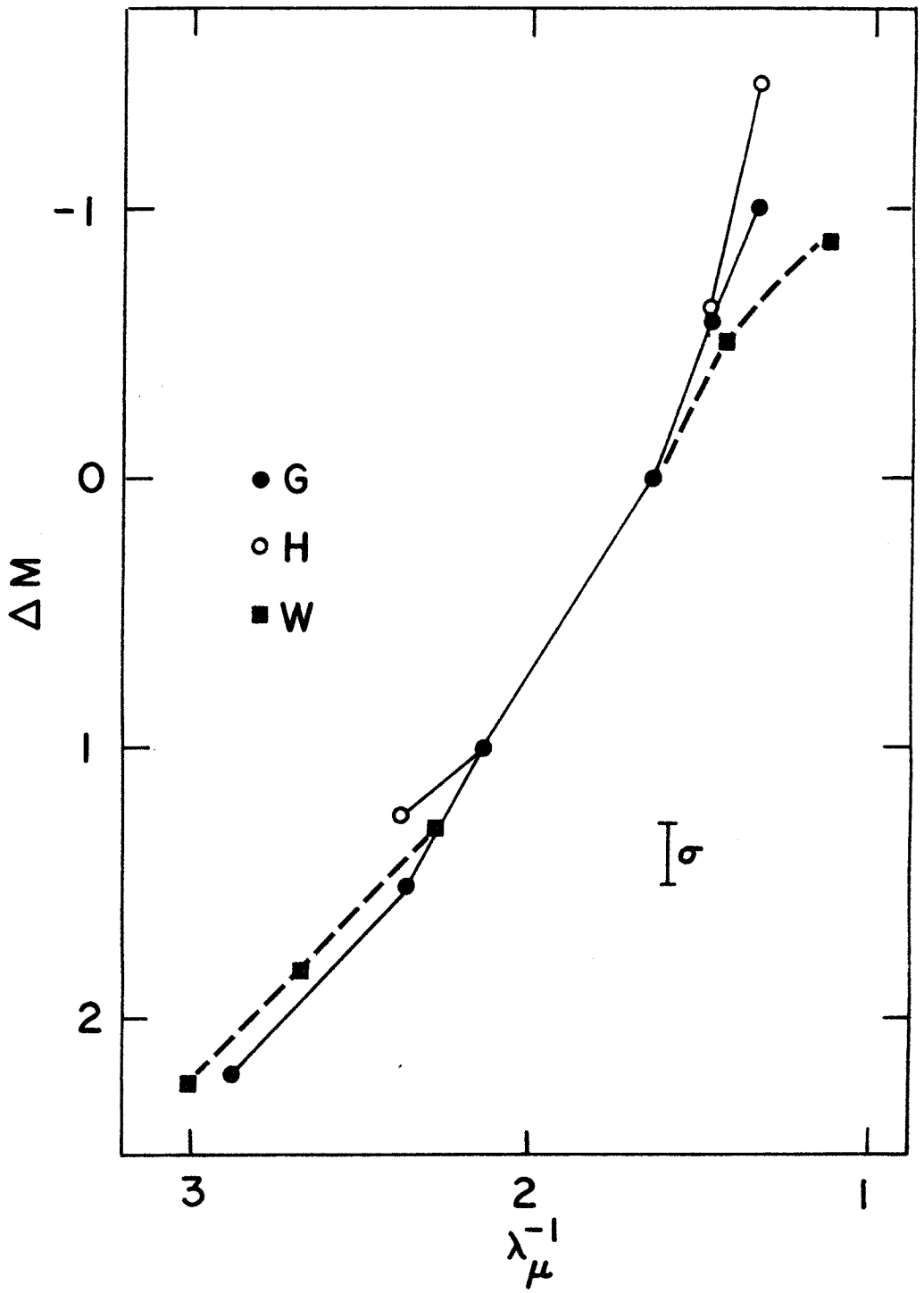
-1
0
1
2
ΔM
● G
○ H
■ W
σ
3
2
1
λ_μ^{-1}

Both curves agree with W below 6000 Å but differ from it above 6000 Å by about one standard deviation in approximately the same manner as does curve M.

Curve M is similar to the anomalous extinction curve found by Johnson (1968) in the Orion Sword region. Nevertheless, it is not necessary to ascribe the infra-red behavior of M to a mean dust grain composition or size distribution different than found in our galaxy. In fact, the analysis of Part III E will show that the reddening law in region B must be very similar to W. Although very different types of grains might exist near region A, curve M is more plausibly explained by a different relative distribution of stars and dust than assumed in calculating curve W. Curve X in Figure 5 represents an extinction curve obtained for a uniform one-dimensional mixture of stars and dust of large total optical depth according to

$$I(\lambda) = \frac{I_0(\lambda)}{\tau_\lambda} \left[1 - e^{-\tau_\lambda}\right] .$$

Here, $I(\lambda)$ is the observed specific intensity at λ, $I_0(\lambda)$ is the specific intensity observed in the absence of dust, and $\tau_\lambda = n \sigma Q_e(\lambda) L$ where n is the number of dust

grains per unit volume, σ is the geometrical cross section of the grains, $Q_e(\lambda)$ is the extinction efficiency factor at λ, and L is the total pathlength through the mixture. We assume the wavelength dependence for the extinction efficiency of the dust grains is given by the Whitford law and that the grains have zero albedo. X is a much better approximation to M than is W.

The following analysis (Parts III E and F) shows that the observations can be reasonably well explained in this way without assuming any large differences between galactic and M82 dust grains. The implication is then that whereas the reddening in M82 B primarily originates in overlying dust clouds, M82 A must itself contain a large admixture of dust.

D Synthesis Procedure

To synthesize the observed composite spectra, we superpose various mixtures of spectra of individual stellar types from Part II, seeking a population model which will reproduce the observations. Population models are developed subject to the following criteria:

1) The population density in the color-magnitude diagram must be smoothly continuous. The relative population of various regions of the diagram must be consistent with our knowledge of stellar evolution. For simplicity, we have assumed the main sequence luminosity function is a monotonically increasing function of absolute magnitude. This is the case for the solar neighborhood luminosity function (McCuskey 1965) in the magnitude interval considered here ($M_V \leq +13$), except for a small dip at $M_V = +7$, which would have negligible influence on integrated properties.

2) In accordance with Part III C, we assume that the extinction efficiency of interstellar grains in M82 is given by the Whitford law except for possible minor variations. We allow only two distributions of stars and dust along the line of sight: (A) all dust lies in a screen between the stars and the observer; and (B) a dust screen overlies a uniform mixture of dust and stars. For the rough analysis performed here, it is not profitable to consider any more elaborate model than the simple one-dimensional uniform mixture neglecting scattering. The importance of scattering in the final adopted models is discussed below. Any foreground galactic reddening, which would amount to only about

E(B-V) = .04 (Peterson 1968), is simply absorbed into this calculation.

3) We exclude non-stellar sources of radiation from the synthesis for region B but consider synchrotron radiation, hydrogen continuum emission and other nonstellar radiation as possible contributors to region A.

4) For lack of observations, we must exclude certain types of stars. The only important objects so excluded are A-K I and II stars, M6+ dwarfs, and stars of low metal content. Many types of objects for which detailed observations are not available (e.g. O-G5 III and IV or M II stars) are indistinguishable in a composite spectrum from adjacent observed types. Their presence must be deduced from condition (1) above. The possible influence of types omitted from the synthesis is discussed below.

The fitting criteria for a successful synthesis are the following:

a) All feature indices must be fit within 4% allowing for the various effects discussed in Parts III A and B. That is, (i) the Balmer indices may be about 7% smaller than observed; (ii) probably $I_{5175} \lesssim .90$; and (iii) roughly allowing for the combined effects of spectral smoothing

and interstellar contributions, I_{3933} should be about as observed and I_{5892} should be larger. We will fit the model to the average value of the indices (except NaD 5892 and the Balmer indices) for A and B.

b) The model should fit the continuum to about 10% over the entire wavelength interval observed. Given the uncertainties involved, especially in the treatment of interstellar extinction, this is not an overgenerous allowance for error.

c) Allowing for the possibly considerable effect of non-luminous matter--40% of the mass in the solar neighborhood remains unidentified (Blaauw 1965)--the predicted M/L must be significantly smaller than M/L observed. Interstellar extinction will have a large influence in determining the predicted M/L.

The value quoted for M/L_V in Table I represents the best available determination for $r < 3$ kpc, but an uncertainty of a factor of 2 is not unlikely. M82 B is probably representative of this region of the galaxy, and hence we will require than $M/L_V(\text{model}) < 6$ for M82 B. The observed mean value of M/L_V does not apply to region A since it is more heavily reddened than its surroundings.

Inasmuch as condition (1) and the fitting criteria cannot be formulated in a simple mathematical way, a trial and error procedure rather than least squares was used to find suitable models. For a given population mixture, however, least squares is useful in determining reddening parameters.

Table IX lists the color-magnitude domains and masses assigned to each stellar group in the synthesis. These quantities have been taken from Schmidt-Kaler (1965) and Harris et. al. (1963).

Finally, we should note that because of the unreliability of the galaxy spectral indices for $\lambda > 8000$ Å and the instrumental or interstellar influences on the Mg I triplet and the D lines, we have lost all spectral sensitivity to stellar luminosity except through I_{4200}. Therefore, the giant-to-dwarf ratio has to be established on the less reliable grounds of conditions (1) and (c) above.

E Synthesis for M82 B

The adopted model for M82 B is presented in Table X. It is normalized such that the F6-9 V population equals 10. Its construction was based on the following considerations:

TABLE IX

GROUP PARAMETERS ASSUMED FOR SYNTHESIS

Group	$\langle M_V \rangle$	$\langle B-V \rangle$	Mass ($M_\odot$)	Color-Magnitude Limits M_V	(B-V)
O V	-5.0	-0.32	30.0	-6.0,-4.2	-0.34,-0.31
B0-4 V	-2.5	-0.26	9.0	-4.2,-1.5	-0.31,-0.20
B5 V	-1.0	-0.17	6.0	-1.5,-0.5	-0.20,-0.15
B6-9 V	0.0	-0.12	3.5	-0.5, 0.75	-0.15,-0.05
A0-4 V	1.5	0.03	2.5	0.75,2.0	-0.05, 0.10
A5-9 V	2.3	0.21	1.7	2.0, 2.7	0.10, 0.27
F0-5 V	3.1	0.37	1.4	2.7, 3.7	0.27, 0.43
F6-9 V	4.2	0.52	1.2	3.7, 4.6	0.43, 0.56
G0-5 V	4.9	0.63	1.0	4.6, 5.3	0.56, 0.69
G6-9 V	5.6	0.74	0.85	5.3, 5.7	0.69, 0.78
K0-2 V	6.1	0.86	0.80	5.7, 6.4	0.78, 0.93
K3-4 V	6.6	1.05	0.75	6.4, 7.0	0.93, 1.10
K5-7 V	7.9	1.30	0.58	7.0, 8.5	1.10, 1.38
M0-2 V	9.6	1.45	0.46	8.5,10.5	1.38, 1.50
M3-4 V	11.4	1.56	0.27	10.5,12.5	1.50, 1.65
M5-6 V	13.2	1.72	0.20	12.5,15.0	1.65, 1.80
G0-5 IV	3.0	0.70	1.1	2.5, 4.0	0.52, 0.75
G6-9 IV	3.1	0.80	1.1	2.5, 5.0	0.75, 0.88
K0-2 IV	3.2	0.95	1.1	2.5, 5.5	0.88, 1.10
B0-6 III	-3.0	-0.22	9.0	-5.0,-2.0	-0.30,-0.16
A5-9 III	1.2	0.22	2.0	1.0, 1.4	0.15, 0.25
F0-5 III	1.6	0.35	2.0	0.7, 2.7	0.25, 0.42
G5-9 III	1.5	0.91	2.0	0.5, 2.5	0.80, 0.98
K0-3 III	0.9	1.15	1.7	-0.2, 1.8	0.98, 1.35
K4-5 III	0.1	1.40	1.7	-0.5, 1.0	1.35, 1.54
M0-2 III	-0.4	1.57	1.7	-1.4, 0.6	1.54, 1.60
M4-5 III	-0.8	1.58	1.7	-1.8, 0.2	
M6-8 III	-1.0	1.55	1.7	-2.0, 0.0	
B0-7 I	-6.2	-0.16	15.0	-7.2,-5.2	-0.27,-0.10
M I-II	-6.0	1.65	15.0	-7.5,-4.5	

TABLE X SYNTHESIS FOR M82 B

Population Model and Spectral Decomposition

Group	Number of Stars	Fraction of Light Contributed at λ								
		λ3620	λ4015	λ4400	λ5050	λ6100	λ7400	λ8400	λ9950	λ10800
B0-B4 V	1.70E-04	0.0036	0.0016	0.0015	0.0011	0.0007	0.0005	0.0004	0.0003	0.0003
B5 V	1.20E-02	0.0455	0.0280	0.0248	0.0190	0.0129	0.0094	0.0073	0.0062	0.0054
B6-B9 V	2.10E-01	0.2291	0.1956	0.1725	0.1334	0.0958	0.0688	0.0569	0.0455	0.0383
A0-A4 V	1.44E 00	0.2420	0.3036	0.2724	0.2240	0.1699	0.1269	0.1049	0.0947	0.0858
A5-A9 V	1.37E 00	0.0903	0.1125	0.1080	0.0981	0.0799	0.0630	0.0568	0.0479	0.0468
F0-F5 V	4.50E 00	0.1414	0.1382	0.1452	0.1444	0.1365	0.1226	0.1140	0.1002	0.0920
F6-F9 V	1.00E 01	0.1059	0.0873	0.0984	0.1097	0.1140	0.1061	0.1036	0.0925	0.0881
G0-G5 V	1.34E 01	0.0632	0.0508	0.0598	0.0748	0.0827	0.0816	0.0822	0.0748	0.0668
G6-G9 V	9.40E 00	0.0162	0.0148	0.0181	0.0255	0.0308	0.0319	0.0331	0.0300	0.0300
K0-K2 V	2.28E 01	0.0204	0.0203	0.0254	0.0382	0.0489	0.0513	0.0529	0.0499	0.0508
K3 V	1.99E 01	0.0069	0.0081	0.0119	0.0187	0.0281	0.0297	0.0340	0.0332	0.0339
K5-K7 V	5.49E 01	0.0037	0.0038	0.0073	0.0119	0.0276	0.0380	0.0446	0.0511	0.0582
M0-M2 V	8.00E 01	0.0	0.0010	0.0017	0.0034	0.0089	0.0193	0.0247	0.0302	0.0329
M3-M4 V	8.40E 01	0.0	0.0002	0.0003	0.0007	0.0017	0.0056	0.0080	0.0102	0.0113
G0-G5 IV	2.00E-01	0.0041	0.0036	0.0044	0.0061	0.0073	0.0076	0.0078	0.0075	0.0072
G6-G9 IV	2.00E-01	0.0032	0.0028	0.0036	0.0054	0.0070	0.0076	0.0081	0.0080	0.0078
K0-K3 IV	2.00E-01	0.0021	0.0022	0.0029	0.0047	0.0063	0.0071	0.0076	0.0076	0.0075
G5-G9 III	8.00E-02	0.0049	0.0047	0.0062	0.0095	0.0119	0.0128	0.0133	0.0134	0.0137
K0-K3 III	1.60E-01	0.0121	0.0133	0.0183	0.0305	0.0425	0.0492	0.0501	0.0532	0.0543
K4-K5 III	6.40E-02	0.0031	0.0045	0.0093	0.0212	0.0413	0.0599	0.0625	0.0721	0.0764
M0-M2 III	3.20E-02	0.0017	0.0024	0.0062	0.0154	0.0352	0.0611	0.0741	0.0923	0.1032
M4-M5 III	6.00E-03	0.0006	0.0008	0.0018	0.0042	0.0100	0.0399	0.0530	0.0793	0.0891

Table X (continued)

Model Indices and Other Parameters

Index	Predicted	Observed	Obs/Pred
H 3798	0.800		
H 3835	0.665	0.715	1.075
CAK 3933	0.853	0.844	0.988
H 4101	0.651	0.717	1.100
CN 4200	0.998	1.046	1.047
G 4305	0.905	0.927	1.025
FS 4430	1.014	0.981	0.968
MGI 5175	0.908	0.959	1.055
NAD 5892	0.932	0.838	0.899
TIO 6180	0.969	0.940	0.970
TIO 7100	0.968	0.976	1.008
NAI 8190	0.994		
CAII 8542	0.920		
TIO 8880	0.990		
CN 9190	0.977		
U/B	0.292	0.295	
B/V	0.539	0.501	
V/R	0.613	0.615	
V/I	0.468	0.535	
V/J	0.372	0.410	

Optical depth in dust: τ_{5500}(external) = 1.04

E(B-V) produced by external cloud: 0.37

Intrinsic M/L_V: 1.12 $M/L_V(\odot)$

Predicted observed M/L_V: 3.12 $M/L_V(\odot)$

Scaling factor for model:

observed V flux corrected for extinction/model V flux

$= 8.5 \times 10^5$

Table X (continued)

Comparison of Predicted and Observed Fluxes

λ (Å)	Intrinsic Model Flux	Predicted Observed Flux	Observed Flux	Obs/Pred
3449.	2.952E-01	1.906E-01	1.690E-01	0.9362
3570.	3.026E-01	1.936E-01	1.941E-01	1.0026
3620.	3.214E-01	2.087E-01	2.032E-01	0.9738
3784.	5.505E-01	3.727E-01	3.664E-01	0.9832
3798.	4.639E-01	3.151E-01	3.532E-01	1.1207
3815.	6.157E-01	4.200E-01	4.246E-01	1.0110
3835.	4.355E-01	2.986E-01	3.192E-01	1.0690
3860.	7.045E-01	4.863E-01	4.742E-01	0.9752
3910.	7.323E-01	5.136E-01	4.966E-01	0.9668
3933.	6.461E-01	4.565E-01	4.285E-01	0.9387
4015.	8.470E-01	6.148E-01	5.495E-01	0.8938
4101.	5.524E-01	4.122E-01	4.169E-01	1.0112
4200.	8.493E-01	6.524E-01	6.486E-01	0.9943
4270.	8.538E-01	6.678E-01	6.486E-01	0.9713
4305.	7.788E-01	6.147E-01	6.138E-01	0.9984
4400.	8.784E-01	7.118E-01	6.982E-01	0.9809
4430.	9.163E-01	7.491E-01	7.047E-01	0.9407
4500.	9.638E-01	8.047E-01	7.656E-01	0.9514
5050.	1.000E 00	1.000E 00	1.000E 00	1.0000
5175.	9.381E-01	9.750E-01	1.028E 00	1.0544
5300.	1.067E 00	1.151E 00	1.148E 00	0.9974
5820.	1.155E 00	1.409E 00	1.542E 00	1.0939
5892.	1.086E 00	1.344E 00	1.330E 00	0.9900
6100.	1.199E 00	1.537E 00	1.722E 00	1.1204
6180.	1.165E 00	1.512E 00	1.660E 00	1.0973
6370.	1.206E 00	1.619E 00	1.871E 00	1.1555
7050.	1.321E 00	2.000E 00	2.148E 00	1.0737
7100.	1.284E 00	1.961E 00	2.109E 00	1.0755
7400.	1.362E 00	2.175E 00	2.228E 00	1.0244
8050.	1.434E 00	2.483E 00	2.270E 00	0.9142
8190.	1.437E 00	2.527E 00	2.421E 00	0.9582
8400.	1.463E 00	2.629E 00	2.421E 00	0.9209
8543.	1.365E 00	2.488E 00	2.109E 00	0.8476
8800.	1.521E 00	2.841E 00	2.606E 00	0.9173
8880.	1.504E 00	2.829E 00	2.559E 00	0.9043
9190.	1.507E 00	2.911E 00	2.805E 00	0.9638
9950.	1.572E 00	3.219E 00	3.133E 00	0.9734
10400.	1.596E 00	3.382E 00	3.192E 00	0.9436
10800.	1.602E 00	3.496E 00	3.373E 00	0.9648

a) We adopt interstellar extinction case A for M82 B because no reasonable model fitting the indices will also fit the near infra-red continuum if any significant amount of reddening occurs internally. The model given, in fact, is slightly too red above 8000 Å, and case B would only increase the discrepancy. For the same reason, we cannot possibly adopt an extinction efficiency curve like curve M of Figure 5 for the dust grains in region B.

As anticipated, the additional degree of freedom introduced by allowing variable reddening renders the continuum above 3900 Å relatively insensitive to stellar content. The Balmer jump, however, is important in determining the population of stars hotter than A0.

b) The character of the upper main sequence is well determined by the spectral indices between 3800 and 5000 Å and the Balmer jump. In Figure 7 we compare the adopted main sequence luminosity function to the solar neighborhood main sequence function (McCuskey 1965, with values converted to surface densities on the plane as in Part III B and corrected for evolved stars using the factors given by Starikova 1960). The two functions are essentially identical for $M_V \leq +4$, except that the M82 B luminosity

function must be truncated at about M_V = -3 to fit the Balmer jump. A model in which the upper main sequence luminosity function is extrapolated to brighter absolute magnitudes from M_V = 0.0 parallel to the solar neighborhood function in Figure 7 would yield 12% more light below 3640 Å than observed. For a good fit to the ultraviolet, stars hotter than B6 cannot contribute more than about 6% of the light at 5050 Å.

c) The problem of the lower main sequence and cool evolved star population must be solved simultaneously. The "minimal" lower main sequence extrapolated from the upper main sequence above which is consistent with condition (1) is, again, essentially the solar neighborhood function (See Figure 7).

In order to fit the TiO indices we need at least 2% M light at 5050 Å. This light cannot entirely originate on the main sequence, because the minimal M/L_V for a late dwarf-enriched model which fits the TiO indices is about 8. Hence, we have assumed in the given model that M light in excess of the "minimal" lower main sequence originates in M0-6 III's. This assumption produces the largest giant-to-dwarf ratio (and smallest M/L) consistent with the

FIGURE 7

Adopted main sequence luminosity functions for M82 A and B taken from Tables X and XI compared to that for the galactic disk in the vicinity of the sun. For $M_V > +4$, the M82 A function is identical to M82 B's. The difference between the two functions for $0 \leq M_V \leq +4$ is not significant. The normalization for all three curves is arbitrary but is the same for M82 A and B.

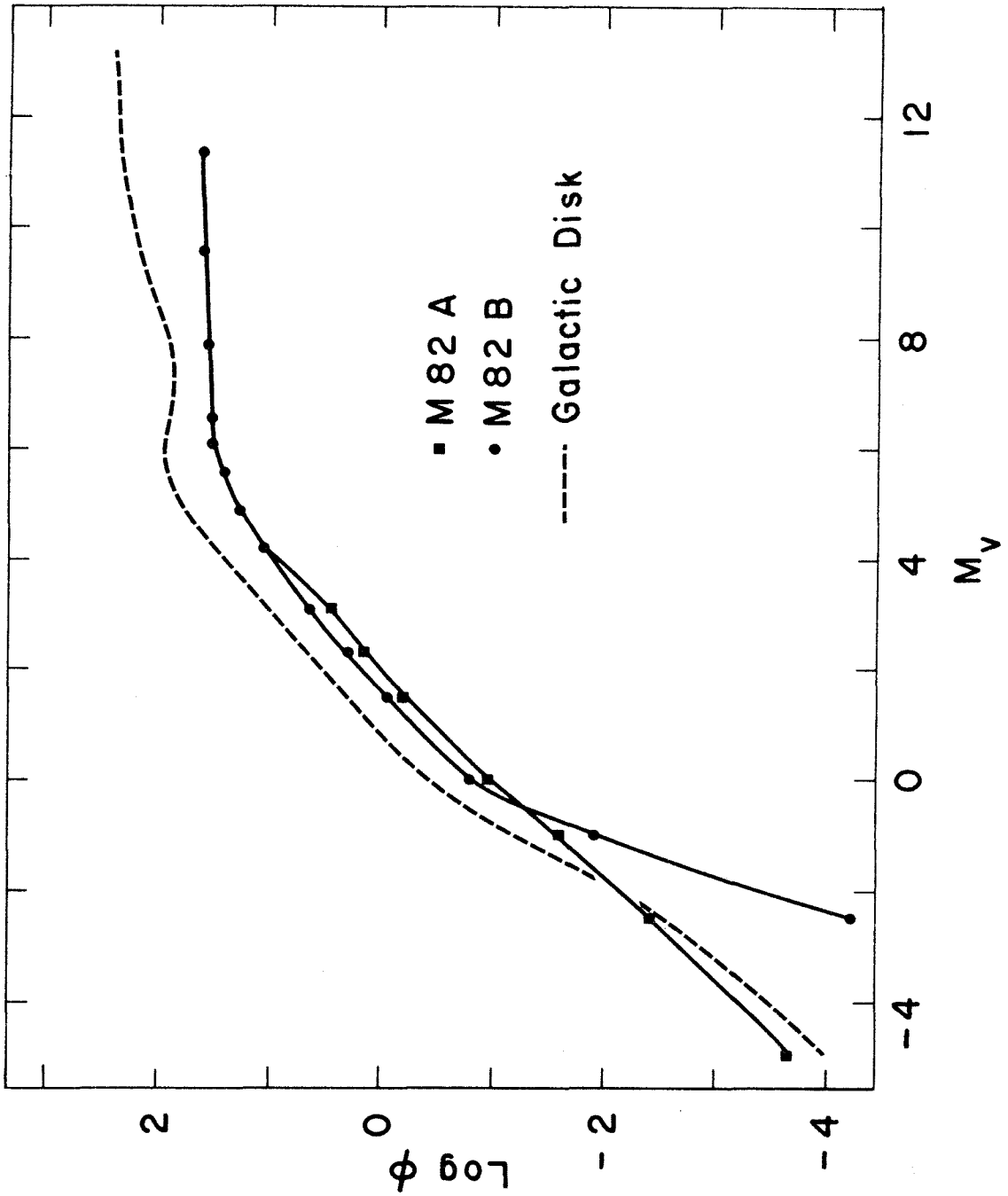
M82 A
M82 B
Galactic Disk
Log φ
2
0
-2
-4
-4
0
4
8
12
M_v

observations. It is, of course, also possible to attribute as much of the M light to dwarfs as is consistent with M/L. Roughly 1/2 of the required M light can be obtained in this way. The M0-6 III contribution is limited to about 4% at 5050 Å by the observed TiO indices and the fit to the near infra-red continuum.

d) As remarked in Part III D, apart from the M III stars, our observations are insensitive to luminosity class III light. The maximum percentage of G6-K5 III light at 5050 Å allowable by I_{3933}, I_{4200} and I_{4305} is about 15%, but this is only a rough upper limit since these indices are more sensitive to hotter stars. A far better hold on G6-K5 III light would be obtained through the 8000-9000 Å indices, particularly CN 9190.

In order to schematically enter G6-K5 III in the model, we have assumed that the relative ratios of numbers of various kinds of luminosity class III stars in M82 are the same as in the solar neighborhood. This is a unsatisfactory assumption because these ratios are dependent on the history of star formation in the solar vicinity, the oldest M III stars (about $1M_{\odot}$) being four times as old as the oldest

G III stars (about $1.5M_{\odot}$). Additionally, the values of these ratios (based on data from McCuskey 1965, Allen 1964, and the stellar groups studied by Eggen 1965) are highly uncertain, perhaps by a factor of 2.

The G-K IV stars have been treated in a similar way.

e) From evolutionary considerations, we expect the presence of stars up to 3^m above the class III stars in Table X as well as large numbers of A-G5 III stars near the main sequence. Such objects are not explicitly included in the model, and it should be supposed that the total light contributed by each spectral type in Table X originates in a somewhat larger range of luminosity than given in Table IX. The resultant corrections to the main sequence luminosity function are not large enough to substantially affect the comparison to the solar neighborhood function.

Further discussion of these results follows a description of the M82 A synthesis.

F Synthesis for M82 A

The synthesis for M82 A has been based on the solution for M82 B adopted above. As described in Part III C, we employ case B for interstellar extinction. In order to fit the continuum between 3700 and 4000 Å, we must extend the upper main sequence obtained for M82 B to O V (see Figure 7). (Again we note that for early spectral types, a large fraction of the model light in "V" stars actually originates in evolved stars of the same temperature.) Condition (1) then requires the presence of a number of B and M supergiants, which have been added in approximately the ratio observed in the galaxy (Stothers 1969). The adopted model is presented in Table XI. Below 3646 Å we have allowed for the presence of Balmer continuum radiation (described below).

The total optical depth in dust internal to M82 A required to fit the near infra-red continuum is a sensitive function of the amount of M I light added to the model. The adopted model possesses the maximum amount of M I light (and hence minimum internal optical depth--4.2 at 5500 Å) consistent with the TiO indices. Reducing the number of M

TABLE XI SYNTHESIS FOR M82 A

Population Model and Spectral Decomposition

Group	Number of Stars	Fraction of Light Contributed at λ								
		λ3620	λ4015	λ4400	λ5050	λ6100	λ7400	λ8400	λ9950	λ10800
O V	4.00E-04	0.0911	0.0447	0.0375	0.0263	0.0165	0.0100	0.0074	0.0049	0.0041
B0-B4 V	1.05E-02	0.1542	0.1004	0.0893	0.0678	0.0445	0.0280	0.0210	0.0149	0.0146
B5 V	2.45E-02	0.0650	0.0564	0.0503	0.0387	0.0253	0.0171	0.0129	0.0102	0.0086
B6-B9 V	1.40E-01	0.1068	0.1287	0.1143	0.0888	0.0615	0.0410	0.0327	0.0245	0.0199
A0-A4 V	8.10E-01	0.0952	0.1685	0.1523	0.1258	0.0921	0.0638	0.0509	0.0430	0.0376
A5-A9 V	1.04E 00	0.0479	0.0843	0.0815	0.0744	0.0584	0.0427	0.0372	0.0294	0.0277
F0-F5 V	2.82E 00	0.0620	0.0855	0.0905	0.0903	0.0824	0.0687	0.0616	0.0507	0.0450
F6-F9 V	1.00E 01	0.0740	0.0861	0.0978	0.1095	0.1098	0.0948	0.0894	0.0746	0.0687
G0-G5 V	1.34E 01	0.0442	0.0501	0.0595	0.0747	0.0797	0.0729	0.0709	0.0604	0.0521
G6-G9 V	9.40E 00	0.0113	0.0146	0.0180	0.0255	0.0297	0.0285	0.0286	0.0242	0.0234
K0-K2 V	2.28E 01	0.0142	0.0200	0.0253	0.0382	0.0472	0.0458	0.0456	0.0403	0.0396
K3 V	1.99E 01	0.0048	0.0080	0.0118	0.0186	0.0270	0.0265	0.0293	0.0268	0.0264
K5-K7 V	5.49E 01	0.0026	0.0037	0.0073	0.0119	0.0266	0.0339	0.0384	0.0412	0.0454
M0-M2 V	8.00E 01	0.0	0.0010	0.0017	0.0034	0.0086	0.0173	0.0213	0.0244	0.0257
M3-M4 V	8.40E 01	0.0	0.0002	0.0003	0.0007	0.0016	0.0050	0.0069	0.0083	0.0088
G0-G5 IV	2.00E-01	0.0029	0.0035	0.0043	0.0061	0.0071	0.0068	0.0067	0.0060	0.0056
G6-G9 IV	2.00E-01	0.0022	0.0028	0.0035	0.0053	0.0067	0.0068	0.0070	0.0065	0.0061
K0-K3 IV	2.00E-01	0.0015	0.0022	0.0029	0.0047	0.0061	0.0064	0.0065	0.0061	0.0059
G5-G9 III	8.00E-02	0.0034	0.0047	0.0062	0.0095	0.0115	0.0115	0.0115	0.0108	0.0107
K0-K3 III	1.60E-01	0.0085	0.0131	0.0182	0.0304	0.0409	0.0440	0.0432	0.0430	0.0423
K4-K5 III	6.40E-02	0.0022	0.0044	0.0093	0.0211	0.0398	0.0535	0.0539	0.0582	0.0596
M0-M2 III	3.20E-02	0.0012	0.0024	0.0061	0.0154	0.0339	0.0546	0.0639	0.0745	0.0805
M4-M5 III	6.00E-03	0.0004	0.0008	0.0018	0.0042	0.0096	0.0356	0.0457	0.0640	0.0695
B0-B7 I	4.00E-04	0.2024	0.1102	0.0996	0.0753	0.0526	0.0329	0.0259	0.0194	0.0161
M I-II	4.00E-04	0.0022	0.0037	0.0107	0.0335	0.0806	0.1519	0.1815	0.2337	0.2560

Table XI (continued)

Model Indices and Other Parameters

Index	Predicted	Observed	Obs/Pred
H 3798	0.848		
H 3835	0.749	0.835 *	1.115
CAK 3933	0.876	0.838	0.957
H 4101	0.731	1.021 *	1.395
CN 4200	1.001	1.032	1.030
G 4305	0.919	0.906	0.985
IS 4430	1.002	0.982	0.980
MGI 5175	0.900	0.940	1.044
NAD 5892	0.909	0.800	0.880
TIO 6180	0.943	0.925	0.980
TIO 7100	0.935	0.958	1.024
NAI 8190	0.992		
CAII 8542	0.904		
TIO 8880	1.005		
CN 9190	0.956		
U/B	0.323	0.384	
B/V	0.318	0.309	
V/R	0.354	0.374	
V/I	0.189	0.219	
V/J	0.101	0.097	

*emission component not removed

Optical depth in dust:

τ_{5500}(internal) = 4.20

τ_{5500}(external) = 1.62

E(B-V) produced by internal extinction: 0.28

E(B-V) " " external " : 0.58

Intrinsic M/L_V: 1.08 $M/L_V(\odot)$

Predicted observed M/L_V: 5.30 $M/L_V(\odot)$

Scaling factor for model:

observed V flux corrected for extinction/model V flux

$= 4.2 \times 10^6$

Table XI (continued)

Comparison of Predicted and Observed Fluxes

λ(Å)	Intrinsic Model Flux	Predicted Observed Flux	Observed Flux	Obs/Pred
3448.	4.445E-01*	1.458E-01*	1.644E-01	1.1278
3570.	4.418E-01*	1.598E-01*	1.959E-01	1.2259
3620.	4.589E-01*	1.715E-01*	2.148E-01	1.2523
3784.	6.468E-01	2.650E-01	2.780E-01	1.0491
3798.	5.642E-01	2.328E-01	2.858E-01	1.2272
3815.	6.871E-01	2.862E-01	2.992E-01	1.0455
3835.	5.371E-01	2.261E-01	2.582E-01	1.1419
3860.	7.542E-01	3.224E-01	3.221E-01	0.9991
3910.	7.796E-01	3.452E-01	3.467E-01	1.0044
3933.	6.978E-01	3.142E-01	2.992E-01	0.9524
4015.	8.568E-01	4.095E-01	3.945E-01	0.9633
4101.	6.240E-01	3.173E-01	4.406E-01	1.3883
4200.	8.544E-01	4.635E-01	4.920E-01	1.0615
4270.	8.571E-01	4.845E-01	5.105E-01	1.0537
4305.	7.949E-01	4.587E-01	4.742E-01	1.0339
4400.	8.820E-01	5.402E-01	5.598E-01	1.0362
4430.	9.089E-01	5.680E-01	5.702E-01	1.0039
4500.	9.635E-01	6.318E-01	6.310E-01	0.9987
5050.	1.000E 00	1.000E 00	1.000E 00	1.0000
5175.	9.357E-01	1.026E 00	1.047E 00	1.0202
5300.	1.077E 00	1.292E 00	1.236E 00	0.9567
5820.	1.183E 00	1.928E 00	2.228E 00	1.1559
5892.	1.088E 00	1.834E 00	1.854E 00	1.0108
6100.	1.242E 00	2.293E 00	2.582E 00	1.1262
6180.	1.177E 00	2.246E 00	2.489E 00	1.1082
6370.	1.250E 00	2.600E 00	2.965E 00	1.1404
7050.	1.422E 00	4.066E 00	4.246E 00	1.0443
7100.	1.342E 00	3.924E 00	4.169E 00	1.0623
7400.	1.522E 00	5.022E 00	5.012E 00	0.9979
8050.	1.642E 00	6.788E 00	6.310E 00	0.9296
8190.	1.649E 00	7.119E 00	6.668E 00	0.9366
8400.	1.694E 00	7.780E 00	7.112E 00	0.9141
8543.	1.566E 00	7.497E 00	7.178E 00	0.9574
8800.	1.807E 00	9.282E 00	8.710E 00	0.9384
8880.	1.807E 00	9.478E 00	9.036E 00	0.9534
9190.	1.765E 00	1.001E 01	1.009E 01	1.0078
9950.	1.944E 00	1.310E 01	1.318E 01	1.0061
10400.	2.004E 00	1.498E 01	1.629E 01	1.0874
10800.	2.051E 00	1.678E 01	1.959E 01	1.1673

* Hydrogen continuum contributes 14% additional flux at these wavelengths

stars by a factor of two would increase the required internal optical depth by about the same factor. In the adopted model, combined internal and external extinction produces an effective E(B-V) of $.85^m$ and a total absorption at 5500 Å of 3.25^m. The effects of grain albedo are discussed in Part III G.

Gaseous emission

M82 A has a low-excitation emission line spectrum which has been discussed by Morgan and Mayall (1959), LS, BBR, van den Bergh (1969), and Bertola et. al. (1969). Photoelectric observations have been published by Peimbert and Spinrad (1970), who conclude that the gas in M82 A is radiatively ionized by hot stars and has a normal He content.

Emission line measures obtained in the course of this program are presented in Table XII. Probable errors in the flux ratios are about 10% unless noted. We have corrected the Balmer line observations for underlying absorption by assuming the absorption line strengths in A are the same as in B. Only the Hγ flux is likely to be appreciably influenced by differences between the two regions. 60" data (12" aperture) has been normalized to the 200" scans (7" aperture). Inasmuch as many of the 200"

TABLE XII

M82 NUCLEAR EMISSION LINE FLUXES

Line	Flux/Hβ	Instrument
[O II] λλ3726,3728	.40	200"
Hγ	.32	200"
Hβ	1.0	200"
[O III] λ5007	.28	200"
Hα	9.3	60"
[N II] λ6583	5.1	60"
[S II] λ6717	1.9	60"
[S II] λ6731	1.2	60"
[O II] λλ7320,7330	.28 ± .08	200"
[S III] λλ9069,9532	9.4 ± 2.0	200"
P_6 λ10938	.74 ± .5	200"

$F_{H\beta} = 5.3 \times 10^{-13}$ ergs sec^{-1} cm^{-2}

observations were taken with the lines off-center in the bandpass, our data is very susceptible to the aperture smoothing problem discussed in Part III A; however, in general, our results are similar to Peimbert and Spinrad's.

Using the effective extinction calculated from the adopted model above and assuming the gas is co-extensive with the stars and dust, we find the intrinsic Balmer decrement Hα:Hβ:Hγ to be 3.6:1.0:.45, which is in good agreement with the theoretical radiative decrement (2.87:1.0:.47 for Case B at $T_e = 10000^o$ from Pengelly 1964) considering the uncertainties involved.

Using this decrement to correct the observed Hδ and H9 absorption line measures for emission, we find the corrected indices to be $I_{4101} = .70$ and $I_{3835} = .73$. The excellent agreement with the predicted values in Table XI must be considered fortuitous.

(Weak [O II] λ3727--2×10^{-14} ergs/sec-cm^2--is detectible in M82 B. If the intrinsic Hδ/[O II] λ3727 ratio is the same in M82 B as in M82 A, the observed flux at Hδ in M82 B must be reduced by only 2% to correct for emission. It is doubtful that emission line ratios in B are similar to those in A since [N II] λ6583, which should be detectible in that

case, does not appear to be present. Observations of Hα place an upper limit of about 3000 cm^{-6} psc on the emission measure in M82 B.)

The observed flux in the hydrogen continuum (bound-free, free-free, and two photon) is given by

$$F_\nu(\lambda) = 4.32 \times 10^{24} \frac{T_4^{3/2}}{b_4} \gamma_\nu e^{-.988/T_4} E_{H\beta} C(\lambda) \text{ ergs sec}^{-1}\text{cm}^{-2}\text{Hz}^{-1}$$

in the notation of Seaton (1960), where $T_4 = T_e/10^{4\circ}K$, $E_{H\beta}$ is the observed Hβ flux (ergs/sec-cm^2), and $C(\lambda)$ is the total extinction at λ relative to the total extinction at Hβ. We have assumed $T_4 = 1.0$ and taken b_4 for Case B from Pengelly (1964). Using the value for $E_{H\beta}$ from Table XII and the effective extinction found from the adopted population model, we find that hydrogen continuous radiation contributes about 12% of the total observed flux for $\lambda < 3646$ Å and is unimportant at longer wavelengths. In particular, the Paschen recombination continuum contributes only about 2% to the observed flux at 8000 Å.

Although our effective interstellar extinction function is different from Peimbert and Spinrad's, it will not alter their conclusions appreciably. We might note that the upper

limit to the electron density in M82 A set by the [SII] doublet ratio is about 10^3 cm^{-3}.

Alternative sources for the infra-red excess; nonstellar radiation

We now consider the possibility that the infra-red excess of Figure 5 originates in a source of radiation not present in M82 B and is not a product of internal dust absorption in M82 A. If we assume that the stellar content of A is identical to B's and take interstellar extinction case A, then we can easily calculate the characteristics of the additional source of radiation required to fit the observed M82 A spectrum. For the range of optical depth in the overlying dust cloud which will best fit M82 A between 4000 and 5500 Å, we find that the color temperature (between 5000 and 11000 Å) of the added source must be between 2200 and 2800° K. The equivalent spectral index, α, ($F_\nu \propto \nu^\alpha$) is $-4 \lesssim \alpha \lesssim -2$. We may then make the following remarks:

i) Although cool stars (e.g. M4-6 III) have almost the requisite continuous energy distributions, adding enough of them to fit the spectrum will yield TiO features much stronger than observed.

ii) Thermal re-radiation from interstellar grains, such as proposed to account for the far infra-red anomaly in Seyfert nuclei (Low and Kleinmann 1968, Pacholczyk and Weymann 1968) cannot generate the near infra-red excess in M82 inasmuch as such grains are presumed to evaporate at temperatures higher than 2000°K.

iii) A non-thermal source (Low 1970) for the far infra-red excess of M82, Seyfert nuclei and quasi-stellar sources is not, of course, subject to this objection. Between 3.4μ and 22μ the far infra-red anomaly of M82 is similar to that of NGC 1068 (Kleinmann and Low 1970). The flattening of M82 A's spectrum between 1.25μ and 3.4μ suggests that starlight begins to dominate the source of the infra-red anomaly at about 3μ; the stellar contribution is, however, strongly dependent on the measuring aperture. To estimate the possible non-thermal contribution to the 6000-11000 Å region of M82 A, we assume the spectral similarity between the far infra-red sources in NGC 1068 and M82 extends to 2.2μ. Extrapolating to shorter wavelengths with allowance for the significant curvature present in the spectrum from 2.2-22μ but neglecting interstellar extinction, we estimate that the far infra-red source in M82 A can produce at most 5% of light at 11000 Å. Hence, it cannot contribute significantly to the 6000-11000 Å excess in M82 A.

iv) Synchrotron radiation from the electron reservoir responsible for 3C 231 probably does not make a measurable contribution to the optical light of M82 A. The contribution at 5050 Å predicted by extrapolation of the radio spectrum from 3000 MHz with $\alpha = -0.6$ is less than .5% without correction for reddening or allowance for the curvature evident between 3000 and 5000 MHz.

Although the 3% polarization of M82 A between 3300 and 6000 Å (Elvius 1963) is suggestive of a small synchrotron contribution, polarization of about 2% has also been found in the strong dust lanes of NGC 5195 by Elvius and Hall (1964). The polarization of M82 B is only .3%.

Sandage and Visvanathan (1969) have suggested that a second, more energetic synchrotron component generates the polarized continuum from the filaments. However, the spectral index for this component ($\alpha \approx -0.2$) is much larger than the maximum allowable index, $\alpha = -2$, capable of producing the near infra-red excess of M82 A.

v) Lynden-Bell (1969) has suggested that the optical spectrum of active galactic nuclei may include composite black body radiation from a dense disk with a large temperature range. As given by Lynden-Bell, the predicted intrinsic spectrum of the disk is too flat to produce the near infra-red excess of M82 A. However, the observed spectrum would be largely determined by the distribution of dust grains (not included in the calculation) in and around the disk and by the aspect from which it is viewed. Lynden-Bell's source could also generate the ultraviolet excess in M82 A since any source of high-temperature continuous radiation is indistinguishable from the O V stars in the adopted model. In order to produce both the near infra-red and ultraviolet excesses of M82 A, a continuous source would require a local flux minimum between 4000 and 6000 Å. Further development of Lynden-Bell's model may well indicate that such a spectrum could be produced. However, since it is not necessary to appeal to unusual mechanisms to explain the spectrum of M82 A, this possibility would not constitute unambiguous evidence for the existence of Lynden-Bell's disks or of any other source of nonstellar radiation in M82.

G Discussion of the Synthesis

Goodness of fit

The adopted models for A and B fit all indices except I_{4200} and I_{5892} to the accuracy specified in Part III D above. Examination of the data in Table B III shows that only a very peculiar population model would yield $I_{4200} > 1.02$. It is possible that the large CN 4200 indices observed for A and B are the result of a small instrumental calibration error. The I_{5892} anomaly is discussed below. Note that the predicted Na I 8190, TiO 8880 and CN 9190 strengths are within the upper limits set by the observations. Observed I_{8542} for M82 B, undoubtedly severely affected by the noise problems described in Appendix A, cannot be synthesized by reasonable population models.

As expected, the fit to the continuum for both models is less successful than that to the indices. In particular, both models are approximately 5% fainter between 5820 and 7100 Å than desirable. It does not appear possible to synthesize the observed flux excess with starlight. Again, this may reflect a small instrumental error. (This is the

spectral region affected by nonlinearity in the S-20 photomultipliers, as described in Appendix A.) On the other hand, a minor change in the assumed extinction efficiency function for M82's interstellar grains could reduce the discrepancy.

Both models show systematic deviations from the observations longward of 7400 Å. The adopted model for B is too bright in this region because of the M stars needed to synthesize the TiO indices. We have allowed the minimum possible M star contribution in the model. Again, the fit in this interval for both A and B could be substantially improved by small modifications in the reddening law.

Table XI indicates that a component not considered in the model may begin to contribute to M82 A between 10000 and 11000 Å. Either M6 III's or the high frequency tail of the far infra-red source described above are likely possibilities for the neglected component.

The D line anomaly

The strength of the sodium D lines in both models is much weaker than observed. Since the discrepancy exists in

both regions of M82, it is not related to the apparent metal enrichment found by Spinrad (1966) and McClure (1969) in galaxy nuclei. In any case, the substitution of SMR stars in the model does not appreciably affect I_{5892}. The D lines may be strengthened relative to the blue indices only by increasing the number of K7-M6 V stars, which in turn increases M/L. It does not appear possible to make $I_{5892} < .88$ for $M/L_V < 10$.

It is entirely possible that the additional Na I absorption (approximately a maximum of 3 Å equivalent width) occurs in the interstellar medium of M82. From Table I, we find a mean H I density $n_{H\ I} = .5\ cm^{-3}$ for M82. For galactic H I region excitation conditions, under which Spitzer (1969) has shown that $n(Na\ I) = 3.8 \times 10^{-8}\ n_H^{1.5}\ cm^{-3}$, we estimate from the curve of growth for a uniform medium with a velocity dispersion of 25 km/sec that a 2.7 Å (D1 + D2) feature will be produced over a 3 kpc pathlength if $n_{H\ I} = .5\ cm^{-3}$. Hence, if interstellar conditions (i.e. abundances, ionizing radiation fields and energetic particle densities) similar to those in our galaxy prevail in M82, an interstellar Na I component of

the strength observed is expected. In view of the smaller relative number of hot stars in M82, it is not clear that this is the case. However, the larger stellar densities near regions A and B (see below) and a possibly higher cosmic ray density produced by the nuclear disturbance may partially or wholly compensate for the lack of hot stars.

Uniqueness

Although the adopted population models for M82 A and B both fit the observations as well as can be expected, the actual stellar population of M82 may differ significantly from the models for two reasons apart from the obvious possibility of observational error: (a) the relative proportions of the components in the adopted models may be varied by significant amounts subject to condition (1) without substantially affecting the fit to the observations; and (b) the actual population may include important stellar types omitted from consideration in the synthesis. We must evaluate the importance of both of these ambiguities.

Regarding alternative solutions employing the same components, we have indicated above that our observations are sensitive primarily to the upper main sequence (spectral

types earlier than G0) and (through TiO) M stars. As a result, we estimate that the population ratio of any two spectral type groups on the upper main sequence is probably determined within a factor of 2. The percentage of M star light in the 6000-7000 Å region is similarly well determined, but the ratio of populations in the three M type luminosity ranges considered (V, III and I) is indeterminate from spectral data alone. Uncertainty is much larger for the remaining types. Considering the upper main sequence fixed, one can vary the proportion of all lower main sequence and/or type III stars (except M stars) by factors of 2-3 without violating the fitting conditions. The subsequent uncertainty in E(B-V) for M82 B and the overlying dust cloud in M82 A is about $\pm.15^{m}$. As noted above, the optical depth at a given wavelength internal to M82 is highly sensitive to the total M star contribution and is probably uncertain by a factor of two. An accurate observation of CN 9190 would set a firm upper limit to the contribution of M I stars.

The omission from the synthesis of M6+ and A-K I stars for lack of adequate data is clearly not serious.

Possible contributions from M5 or later dwarfs are negligible in the framework of the adopted models (note the percentage contributions from M3-4 V's). In any case, the upper limit to the M6+ V contribution at 5050 Å set by observed M/L_V is .5%. There is no evidence that M6-8 III's make any significant contribution ot M82 B below 11000 Å; however, as noted above, they may influence M82 A's spectrum between 10000 and 11000 Å. In the solar neighborhood, such stars are only 1% as populous as M0-2 III's (Blanco 1965). The M6-8 III contribution could be easily established by observation of TiO 8880.

Based on the galactic supergiant compilation of Stothers (1969), A-K I's will contribute only about 1% of the light at any wavelength in the adopted M82 A model. In addition, Wooley (1963) finds that such stars are very rare in the Large Magellanic Cloud.

We have neglected metal-poor stars in the synthesis, and it is important to estimate their population in M82. The successful fit to the indices in terms of stars of normal metal content indicates that objects with metal abundances below 20% of solar values do not make large contributions to the light of M82. For example, it would

have been impossible to synthesize both the Balmer jump and Balmer line indices and the K line with B-F stars as deficient in calcium as HD 161817 (cf. Figure B4). Similarly, the strength of the TiO indices, which should be sensitive to metal content, suggests that cool stars in M82 have normal metal abundances.

On the other hand, there is no evidence that M82 contains fewer metal-poor stars than the solar neighborhood. The actual composite spectrum of the solar vicinity would probably be little influenced by Pop II stars even though they constitute 60% of the surface density of 1 $M_{\odot}$ stars near the sun (Dixon 1965, 1966). We estimate that such stars would add only about 5% to the light from 3300-5000 Å of the solar vicinity composite model of Table VIII. Furthermore, the majority of these stars have metal contents between 10% and 60% of the solar content (Dixon 1966). From Figures B2-B16, we find that stars with such abundances (e.g. μ Cas, which has a mean metal content about 25% of the solar value according to Cohen 1969) are likely to have little influence on feature strengths in a composite spectrum. Hence, since hot stars are relatively more

important in M82 than in the solar neighborhood, the spectral effects of a metal-poor population similar to that in the galaxy near the sun would probably not be detectible. We therefore suggest that the metal-deficient population of M82 is not unlike that of the solar neighborhood.

The giant-to-dwarf ratio

Because it has important evolutionary implications, we should comment on the giant-to-dwarf ratio calculated in the adopted models. In these models, the ratio of numbers of G-M III stars to their main sequence progenitors (A0-F5 V stars) is .04. The corresponding ratio in the solar neighborhood is .17 (McCuskey 1965). We do not expect our giant-to-dwarf ratio to be more uncertain than a factor of 3. Hence, M82 is apparently somewhat deficient in giants relative to the solar neighborhood. However, this is a marginal result which is subject to further observational confirmation--particularly through more careful observations of CN 4200, Ca II 8542 and CN 9190. If corroborated, the deficiency implies that if stars in M82 evolve as they do in the solar neighborhood, then star formation has proceeded at a higher rate in M82 over the

past 5×10^8 years relative to earlier times than in the solar neighborhood.

We wish to emphasize that there is no evidence in either the spectrum or mass-to-light ratio of M82 for the presence of stars older than 10^9 years. The only stellar groups considered whose age is unambiguously larger than 10^9 years are the class IV stars; their presence in the models is purely schematic, and there is no direct evidence for their existence in M82.

Properties of region B and the disk of M82

Properties for region B calculated from our adopted model are presented in Table XIII. UBV colors are calculated from our U/B and B/V continuum indices by means of the absolute calibration of the UBV system given by Johnson (1966a). The uncertainty in the transformations is probably about $\pm .05^m$ in each color. In the two-color diagram, M82 B falls close to the dwarf star relation at (B-V) = +0.4 as a result of its large Balmer discontinuity. It lies about 0.4^m in (U-B) below the locus for late-type spiral and irregular galaxies given by de Vaucouleurs (1961b). No other object observed by de Vaucouleurs in his survey of bright galaxies has similar colors.

TABLE XIII

INTRINSIC PROPERTIES OF M82 B

Volume observed: 3.0×10^{6} psc^{3}

Intrinsic luminosity: $L_V = 1.3 \times 10^{8} L_V(\odot)$
$= 5.5 \times 10^{40}$ erg sec^{-1}

Intrinsic UBV colors:
(U-B) = +0.08
(B-V) = +0.44

Intrinsic surface brightness: σ_V = 16.0 V/□"

Volume emissivity: 43 $L_V(\odot)$/psc^{3}

Stellar mass: 1.4×10^{8} $M_\odot$

Stellar mass density: 46 $M_\odot$/psc^{3}

Stellar mass surface density: 1.5×10^{4} $M_\odot$/psc^{2}

The intrinsic surface brightness and corresponding mass density (calculated from M/L_V) of region B are quite high. (The masses quoted here and in the next section are lower limits because we have not allowed for non-luminous matter.) The B-magnitude surface brightness of M82 B is approximately equal to the apparent surface brightness of the nucleus of M31 when observed through a 4.86" aperture (Sandage et al. 1969). The mass density of region B is 300 times the density found in the solar neighborhood (Oort 1965) and 40 times the mean density for $r < 3$ kpc in M82 computed from Table I. To estimate the volume producing the emission in M82 B, we have assumed the line-of-sight depth is equal to the lateral extent (330 pscs) of the bright region including B. This region has a surface brightness 3-4 times higher than surrounding areas, and it is therefore improbable that we have underestimated the volume contributing to our observations by more than a factor of 2-3 except in the unlikely instance that the region is the cap of an elongated cylinder fortuitously viewed end-on. Such a situation could arise if dust were anomalously depleted in the direction of B compared to surrounding areas; but the similarity of energy distributions

(see Part I) for all regions on the NE half of M82 except the dust lanes suggests that differential reddening does not cause the relative brightness of region B. Therefore, it appears that region B has a mass density considerably in excess of that typically encountered in late-type galaxies. The given density is equal to the relatively high central density of the Sb galaxy NGC 5055 (Burbidge, Burbidge and Prendergast, 1960).

Interference filter photometry described in Part I shows that the energy distribution of M82 B is similar to those of the other disk regions of M82 for $r < 3$ kpc. Therefore, although we expect some differences in detail because the spectral type of the other disk regions is somewhat later than M82 B's, the model of Table X is probably representative of the average stellar population in the disk of M82.

The adopted population model for M82 B differs from the solar neighborhood in only two ways: there are relatively fewer stars brighter than $M_V = -3$ in M82 B, and its giant-to-dwarf ratio is probably smaller. The implications of the latter departure have been discussed above. Although the relative depression of the upper main sequence in

M82 B is not large, it has important consequences for the population of stars brighter than $M_V = -5$ because the solar neighborhood itself is deficient in such stars relative to "Population I" regions of the Magellanic Clouds (McCuskey 1965).

The absence of massive stars in the disk of M82 is therefore suggested by three independent pieces of evidence: (a) the results of the synthesis; (b) the absence of resolved stars; and (c) the contrast between the amount of H I and the low level of general interstellar excitation inferred from direct spectra and the photoelectric upper limit on the emission measure in M82 B.

In the next section we show that the initial luminosity function for stars brighter than $M_V = 0.0$ in M82 A may resemble that in the galaxy. Furthermore, the form of the main sequence luminosity function in M82 B is essentially identical to the solar neighborhood function for $-1 \lesssim M_V \lesssim +4$. It is therefore reasonable to assume that the form of the initial luminosity function everywhere in M82 is similar to that of the galaxy and that the absence of massive stars in the disk of M82 is a manifestation of the time dependence (and not mass dependence) of star

formation. This then implies that star formation in the disk of M82 has been suppressed during the last 10^7 years even though the density of interstellar gas in M82 is probably similar to that of the solar neighborhood. It is tempting to link this suppression to the violent activity in M82's nucleus. Although motions in the filaments indicate that they were ejected only a few million years ago (LS, BBR), previous disturbances may well have occurred inasmuch as the phase of similar activity in Seyfert nuclei lasts at least 10^8 years (Burbidge and Hoyle 1968). We will not speculate extensively on possible mechanisms coupling nuclear activity to star formation in the disk. However, one obvious way in which a strong disturbance propagating through an interstellar medium can inhibit star formation is through the disruption of proto-cluster cloud complexes, in which at least all early main sequence stars originate according to Ebert, von Hoerner and Temesvary (1960).

Properties of region A

In calculating interstellar extinction internal to region A, we have neglected light scattering by grains,

which is likely to be significant because grain albedos are probably greater than .5 at 5000 Å (Wickramasinghe 1967). Numerical calculations of radiative transfer including scattering in spherical nebulae have been performed by Mathis (1970). Apart from the probably unimportant difference in geometry, our case B corresponds to Mathis' case 1, and we may use his results to estimate the influence of scattering in our model for any given albedo and optical depth. For the range of total optical depth (1.5 to 6.8) encountered between 3400 and 11000 Å in the adopted model for M82 A, Mathis' calculations show that if the grains have a wavelength-independent albedo of .5, then scattering will increase the observed flux at any wavelength by about 40%. However, the shape of the apparent extinction curve is almost unchanged, fluxes relative to 5000 Å being identical below 5000 Å and increasing a maximum of 10% longward of 8000 Å. Mathis' results show that for any albedo up to .7, distortions in the extinction curve may be kept to a few percent if all optical depths in the observed wavelength interval are greater than a certain minimum; for an albedo of .5, this minimum depth is 4.0 on a diameter across the nebula. Distortions of shape

naturally increase with the albedo of the grains and with the wavelength dependence of the albedo.

We have already indicated that the total optical depth in dust internal to A in the adopted model is uncertain by a factor of about 2. Hence, it is evident that allowance for scattering will not substantially affect our ability to fit the observations of A with a model similar to the adopted one as long as grain albedos are not strongly wavelength dependent or much larger than 0.6.

Allowing for a 50% increase in flux due to scattering, we find that probable values for the total extinction at 5500 Å suffered by light from region A range from 2.5^m to 4^m. We have used a value of 2.9^m, corresponding to the adopted model, to compute the various intrinsic properties for region A tabulated in Table XIV. The corresponding extinction at H_β is 3.2^m; hence, all intrinsic emission line fluxes given by Peimbert and Spinrad (1970) should be reduced a factor of 2.5 to conform to our results.

The surface brightness, mass density and volume emissivity of M82 A given in Table XIV are clearly in accord with those of galactic nuclei, as we suggested in Part I. Even without including the effects of extinction internal

TABLE XIV

INTRINSIC PROPERTIES OF M82 A

Volume observed: 2.3×10^5 psc^3

Intrinsic luminosity: $L_V = 6.6 \times 10^8 L_V(\odot)$
$= 3.0 \times 10^{41}$ erg sec^{-1}

UBV colors (including hydrogen continuum):

	intrinsic	including internal extinction
(U-B)	-0.44	-0.29
(B-V)	+0.45	+0.74

Surface brightness:

intrinsic $\sigma_V = 14.1$ V/□"

$\sigma_V = 15.6$ V/□" including internal extinction

Volume emissivity: $2.9 \times 10^3 L_V(\odot)$/psc^3

Stellar mass: $7.2 \times 10^8 M_\odot$

Stellar mass density: $3.1 \times 10^3 M_\odot$/psc^3

Mass of dust producing internal extinction: $10^3 M_\odot$

to M82 A, the luminosity in the V band is two orders of magnitude smaller than the luminosity of the postulated Seyfert nucleus in Solinger's (1969) model for the continuum of the filaments. In order that M82 A produce the filamentary continuum at a radius of 2 kpc by electron scattering, the electron density in the filaments would have to be 10^3 cm^{-3} and furthermore the optical path from M82 A to the filaments would have to be relatively free of dust. In addition, the position of the filaments in the two color diagram (Sandage and Visvanathan 1969) is such that they cannot be reached by reddening from that of M82 A when internal extinction in the nucleus is taken into consideration. Hence, our model suggests that the filamentary continuum does not originate by Thompson scattering from the light of M82 A, unless its properties have changed drastically during the light travel time (a few thousand years) between itself and the filaments. Luminous, high surface brightness regions like those including B are perhaps more likely candidates for sources of scattered radiation. However, similar remarks regarding the UBV colors apply here.

The intrinsic colors of M82 A resemble those for emission line objects like the Haro galaxies (Haro 1956, Hiltner and Iriarte 1958).

It is evident that a modest amount of dust distributed throughout M82 A will produce the reddening required of our model. We note that if the dust-to-gas ratio in M82 A is comparable to that in the galaxy (10^{-2}), then Peimbert and Spinrad's (1970) determination of the amount of ionized material in the nuclear region (appropriately corrected for our adopted extinction) indicates that 20 times this amount would be present. The existence of dust in the nucleus of M82 is clearly not unprecedented in view of its apparent presence in Seyfert nuclei (Wampler 1968) and its association with violent activity in radio galaxies (Burbidge, Burbidge and Sandage 1963). Hoyle and Wickramasinghe (1968) have suggested that dust condenses during nuclear outbursts; if this occurred in M82, then our results indicate that dust produced in this manner is closely similar to the "common" dust of the solar neighborhood.

Our adopted model for the stellar population of M82 A demands that, in contrast to the disk of M82, star formation

in the nucleus has continued during the last few million years in spite of the probably severe disturbances associated with the ejection of the filaments. (The Lasker photometry of Part I also suggests the presence of O stars in region C adjacent to A.) Perhaps this is a consequence of the higher stellar and gas densities in region A. The adopted luminosity function for stars brighter than $M_V = 0$ in M82 A is parallel to the initial luminosity function of Limber (1960) when weighted by main sequence lifetimes. Hence, as mentioned above, it is possible that the initial luminosity function in M82 resembles that in the solar neighborhood.

Peimbert and Spinrad (1970) concluded that the gas in M82 A is radiatively ionized. The Balmer decrement (discussed above) agrees with this interpretation. Furthermore, using Mihalas' (1965) model atmospheres, we estimate that the amount of radiation emitted below 912 Å by stars hotter than B0 in our model is ten times the amount required by Peimbert and Spinrad to maintain ionization in the nuclear region. There is great uncertainty in all quantities involved here, and the influence of dust on the ultraviolet radiation field is probably large. However, we

can almost certainly conclude that gaseous emission from M82's nucleus is sustained by hot stars.

H Summary

Our major conclusions regarding the nature of M82 are summarized below:

a) The absorption line spectrum of M82 (with the exception of the sodium D lines) can be satisfactorily interpreted in terms of common galactic stars of normal metal content. There is no evidence for any kind of abundance anomaly. No nonstellar source of radiation other than continuous emission from hydrogen is required to interpret the spectrum.

b) The main sequence luminosity function for $M_V < +4$ in both nuclear and disk regions of M82 closely resembles that of the galactic disk in the solar vicinity except that there is a defieiency of stars brighter than $M_V = -3$ in the disk and an excess in the nucleus.

c) The extinctive properties of dust grains in M82 are very similar to those of grains in our galaxy (as represented by the Whitford law). Extinction in region B takes

place in an overlying dust cloud, while additional extinction occurs internally in region A.

d) A significant fraction of the total sodium D line absorption in regions A and B occurs in the interstellar medium of M82.

e) M82 A has intrinsic properties comparable to those of galactic nuclei and is probably the origin of the violent outburst which ejected the filaments. It is doubtful that scattered light from M82 A produces the polarized continuum in the filaments. Ionization of gas in region A is maintained by ultraviolet radiation from hot stars.

f) M82 B has a surface brightness and mass density much higher than found in the disks of typical late-type galaxies. Therefore, apart from the prevalence of dust and lack of massive stars, both of which may be related to nuclear activity, M82 cannot properly be regarded as a normal late-type system.

Somewhat weaker conclusions and inferences are the following:

g) The initial luminosity function in M82 is probably similar to that in the solar neighborhood. The lack of

massive stars in the disk is therefore interpreted as due to a suppression of star formation during the last 10^7 years.

h) The giant-to-dwarf ratio in M82 is smaller than in the solar neighborhood. Taken together with (g), this implies that a local maximum (relative to rates in the solar vicinity) of star formation occurred between 10^7 and 5×10^8 years ago in the disk of M82.

APPENDIX A

OBSERVATIONS AND REDUCTIONS

I Introduction

The stellar survey for this program was carried out with the Cassegrain scanner at the Mt. Wilson 60" telescope. Observations of M82 were made both with this instrument and with the 200" multi-channel spectrometer. Additional galaxy observations were made with interference filters. The absolute calibration for all photometry is that of Oke (1964) with $.06^m$ added to all points below 3700 Å.

II Scanner Bandpass Selection

The bandpass sequence selected for the spectrophotometry emphasizes spectral features useful for typical early-type composite spectra and not necessarily M82 alone. It is tabulated in Table IV.

Bandpasses were selected according to the following criteria:

1) The features observed must be strong--at least 2 Å equivalent width at maximum strength--and as sensitive to stellar temperature or luminosity as possible. They must be common in the spectra of EST galaxies.

2) The features should be isolated from other strong

features in their neighborhood and free from the emission lines commonly found in EST galaxies. Bandpasses selected to measure the continuum in a given spectral region must contain as little blanketing as possible in those stars where the neighboring spectral features are strongest. Further, it is desirable that they be as close as possible to the features for which they serve as reference. Convenient references for the choice of continuum bandpasses include Minnaert (1940), Griffin (1968), Oke and Conti (1966), and Wildey et. al. (1962).

The blue spectral regions of EST galaxies are dominated by hydrogen lines and the H and K lines of Ca II. It was thought desirable to observe at least two Balmer lines, one of which is as blue as possible to minimize the influence of emission. Study of various plates taken at Mt. Wilson-Palomar and photographs reproduced by Mayall (1958, 1960) indicates that the bluest Balmer lines which are strong in EST galaxies and which are not severely blended are H9 and H10. The reddest line which is likely to be free of emission is Hδ. All three of these lines were included in the program. The λ3815 sideband for H9 and H10 includes He I λ3819, which reaches about 1.5 Å equivalent width in early B stars (Tinsley 1967). The λ3860 sideband is susceptible to contamination from [Ne III] λ3869 but was included as the nearest bandpass redward of H9 relatively clear of depression by Balmer line wings.

Of the Ca II lines, only K is appropriate for observation because H is blended with Hϵ. Several useful spectral features in the blue for stars later than KO such as CN λ3883, Ca I λ4227 and MgH λ4800 (Spinrad, 1966; Morgan, 1960) were not expected to attain reasonable strengths in competition with early-type starlight and were excluded. However, the G band, occurring in stars of earlier type, was included. CN λ4200 was also included as it is a unique indicator of K giant light, which is very important in k-nuclei.

Since reddening was expected to be appreciable in some EST galaxies, an interstellar absorption feature was experimentally included. The λ4430 feature is the strongest interstellar feature not also present in stellar spectra; it is correlated with color excess (Stoeckly and Dressler, 1964).

Spectra beyond 5000 Å are not readily available for EST galaxies. However, because of their high degree of compositeness, EST galaxy spectra are expected to contain the same features as k-nuclei spectra in the yellow and red. Hence the wavelength sequence in this region was patterned after those of Wood (1966) and Spinrad (1966). The λ7050 continuum bandpass was placed so as to avoid terrestrial water vapor near 7000 Å and contains the TiO bandhead at λ7054. However, the effect of TiO absorption on λ7050 is small enough that it is still useful as a sideband for the λ7100 bandpass.

The features observed between 8000 and 9200 Å are primarily luminosity discriminants for M stars and are important to the detection of possible M supergiant light. Again, the wavelength sequence is patterned after Spinrad (1966); however, Ca II λ8542, the strongest member of the Ca II triplet, was given preference over Ca II λ8662. Continuum points with minimal blanketing in M stars were selected from Sharpless (1956), Wing (1966) and Wing et. al. (1967). Their strong contribution in the blue notwithstanding, O-F stars are not expected to make an appreciable contribution to near infra-red light, so no Paschen lines are explicitly observed. The bandpasses between 8190 and 9950 Å are, however, influenced by Paschen line absorption.

The bandwidths selected are compromises between the opposing demands of resolution and signal-to-noise ratio. Bandwidths smaller than about 10 Å are also to be avoided as being too susceptible to seeing and to guiding inaccuracies. For similar reasons, the central wavelengths of bandpasses measuring molecular features are usually placed such that the bandhead is not included.

A more complete discussion of background line blanketing and the temperature and luminosity dependence of each feature may be found in Part II.

III General Scanner Technique

The major portion of program data was obtained with the Cassegrain scanner at the Mt. Wilson 60" telescope operated in conjunction with a pulse-counting data system. The equipment and standard observing and calibrating procedures have been described in detail by Oke (1965), C. Anderson (1968) and K. Anderson (1968). In general, these procedures have been adopted in the present program and need no further discussion. However, several aspects of observing technique and reduction pertinent to the particular nature of this program require comment.

1) The major calibration problem encountered with the scanner is the determination of the instrumental response function. (This function, measured in magnitudes is denoted OB-AB.) In spectral regions where there are strong absorption features in the standard stars (e.g. λλ3650-4000 and λλ8400-9000) it is necessary to interpolate OB-AB both because direct observation yields results which depend on the bandwidth and because the calibration of the standards is itself uncertain. Particular difficulty was encountered in the λλ8800-8900 region in which neither directly-observed nor interpolated values of OB-AB yielded the smooth continua expected for stars of middle type (F5-K0). The effects were in opposite senses, directly-observed OB-AB placing the points at λλ8800 and 8880 $.07^m$ below the continuum

interpolated from either side, and interpolated OB-AB, $.06^m$ above. The anomaly, which is apparently a characteristic of the scanner itself, was present in all 60" data and appeared to be sufficiently stable that it could be removed by merely adding $.06^m$ to the λλ8800 and 8880 observations derived from interpolated OB-AB. This correction has been made to all group mean data presented in Table B II. Although the AB magnitudes derived in this manner for λλ8800 and 8880 must be regarded as of slightly lower quality than those at neighboring points, the intercomparison of spectra all treated in this way is not, of course, affected. A similar problem does not seem to exist in the other region (λλ3650-4000) affected by hydrogen lines in the standards, although it is more difficult to evaluate here due to the heavy line blanketing present in almost all kinds of stars.

2) The presence of large amounts of dust and smog in the atmosphere over Mt. Wilson often causes temporal changes in the extinction. Fluctuations of up to $.1^m$ in 30 minutes are not uncommon. Nevertheless, the extinction changes are usually almost wavelength independent. When an actual extinction coefficient can be calculated, it typically varies less than $.03^m$ from 3500 to 5000 Å. Fluctuations such as these naturally increase the uncertainty in OB-AB over photon-statistical uncertainty. Mean values during the course of this program for the standard deviation in OB-AB at a given wavelength and in its color (relative to

a fixed wavelength) are $.035^m$ and $.020^m$ respectively. Since colors are not substantially influenced by this "grey" term, no attempt was made to remove it from stellar observations. Its effect was additionally minimized by observing stars rapidly and within one hour of the meridian wherever possible.

Water vapor absorption, which is present in several of the infra-red bands ($\lambda\lambda$7050, 8190, and 9190), is not included in the standard extinction law and must be determined nightly. Because the water vapor bands are highly structured, it is important that the standards be observed with the same bandwidth as the unknowns and at exactly the same central wavelength. In practice, it was found that only λ8190 suffered significant water vapor absorption, extinction at this wavelength being consistently about $.1^m$ higher than at surrounding points. Due to saturation of the water vapor bands, the amount of this extra absorption was normally found to be independent of zenith distance and could therefore be treated simply as part of the instrumental response function. The dispersion in OB-AB for λ8190 was normally no larger than for any other point in its neighborhood.

3) Accurate measurement of absorption features requires that bandwidths and bandpass centering be made as uniform as possible for all objects. Therefore, special care was taken in setting the exit slit and in calibrating the wavelength readout scale. If one takes backlash in the grating drive mechanism into account during calibration, the final

accuracy of the wavelength scale can be made somewhat better than 1 Å in the second order (2 Å in the first order).

Since the scanner is operated as a slitless spectrograph, the central wavelength of a bandpass and the bandwidth are influenced by the position and size of the stellar image. Hence, guiding was made as accurate as possible, and observations were not taken when the seeing image was larger than 5". (One second of arc at the 60" Cassegrain is equivalent to 1.2 Å in the second order at the scanner exit plane.) In general, the actual wavelength or effective bandwidth for a given observation may be assumed to lie within 1-2 Å (second order) of the quoted values.

The influence of essentially random guiding errors or sudden seeing fluctuations on the averaged group data discussed in Part II B is naturally rather small; but it should be noted that such errors, when important, almost always act to reduce the strength of the feature being measured.

IV Stellar Observations

A complete stellar observation was made in two or three scan segments. Below 5050 Å, 1P21's, S-20's or S-17's were used in the second order. S-17 and S-20 use was restricted to points longward of λλ3800 and 4200, respectively, due to first order contamination which could not be filtered out successfully. Above 5050 Å, S-20's (to 8400 Å only) and S-1's were employed in the first order. Each scan segment

was overlapped for several bandpasses with its neighbor at their common boundary.

Integration times were normally adjusted to provide at least 2000 net counts at each wavelength per scan. However, the minimum acceptible count level was reduced in the extreme ultra-violet and infra-red regions. Sky and dark current were subtracted from the total count when they reached about 1% of the signal.

Unfortunately, time did not allow more than a single complete observation of most stars, and reobservations were usually made only when a pecularity was detected in the reduction. Complete scans are available for only 70% of the stars listed in Table B I. For a given stellar type preference was always given to obtaining those scan segments of greatest importance to a composite spectrum--i.e., the blue segments ($\leq$5050 Å) for hot stars, and the red for cool stars. For K stars, special emphasis was given to the interval $\lambda\lambda$5050-7400, where feature strengths show large cosmic dispersion. M dwarfs were not observed below 3900 Å due to the prohibitively long integration times required. A number of stars were observed at points above 5050 Å with both 30 Å and 40 Å resolution, as discussed in Part III A.

The two or three segments of the complete scan were shifted in magnitude such that the mean residual in the overlapping spectral regions (apart from λ5175) vanished. Owing to grey extinction changes, the shifts required were as large as $.15^{m}$.

The average accuracy of the stellar data is on the order of 3% and may be estimated from the following considerations:

a) A fundamental limitation to the quality of the data on a given night is set by the accuracy with which OB-AB is known. As indicated above, the average standard deviation in the color of OB-AB is about $.02^m$.

b) The standard deviation of the two measures taken at a given wavelength during any scan indicates the influence of photon statistics, seeing or guiding fluctuations, errors in setting the grating tilt, and short term extinction changes. This quantity averages about $.01^m$.

c) The standard deviation in color between adjacent scan segments at the wavelengths overlapped combines the influences of (a) and (b). Its average value is $.02^m$.

d) For those objects where more than one scan under good conditions is available, the agreement is generally better than $.03^m$.

e) As discussed in Part II, agreement of feature strength measures among stars of similar types for which cosmic abundance variations are not suspected is usually better than 3%. Furthermore, where a correlation can be determined between feature strengths measured here and similar measurements by another observer, the average deviation from the mean relationship is about 3%.

These remarks apply generally to most regions of the spectrum except the extreme ultra-violet and infra-red and

to those stars whose AB at a given wavelength is smaller than 5.5^m in the red and 7.0^m in the blue. 5% can be considered the minimum average quality for the stellar data. Again, due to calibration uncertainties, $\lambda\lambda$8800 and 8880 must be regarded as of slightly lower quality than other points in their vicinity.

V Galaxy Spectrophotometry

60" Observations

Observations of M82 taken with the 60" Cassegrain scanner differed from stellar observations in several respects.

All wavelengths were corrected for the galaxy's redshift. Corrections were determined separately for regions A and B from the absorption line rotation curve given by Burbidge, Burbidge, and Rubin (1963).

Measurements of the sky plus dark current had to be taken at every wavelength. A preselected region of the sky free from possible contamination from the filaments about 5' north of the galaxy was used as reference. Since no chopper was available, the telescope was offset to this region for each measurement. The absence of a chopper also limited the maximum meaningful integration time to 100^s because non-random fluctuations in both the sky brightness and the dark current occurred in times of this order. Non-random dark current fluctuations were particularly

troublesome for the 1P21, where they were, next to grey extinction changes, the major source of uncertainty. Whenever possible, S-17's or S-20's were used because of their high sensitivities and low, stable dark currents.

The large grey shifts in the extinction mentioned above create a considerable problem for galaxy observations, where long integration times are necessary. Semi-continuous evaluation of the grey term was necessary and was accomplished by observing a particular bandpass in the wavelength sequence every fifteen to twenty minutes. Systematic magnitude changes in this reference bandpass larger than a photon-statistical standard deviation were ascribed to grey shifts, and appropriate corrections were applied to observations in other bandpasses. Only a few nights lacked an appreciable shift. Typically, shifts of $.15^{m}$ were encountered.

This correction procedure is not entirely satisfactory; the grid of grey term measurements is too coarse in time, and photon noise in the reference channel is larger than desirable. As a result, grey shifts contribute the largest uncertainty to the observations. These shifts are probably best evaluated by continuous broad-band monitoring of the galaxy or a nearby star.

Unfortunately, the relatively inefficient observing procedure dictated by the combined difficulties of low signal-to-noise ratio, grey shifts, inefficient optics, and the lack of a chopper resulted in data being accumulated

slowly. Even where counting rates were highest, total observing times of 1000^s per bandpass (including sky) were required to reach $.05^m$ accuracy. This is a factor of about 5 larger than the times estimated from photon statistics alone. Data below 3800 Å or above 7400 Å could only be obtained with 50 Å resolution and larger entrance apertures and was accurate only to about 15%. The only 60" data deemed to be of sufficient quality ($.03^m$ to $.05^m$ standard deviation) for inclusion in the synthesis program was that obtained between 5050 and 6370 Å. This data has been given equal weight with the 200" data described below.

200" Observations

Galaxy data of far greater quality than that gathered with the 60" was obtained on two nights in February and May of 1969 with the recently-completed 200" multi-channel spectrometer (MCSP). This instrument has been described by Oke (1969). Since at least eighteen channels were operated per night, a large amount of data at non-program wavelengths was acquired. The resulting coverage of the spectrum is essentially complete from 3400 to 11000 Å with observations spaced on an average of 20 Å below 5000 Å and 50 Å above 5000 Å. Integration times of 100^s were used throughout, and the resulting photon-statistical accuracies range from 1% to 3% for all except points blueward of 3600 Å and redward of 10700 Å. However, a variety of difficulties lower the actual accuracy of the observations:

1) In regions affected by absorption lines in the standards, OB-AB interpolation is somewhat less accurate than with the Cassegrain scanner because the slewing range of the MCSP grating is not large enough to provide all channels with line-free standard star observations on either end of the bandwidth accessible to them. This problem is further complicated longward of 8000 Å by the presence of highly structured water vapor absorption. The average resultant uncertainty at the program wavelengths involved is probably less than 3%.

2) Continuous sky measurement was impossible because M82 is larger than the separation of the two MCSP entrance apertures (40" arc). To conserve time, only one complete sky measurement was made per night; measurements at a few grating tilts before and after the M82 observations served as a check on systematic sky drifts, which were not found in most channels. However, significant fluctuations (due mainly to night sky OH emission) occurred in many bandpasses longward of 8000 Å and introduced a few percent additional uncertainty. In addition, one or two channels on each night suffered higher than normal dark count, which would best have been continously monitored. Unfortunately, one of these channels (λλ8000-8600) included four important program wavelengths for which accuracies of only 6% were achieved.

3) The February data on both M82A and B had to be corrected

for guiding errors, which occur easily with the small entrance aperture used. Since such errors appear in the data as grey shifts which are the same in all channels for a given grating tilt, they may be detected and eliminated with a fair degree of confidence. Although the corrections for guiding are uncomfortably large (up to $.1^m$), independent reduction of two scans of M82 A yielded results which agreed to within about $.03^m$ in all channels. Corrections to M82 B data were small.

4) In May the ITT FW 130 (S-20) photomultipliers exhibited gains which depended on the incident photon flux in such a way that the efficiency of the S-20 channels when used to observe M82 was overestimated. Corrections for the resultant depression of the S-20 channels in the galaxy energy distribution were made by interpolating the continuum between the S-17 and S-1 channels, making it parallel to the continuum in the various S-20 channels. Each S-20 channel was then shifted to match the interpolation; corrections on the order of $.05^m$ were required. Uncertainties of about 3% are introduced by this process but do not, of course, apply to relative fluxes within a given channel.

5) Observations in May were made at an air mass of 1.75 where differential refraction between 5000 and 3500 Å amounts to 2.5". Apparently, this displacement was large enough that the 7" entrance aperture partially occulted the ultraviolet image because May data at wavelengths shorter than

3900 Å falls well below February data. Hence, the May scans below 3900 Å were discarded. Refraction at 10000 Å would produce a relative image displacement of 1.5", which is probably not large enough to cause a similar problem.

VI Lasker Interference Filter Photometry

Supplementary surface photometry of M82 and the nuclei of a number of other galaxies was performed with the Mt. Wilson 60" telescope and the set of intermediate-bandwidth filters chosen by Lasker (1966, 1968, and 1970) to study the continua of galaxies. The properties of these filters are summarized by Lasker (1970) and Scargle (1969); with the exception of the filters centered at λλ3474 and 6784, they are not greatly influenced by the common absorption or emission features of galaxy spectra.

The photometry was calibrated with a set of well-observed 6-8^{m} standards provided by Oke. Since the filter bandwidths are relatively small, color terms in the atmospheric extinction could be ignored for all except the λ3474 filter, for which the color term is very difficult to determine. Hence, all filter data was reduced in exactly the same manner as scanner data to monochromatic AB magnitudes at the eight filter central wavelengths. Only the λ3474 filter is broad enough to produce results which differ significantly from the monochromatic magnitudes at the central wavelength which would be determined by higher resolution spectrophotometry.

A correction for the red leak of the λ3474 filter (which reaches a maximum of 2% transmission at 7000 Å) is necessary but for most spectra is smaller than the observational uncertainty.

Offsets from BD + 70°587 to various regions on M82 were taken from a 200" plate kindly lent by Sandage. The ultimate positional accuracy attained with the Mt. Wilson offset photometer base is better than 1" arc. Diaphrams with diameters ranging from 8"-20" were employed. Observations of the dust lanes in M82 were carefully made with the smallest apertures to avoid contamination from adjacent bright regions.

The accuracy of the photometry on brighter objects is indicated by its agreement to within a few percent in color with direct scans of M82A and B except in the λ3474 filter, which is expected to be less reliable due to the various factors mentioned above.

Lasker energy distributions for a variety of objects are displayed in Figures 2 and 3. Counting rates in the λ7953 filter were often too low for accurate observation. Fluctuations of [O I] λ5577 in the night sky often hindered observations on fainter objects. These points are not always included in the plots. The average accuracy of the plotted photometry is $.05^{m}$.

APPENDIX B

DATA FOR THE STELLAR SURVEY

Data and figures relating to the stellar survey are contained in Appendix B.

All objects observed in the survey are listed in Table B I by the spectral type groups to which they are assigned. Color-magnitude domains for these groups are given in Table IX. Relative fluxes per unit frequency normalized at 5050 Å are tabulated for each group in Table B II. Zero entries here and in Table B III correspond to spectral regions where no observations are available. Parts of the energy distributions for G6-9 V, M3-4 V and M5-6 V do not correspond to actual observations (see Part II A). Continuum and feature indices formed from the data in Table B II are presented in Table B III. The bandpasses employed in calculating these indices are given in Table V.

With the exception of Figure B 1, all figures present absorption feature index values for the stellar groups plotted against the temperature index V/R. V/R is an increasing function of temperature. Figure B 1 shows the correlation between spectral classification and V/R for all objects in Table B I with both available. The solid line is the locus for black bodies described in the text.

For comparison purposes, two individual metal-poor objects (HD 161817, at V/R = 1.03, and μ Cas, at V/R = 0.74) are plotted in most figures. Data for these is given in Table B IV. Since this data represents only a single observation of each object, it is of lower quality than the averaged group data. Observations longward of 7000 Å for HD 161817 are of particularly low accuracy and

have not been included in the figures.

The legend for all figures except B 8, where no luminosity class distinctions are made, is the following:

- • V
- ⊙ IV
- O III
- △ I-II
- ⊡ IV SMR
- □ III SMR
- ■ metal-poor (including Pop II gi)

TABLE BI

THE STELLAR SURVEY

HD/BD	HR	Sp	V	V/R	Notes
			O V		
46223		O5	7.28		p
199579	8023	O6	5.96	1.42	
24912	1228	O7	4.02	1.52	
14633		O8	7.47	1.49	p
			B0-4 V		
35299	1781	B2 V	5.71	1.40	
74280	3454	B3 V	4.31		p, Oke standard (2)
			B5 V		
4727	226	B5 V	4.52	1.34	
			B6-9 V		
42784	2207	B8 V	6.20	1.26	
196867	7906	B9 V	3.77	1.27	
			B0-6 III		
37756	1952	B3 III	4.93		p
182255	7358	B6 III	4.89	1.32	
			B I		
2905	130	B1 Ia	4.16	1.39	
40111	2084	B1 Ib	4.81	1.39	
13267	627	B5 Ia	6.35	1.31	p
183143		B7 Ia	6.87	1.28	
			A0-4 V		
130109	5511	A0 V	3.75	1.20	Oke standard (2)
21447	1046	A1 V	5.06	1.22	
150483	6203	A2 V	5.94	1.21	
195050	7826	A3 V	5.38	1.15	

Table B I (continued)

HD/BD	HR	Sp	V	V/R	Notes
			A5-9 V		
116842	5062	A5 V	4.01		p
160054	6570	A7 V	5.71	1.12	
205767	8264	A7 V	4.68	1.09	
			A5-9 III		
13161	622	A5 III	3.00	1.10	
147547	6095	A9 III	3.74	0.97	
			F0-5 V		
58946	2852	F0 V	4.16	0.92	
173649	7057	F0 IV	5.74	0.93	
128167	5447	F2 V	4.45	0.91	
			F5-9 V		
30652	1543	F6 V	3.16	0.90	A
173667	7061	F6 V	4.20	0.88	VI according to (3)
157482*	6469	dF8	5.60	0.74	spec. binary (1)
198084	7955	F8 IV-V	4.57	0.82	
			F0-5 III		
21770	1069	F4 III	5.30		p
43905	2264	F5 III	5.35	0.84	
			G0-5 V		
19373	937	G0 V	4.04	0.83	A
141004	5868	G0 V	4.43	0.79	
186408	7503	G2 V	5.96	0.78	A
186427	7504	G5 V	6.20	0.77	A
			G6-9 V		
101501	4496	G8 V	5.35	0.75	p
182488	7368	G8 V	6.38	0.75	p; spectral type from (4)
			G0-5 IV		
82210	3771	G5 IV	4.58	0.71	spectral type from (5)
161797	6623	G5 IV	3.35	0.78	

Table B I (continued)

HD/BD	HR	Sp	V	V/R	Notes
			G6-9 IV		
67767	3191	G6 IV	5.73	0.67	IV assignment by (6)
139641	5823	G8 IV	5.27	0.67	III-IV (7)
			G5-9 III		
27022	1327	G5 III	5.27	0.72	
62345	2985	G8 III	3.57	0.68	A
191046*		G9 III	7.05	0.59	CN^-; A; high velocity (8)
			K0-2 V		
3651	166	K0 V	5.84	0.72	SMR (13)
145675		K0 V	6.65	0.73	SMR (13)
149661	6171	K0 V	5.74	0.73	
10476	493	K1 V	5.23	0.70	abundance analysis (7)
			K3-4 V		
110833		K3 V	7.03	0.69	p
160346		K3 V	6.53	0.65	p
219134	8832	K3 V	5.57	0.64	A
190007*		K4 V	7.4	0.59	p
			K5-7 V		
154363		K5 V	7.73	0.52	p
201091	8085	K5 V	5.19	0.54	
157881		K7 V	7.54	0.45	
201092	8086	K7 V	6.02	0.44	
			K0-3 IV		
23249	1136	K0 IV	3.55	0.69	A
198149	7957	K0 IV	3.43	0.67	p;A
111028	4849	K1 IV	5.67	0.64	
			K0-3 IV SMR		
10486	495	sgK2	6.28	0.68	
121146	5227	sgK2	6.28	0.58	p

Table B I (continued)

HD/BD	HR	Sp	V	V/R	Notes
			K0-3 III		
19476	941	K0 III	3.89	0.66	p
40035	2077	K0 III	3.69	0.65	
27971	1390	K1 III	5.18	0.68	
55280	2715	K2 III	5.22	0.63	p
137759	5744	K2 III	3.26	0.61	p
9927*	464	K3 III	3.56	0.56	p
155410*	6388	K3 III	5.00	0.56	p
			K0-3 III SMR		
85503	3905	K2 III	3.94	0.61	
132345	5582	K3 III-IV	6.02	0.61	
188056	7576	K3 III	5.00	0.59	abundance analysis (12)
			K4-5 III		
10380	489	K3 III	4.43	0.51	A
69267	3249	K4 III	3.52	0.48	
15656	736	K5 III	5.23	0.46	p
149161	6159	K5 III	4.85	0.44	p
			K4-5 III SMR		
209747	8413	K4 III	4.84	0.49	
			M0-2 V		
111631*		M0.5 V	8.49	0.42	p
1326 A		dM1	8.07	0.32	
36395		dM1	7.97	0.32	
45735		M2 V	7.49	0.29	
216899		dM2	8.65	0.31	
			M3-4 V		
173739		dM3.5	8.90	0.25	p
173740		dM4	9.69	0.22	p
Kreuger 60 A+B		dM4.5e	9.59	0.21	p
			M5-6 V		
1326 B		dM6	11.04	0.18	p

Table B I (continued)

HD/BD	HR	Sp	V	V/R	Notes
			M0-M2 III		
95578	4299	K5 III	4.73	0.40	p
6860	337	M0 III	2.03	0.40	
18884	911	M2 III	2.52	0.35	
218329	8745	M2 III	4.50	0.39	metal richness influences classification (9)
			M3-5 III		
123657	5299	M4 III	4.22	0.19	p
145713	6039	M4 III	5.96	0.18	variable
132813	5589	M5 III	4.69	0.18	p
			M6-8 III		
148783	6146	M6 III	4.4	0.10	variable
14386	681	M6-8	2.0	0.11	p; variable
R Cas*		M6-8	5.5	0.07	p; variable
207076		M7	7.2	0.07	p
			M I		
206936	8316	M2 Ia	3.99	0.31	
36389	1845	M2 Ib	4.73	0.29	
YZ Per		M2.5 Iab	7.66	0.31	H & χ Persei (10); var.
40239*	2091	M3.5 II	4.44	0.32	
14469*		M4 Iab	7.69	0.22	H & χ Persei (10); p; variable
			Population II Giants		
165195		Pop II Gi	7.35	0.57	A
221170		Pop II Gi	7.68	0.57	A
			Miscellaneous		
161817*		Hor. Br. A2	6.95	1.03	A
6582*	321	G5 sd	5.12	0.74	abundance analysis (11); astrometric binary, $\Delta v = 3^m$ (14)
192909*	7751	K5+B8	3.90	0.43	composite

Table B I (continued)

* = star not included in group data
p = partial scan only. A "complete" M V scan extends from 3910-10800 Å.
A = abundance analysis listed by Cayrel and Cayrel de Strobel (1966)

References

1 Hoffleit (1964)
2 Oke (1964)
3 Strom and Strom (1967)
4 Whiteoak (1967)
5 Roman (1952)
6 Wilson (1962)
7 Price (1966)
8 Greenstein and Keenan (1958)
9 Spinrad and Taylor (1969)
10 Wildey (1964)
11 Cohen (1968)
12 Helfer and Wallerstein (1968)
13 Taylor (1969)
14 Wehinger and Wyckoff (1966)

TABLE B II MEAN STELLAR FLUXES

LAMBDA	O V	B0-4 V	B5 V	B6-9 V	A0-4 V	A5-9 V	F0-5 V	F6-9 V	G0-5 V	G6-9 V	K0-2 V	K3 V
3448.	1.69E 00	1.07E 00	7.85E-01	5.46E-01	3.31E-01	2.72E-01	2.83E-01	2.73E-01	2.17E-01	1.55E-01	1.24E-01	8.37E-02
3571.	1.58E 00	1.05E 00	7.70E-01	5.43E-01	3.38E-01	2.87E-01	3.06E-01	2.99E-01	2.37E-01	1.61E-01	1.23E-01	8.04E-02
3620.	1.59E 00	1.04E 00	7.71E-01	5.52E-01	3.47E-01	2.96E-01	3.15E-01	3.10E-01	2.71E-01	2.04E-01	1.71E-01	1.19E-01
3784.	1.58E 00	1.26E 00	1.07E 00	9.49E-01	6.77E-01	5.60E-01	5.35E-01	4.80E-01	3.96E-01	2.94E-01	2.43E-01	1.82E-01
3798.	1.50E 00	1.08E 00	9.15E-01	7.89E-01	5.47E-01	4.60E-01	4.74E-01	4.30E-01	3.54E-01	2.51E-01	2.00E-01	1.44E-01
3815.	1.58E 00	1.27E 00	1.18E 00	1.10E 00	8.37E-01	6.56E-01	6.05E-01	4.90E-01	3.47E-01	2.29E-01	1.71E-01	1.21E-01
3835.	1.49E 00	1.08E 00	9.18E-01	7.94E-01	5.42E-01	4.48E-01	4.67E-01	3.65E-01	2.51E-01	1.61E-01	1.16E-01	8.51E-02
3860.	1.59E 00	1.37E 00	1.29E 00	1.23E 00	1.01E 00	7.96E-01	7.04E-01	5.30E-01	3.42E-01	2.14E-01	1.50E-01	1.08E-01
3910.	1.56E 00	1.37E 00	1.29E 00	1.23E 00	1.04E 00	7.97E-01	6.92E-01	5.47E-01	4.21E-01	3.18E-01	2.67E-01	1.89E-01
3933.	1.52E 00	1.34E 00	1.31E 00	1.25E 00	1.03E 00	6.99E-01	5.30E-01	3.39E-01	2.34E-01	1.80E-01	1.53E-01	1.08E-01
4015.	1.46E 00	1.27E 00	1.25E 00	1.24E 00	1.15E 00	9.71E-01	8.11E-01	6.74E-01	5.75E-01	4.91E-01	4.50E-01	3.66E-01
4101.	1.24E 00	9.78E-01	8.57E-01	7.52E-01	5.59E-01	5.23E-01	5.74E-01	5.72E-01	5.37E-01	4.83E-01	4.56E-01	4.00E-01
4200.	1.30E 00	1.24E 00	1.21E 00	1.17E 00	1.12E 00	9.82E-01	8.46E-01	7.23E-01	6.19E-01	5.10E-01	4.56E-01	3.91E-01
4270.	1.31E 00	1.20E 00	1.19E 00	1.17E 00	1.10E 00	9.83E-01	8.65E-01	7.39E-01	6.13E-01	5.21E-01	4.76E-01	4.02E-01
4305.	1.30E 00	1.20E 00	1.18E 00	1.15E 00	1.02E 00	8.85E-01	7.91E-01	6.34E-01	4.81E-01	4.06E-01	3.69E-01	3.47E-01
4400.	1.26E 00	1.16E 00	1.15E 00	1.14E 00	1.07E 00	9.67E-01	8.83E-01	7.87E-01	7.02E-01	6.74E-01	5.85E-01	5.58E-01
4430.	1.22E 00	1.16E 00	1.15E 00	1.14E 00	1.09E 00	1.01E 00	9.14E-01	8.30E-01	7.68E-01	7.04E-01	6.73E-01	6.39E-01
4500.	1.24E 00	1.15E 00	1.15E 00	1.13E 00	1.09E 00	1.02E 00	9.55E-01	8.91E-01	8.56E-01	8.22E-01	8.06E-01	8.23E-01
5050.	1.00E 00	1.00E 00	1.00E 00	1.00E 00	1.00E 00	1.00E 00	1.00E 00	1.00E 00	1.00E 00	1.00E 00	1.00E 00	1.00E 00
5175.	9.82E-01	9.90E-01	9.57E-01	9.76E-01	9.66E-01	9.55E-01	9.78E-01	9.54E-01	9.06E-01	8.85E-01	7.87E-01	7.24E-01
5300.	9.53E-01	9.54E-01	9.76E-01	9.70E-01	9.84E-01	1.00E 00	1.04E 00	1.08E 00	1.10E 00	1.16E 00	1.17E 00	1.28E 00
5820.	8.13E-01	8.54E-01	8.85E-01	8.71E-01	9.12E-01	9.83E-01	1.10E 00	1.20E 00	1.26E 00	1.40E 00	1.45E 00	1.71E 00
5892.	7.70E-01	8.13E-01	8.38E-01	8.58E-01	9.00E-01	9.53E-01	1.08E 00	1.15E 00	1.22E 00	1.31E 00	1.30E 00	1.42E 00
6100.	7.81E-01	8.16E-01	8.14E-01	8.61E-01	9.09E-01	9.75E-01	1.13E 00	1.24E 00	1.32E 00	1.45E 00	1.53E 00	1.80E 00
6180.	7.58E-01	7.76E-01	8.23E-01	8.40E-01	8.84E-01	9.56E-01	1.13E 00	1.22E 00	1.31E 00	1.45E 00	1.52E 00	1.78E 00
6370.	7.22E-01	7.22E-01	7.83E-01	8.01E-01	8.68E-01	9.38E-01	1.13E 00	1.25E 00	1.36E 00	1.53E 00	1.58E 00	1.93E 00
7050.	6.23E-01	6.50E-01	7.12E-01	7.37E-01	8.13E-01	9.13E-01	1.17E 00	1.32E 00	1.50E 00	1.71E 00	1.82E 00	2.25E 00
7100.	6.18E-01	6.57E-01	7.12E-01	7.33E-01	8.10E-01	9.07E-01	1.16E 00	1.34E 00	1.48E 00	1.70E 00	1.80E 00	2.22E 00
7400.	5.77E-01	6.29E-01	6.75E-01	7.03E-01	7.72E-01	8.75E-01	1.16E 00	1.32E 00	1.49E 00	1.70E 00	1.83E 00	2.16E 00
8050.	4.91E-01	5.59E-01	5.89E-01	6.41E-01	7.15E-01	8.49E-01	1.13E 00	1.33E 00	1.56E 00	1.84E 00	1.95E 00	2.52E 00
8190.	5.08E-01	5.38E-01	6.10E-01	6.35E-01	7.06E-01	8.43E-01	1.13E 00	1.35E 00	1.57E 00	1.86E 00	1.93E 00	2.54E 00
8400.	4.73E-01	5.25E-01	5.66E-01	6.24E-01	6.85E-01	8.47E-01	1.15E 00	1.38E 00	1.61E 00	1.90E 00	2.03E 00	2.66E 00
8546.	4.74E-01	5.20E-01	5.81E-01	6.26E-01	6.71E-01	7.70E-01	1.09E 00	1.26E 00	1.48E 00	1.72E 00	1.86E 00	2.43E 00
8800.	4.42E-01	4.94E-01	5.88E-01	6.51E-01	7.40E-01	8.68E-01	1.13E 00	1.35E 00	1.57E 00	1.82E 00	2.02E 00	2.66E 00
8880.	4.39E-01	5.14E-01	5.34E-01	6.29E-01	6.46E-01	7.93E-01	1.13E 00	1.34E 00	1.59E 00	1.85E 00	2.11E 00	2.76E 00
9190.	4.06E-01	4.48E-01	5.30E-01	6.04E-01	6.88E-01	8.08E-01	1.12E 00	1.34E 00	1.55E 00	1.85E 00	2.06E 00	2.72E 00
9950.	3.65E-01	4.29E-01	5.14E-01	5.36E-01	6.65E-01	7.67E-01	1.09E 00	1.32E 00	1.57E 00	1.85E 00	2.05E 00	2.79E 00
10400.	3.23E-01	4.16E-01	4.65E-01	5.02E-01	6.27E-01	7.58E-01	1.07E 00	1.29E 00	1.58E 00	1.91E 00	2.12E 00	3.01E 00
10800.	3.20E-01	4.43E-01	4.54E-01	4.60E-01	6.14E-01	7.65E-01	1.02E 00	1.29E 00	1.43E 00	1.89E 00	2.13E 00	2.91E 00

TABLE B II (continued)

LAMDBA	K5-7 V	M0-2 V	M3-4 V	M5-6 V	G0-5 IV	G6-9 IV	K0-3 IV	K0-3 IV SMR	B0-6 III	A5-9 III	F0-5 III	G5-9 III
3448.	7.08E-02	0.0	0.0	0.0	1.65E-01	1.41E-01	1.02E-01	8.02E-02	6.77E-01	2.51E-01	2.72E-01	1.20E-01
3571.	6.51E-02	0.0	0.0	0.0	1.75E-01	1.42E-01	9.98E-02	6.40E-02	6.77E-01	2.63E-01	2.90E-01	1.22E-01
3620.	1.01E-01	0.0	0.0	0.0	2.17E-01	1.93E-01	1.43E-01	1.14E-01	6.85E-01	2.75E-01	3.07E-01	1.67E-01
3784.	1.37E-01	0.0	0.0	0.0	3.14E-01	2.66E-01	2.05E-01	1.49E-01	1.13E 00	5.64E-01	5.01E-01	2.35E-01
3798.	1.27E-01	0.0	0.0	0.0	2.67E-01	2.26E-01	1.67E-01	1.19E-01	9.63E-01	4.71E-01	4.43E-01	1.97E-01
3815.	1.02E-01	0.0	0.0	0.0	2.57E-01	2.12E-01	1.46E-01	9.60E-02	1.20E 00	6.64E-01	5.39E-01	1.82E-01
3835.	8.96E-02	0.0	0.0	0.0	1.81E-01	1.44E-01	9.72E-02	7.52E-02	9.54E-01	4.53E-01	4.05E-01	1.33E-01
3860.	1.06E-01	0.0	0.0	0.0	2.18E-01	1.71E-01	1.19E-01	8.02E-02	1.30E 00	7.98E-01	6.11E-01	1.45E-01
3910.	1.44E-01	1.40E-01	0.0	0.0	3.43E-01	2.94E-01	2.35E-01	2.04E-01	1.32E 00	7.91E-01	5.98E-01	2.79E-01
3933.	1.03E-01	1.11E-01	0.0	0.0	2.00E-01	1.59E-01	1.23E-01	1.14E-01	1.33E 00	6.52E-01	3.87E-01	1.37E-01
4015.	2.68E-01	2.39E-01	2.17E-01	2.03E-01	5.01E-01	4.44E-01	3.97E-01	3.70E-01	1.26E 00	9.49E-01	7.24E-01	4.22E-01
4101.	3.07E-01	2.53E-01	2.35E-01	2.09E-01	5.01E-01	4.63E-01	4.10E-01	3.51E-01	9.76E-01	5.49E-01	5.65E-01	4.31E-01
4200.	3.43E-01	2.87E-01	2.63E-01	2.17E-01	5.24E-01	4.64E-01	4.05E-01	3.43E-01	1.25E 00	9.48E-01	7.59E-01	4.27E-01
4270.	3.36E-01	2.62E-01	2.33E-01	2.00E-01	5.43E-01	4.90E-01	4.38E-01	4.27E-01	1.22E 00	9.60E-01	7.88E-01	4.95E-01
4305.	3.42E-01	2.92E-01	2.56E-01	2.27E-01	4.29E-01	3.72E-01	3.33E-01	3.24E-01	1.20E 00	8.68E-01	6.98E-01	3.74E-01
4400.	5.41E-01	4.31E-01	4.06E-01	3.84E-01	6.33E-01	5.83E-01	5.47E-01	5.18E-01	1.18E 00	9.44E-01	8.14E-01	5.78E-01
4430.	5.91E-01	4.59E-01	4.66E-01	4.49E-01	7.10E-01	6.64E-01	6.31E-01	6.11E-01	1.18E 00	9.80E-01	8.44E-01	6.37E-01
4500.	8.35E-01	6.75E-01	6.14E-01	6.25E-01	8.08E-01	7.77E-01	7.70E-01	7.33E-01	1.17E 00	1.00E 00	8.99E-01	7.45E-01
5050.	1.00E 00	1.00E 00	1.00E 00	1.00E 00	1.00E 00	1.00E 00	1.00E 00	1.00E 00	1.00E 00	1.00E 00	1.00E 00	1.00E 00
5175.	8.02E-01	9.42E-01	8.93E-01	9.06E-01	9.12E-01	9.45E-01	8.84E-01	8.57E-01	9.80E-01	9.63E-01	9.76E-01	9.45E-01
5300.	1.53E 00	1.59E 00	1.63E 00	1.89E 00	1.14E 00	1.16E 00	1.21E 00	1.28E 00	9.62E-01	1.02E 00	1.06E 00	1.15E 00
5820.	2.46E 00	2.63E 00	2.46E 00	2.75E 00	1.37E 00	1.45E 00	1.50E 00	1.69E 00	8.84E-01	1.04E 00	1.16E 00	1.42E 00
5892.	1.75E 00	1.49E 00	1.20E 00	1.17E 00	1.28E 00	1.40E 00	1.42E 00	1.49E 00	8.25E-01	1.00E 00	1.19E 00	1.36E 00
6100.	2.78E 00	3.12E 00	2.89E 00	3.22E 00	1.45E 00	1.56E 00	1.61E 00	1.79E 00	8.28E-01	1.03E 00	1.23E 00	1.51E 00
6180.	2.65E 00	2.40E 00	1.92E 00	1.92E 00	1.42E 00	1.55E 00	1.61E 00	1.81E 00	8.27E-01	1.00E 00	1.21E 00	1.51E 00
6370.	2.97E 00	3.39E 00	3.33E 00	3.66E 00	1.50E 00	1.65E 00	1.71E 00	1.92E 00	7.80E-01	1.03E 00	1.27E 00	1.60E 00
7050.	3.93E 00	6.01E 00	7.37E 00	8.55E 00	1.67E 00	1.93E 00	2.00E 00	2.32E 00	7.12E-01	1.01E 00	1.34E 00	1.82E 00
7100.	3.89E 00	5.02E 00	5.39E 00	6.14E 00	1.69E 00	1.89E 00	2.00E 00	2.33E 00	7.13E-01	1.02E 00	1.31E 00	1.80E 00
7400.	4.34E 00	7.66E 00	1.08E 01	1.34E 01	1.71E 00	1.94E 00	2.06E 00	2.41E 00	6.91E-01	9.83E-01	1.33E 00	1.84E 00
8050.	5.11E 00	9.87E 00	1.46E 01	1.77E 01	1.83E 00	2.13E 00	2.26E 00	2.72E 00	6.11E-01	9.65E-01	1.31E 00	1.99E 00
8190.	4.96E 00	9.39E 00	1.43E 01	1.85E 01	1.81E 00	2.11E 00	2.16E 00	2.68E 00	6.10E-01	9.50E-01	1.34E 00	2.01E 00
8400.	5.48E 00	1.05E 01	1.66E 01	2.15E 01	1.88E 00	2.21E 00	2.35E 00	2.86E 00	5.62E-01	9.56E-01	1.38E 00	2.05E 00
8546.	5.21E 00	1.05E 01	1.60E 01	2.11E 01	1.73E 00	2.06E 00	2.19E 00	2.71E 00	5.84E-01	8.93E-01	1.25E 00	1.88E 00
8800.	5.69E 00	1.15E 01	1.83E 01	2.40E 01	1.89E 00	2.26E 00	2.38E 00	2.98E 00	5.84E-01	1.00E 00	1.35E 00	2.13E 00
8880.	6.01E 00	1.19E 01	1.87E 01	2.33E 01	1.91E 00	2.24E 00	2.47E 00	3.08E 00	5.23E-01	9.26E-01	1.34E 00	2.15E 00
9190.	6.06E 00	1.25E 01	2.05E 01	2.99E 01	1.86E 00	2.24E 00	2.33E 00	2.88E 00	5.44E-01	9.36E-01	1.29E 00	2.03E 00
9950.	6.74E 00	1.38E 01	2.29E 01	3.37E 01	1.94E 00	2.36E 00	2.52E 00	3.31E 00	5.02E-01	9.49E-01	1.28E 00	2.22E 00
10400.	7.01E 00	1.46E 01	2.54E 01	3.66E 01	1.97E 00	2.36E 00	2.58E 00	3.45E 00	4.64E-01	9.17E-01	1.24E 00	2.23E 00
10800.	7.83E 00	1.53E 01	2.57E 01	4.09E 01	1.89E 00	2.34E 00	2.56E 00	3.53E 00	4.46E-01	8.91E-01	1.17E 00	2.32E 00

TABLE B II (continued)

LAMBDA	K0-3 III	K0-3 III SMR	K4-5 III	K4-5 III SMR	M0-2 III	M4-5 III	M6-8 III	B0-7 I	M I-II	Pop II gi
3448.	8.68E-02	6.84E-02	3.38E-02	3.12E-02	2.60E-02	2.94E-02	3.90E-02	1.27E 00	4.04E-02	9.96E-02
3571.	8.33E-02	4.30E-02	3.46E-02	2.71E-02	2.28E-02	2.81E-02	4.59E-02	1.23E 00	2.04E-02	1.19E-01
3620.	1.27E-01	6.81E-02	4.70E-02	4.48E-02	3.46E-02	4.59E-02	7.43E-02	1.23E 00	2.95E-02	1.36E-01
3784.	1.67E-01	8.60E-02	7.22E-02	6.52E-02	5.18E-02	7.03E-02	1.48E-01	1.32E 00	4.55E-02	2.20E-01
3798.	1.42E-01	7.02E-02	5.61E-02	5.27E-02	4.64E-02	6.18E-02	1.29E-01	1.26E 00	4.08E-02	2.18E-01
3815.	1.15E-01	5.88E-02	5.09E-02	4.63E-02	4.10E-02	5.74E-02	1.21E-01	1.33E 00	3.96E-02	2.21E-01
3835.	9.05E-02	4.57E-02	3.91E-02	3.62E-02	3.72E-02	5.74E-02	1.14E-01	1.28E 00	3.99E-02	2.05E-01
3860.	9.44E-02	5.15E-02	4.84E-02	4.61E-02	4.42E-02	6.29E-02	1.27E-01	1.34E 00	4.09E-02	2.48E-01
3910.	2.09E-01	1.19E-01	8.04E-02	7.78E-02	6.00E-02	8.28E-02	1.70E-01	1.34E 00	4.78E-02	2.56E-01
3933.	1.03E-01	5.92E-02	3.81E-02	3.86E-02	3.19E-02	4.36E-02	7.58E-02	1.30E 00	2.73E-02	1.53E-01
4015.	3.68E-01	2.55E-01	1.79E-01	1.85E-01	1.33E-01	1.60E-01	3.32E-01	1.25E 00	9.47E-02	3.44E-01
4101.	3.69E-01	2.44E-01	2.01E-01	1.99E-01	1.60E-01	2.08E-01	4.18E-01	1.13E 00	1.19E-01	3.82E-01
4200.	3.59E-01	2.36E-01	2.07E-01	1.99E-01	1.80E-01	2.46E-01	4.50E-01	1.21E 00	1.43E-01	4.20E-01
4270.	4.30E-01	3.31E-01	2.65E-01	2.72E-01	2.23E-01	2.70E-01	4.19E-01	1.19E 00	1.94E-01	4.57E-01
4305.	3.36E-01	2.71E-01	2.36E-01	2.36E-01	2.25E-01	2.77E-01	4.11E-01	1.18E 00	1.88E-01	4.02E-01
4400.	5.27E-01	4.50E-01	3.86E-01	4.00E-01	3.50E-01	3.78E-01	4.92E-01	1.17E 00	2.81E-01	5.45E-01
4430.	5.95E-01	5.22E-01	4.43E-01	4.76E-01	4.09E-01	3.98E-01	4.21E-01	1.10E 00	2.89E-01	5.77E-01
4500.	7.20E-01	6.60E-01	5.91E-01	6.27E-01	5.59E-01	4.89E-01	4.86E-01	1.16E 00	4.33E-01	6.65E-01
5050.	1.00E 00	1.00E 00	1.00E 00	1.00E 00	1.00E 00	1.00E 00	1.00E 00	1.00E 00	1.00E 00	1.00E 00
5175.	9.00E-01	8.40E-01	8.54E-01	8.42E-01	8.26E-01	7.49E-01	9.18E-01	9.78E-01	8.36E-01	1.05E 00
5300.	1.22E 00	1.32E 00	1.36E 00	1.43E 00	1.46E 00	1.59E 00	1.82E 00	9.80E-01	1.45E 00	1.23E 00
5820.	1.58E 00	1.83E 00	2.07E 00	2.20E 00	2.28E 00	2.04E 00	2.74E 00	8.99E-01	2.29E 00	1.58E 00
5892.	1.46E 00	1.55E 00	1.82E 00	1.80E 00	1.75E 00	1.25E 00	1.35E 00	8.54E-01	1.63E 00	1.54E 00
6100.	1.67E 00	1.97E 00	2.34E 00	2.48E 00	2.73E 00	2.84E 00	3.89E 00	8.69E-01	2.99E 00	1.74E 00
6180.	1.68E 00	1.96E 00	2.27E 00	2.38E 00	2.26E 00	1.54E 00	1.91E 00	8.37E-01	2.11E 00	1.78E 00
6370.	1.79E 00	2.03E 00	2.56E 00	2.64E 00	2.93E 00	3.16E 00	4.58E 00	8.05E-01	3.19E 00	1.91E 00
7050.	2.15E 00	2.56E 00	3.47E 00	3.53E 00	4.38E 00	6.81E 00	1.46E 01	7.13E-01	5.16E 00	2.34E 00
7100.	2.12E 00	2.49E 00	3.30E 00	3.28E 00	3.70E 00	3.91E 00	6.98E 00	7.21E-01	3.82E 00	2.49E 00
7400.	2.20E 00	2.68E 00	3.85E 00	3.86E 00	5.40E 00	1.29E 01	3.66E 01	6.66E-01	6.90E 00	2.58E 00
8050.	2.43E 00	3.05E 00	4.53E 00	4.48E 00	6.53E 00	1.68E 01	5.64E 01	6.25E-01	8.38E 00	2.83E 00
8190.	2.35E 00	2.91E 00	4.47E 00	4.60E 00	6.68E 00	1.88E 01	8.15E 01	6.12E-01	8.51E 00	2.96E 00
8400.	2.40E 00	3.17E 00	4.32E 00	4.75E 00	7.03E 00	1.85E 01	6.58E 01	5.83E-01	9.18E 00	3.02E 00
8546.	2.29E 00	2.96E 00	3.95E 00	4.47E 00	6.36E 00	1.58E 01	5.18E 01	5.91E-01	8.09E 00	2.87E 00
8800.	2.58E 00	3.37E 00	4.67E 00	5.17E 00	7.81E 00	2.27E 01	1.04E 02	5.97E-01	1.10E 01	3.11E 00
8880.	2.67E 00	3.56E 00	4.89E 00	5.52E 00	8.12E 00	2.09E 01	7.73E 01	5.83E-01	1.12E 01	3.23E 00
9190.	2.45E 00	3.16E 00	4.53E 00	5.02E 00	7.81E 00	2.53E 01	1.31E 02	5.64E-01	1.02E 01	3.07E 00
9950.	2.74E 00	3.78E 00	5.35E 00	6.00E 00	9.40E 00	2.97E 01	1.62E 02	5.01E-01	1.36E 01	3.38E 00
10400.	2.82E 00	4.02E 00	5.61E 00	6.40E 00	1.00E 01	3.23E 01	1.87E 02	4.61E-01	1.46E 01	3.49E 00
10800.	2.85E 00	4.10E 00	5.78E 00	6.81E 00	1.07E 01	3.40E 01	2.01E 02	4.40E-01	1.57E 01	3.62E 00

MEAN STELLAR INDICES

TABLE B III

INDEX	O V	B0-4 V	B5 V	B6-9 V	A0-4 V	A5-9 V	F0-5 V	F6-9 V	G0-5 V	G6-9 V	K0-2 V	K3 V	K5-7 V	M0-2 V	M3-4 V
H 3798	0.950	0.858	0.819	0.777	0.731	0.763	0.837	0.888	0.945	0.947	0.945	0.931	1.043	0.0	0.0
H 3835	0.940	0.817	0.747	0.686	0.593	0.625	0.720	0.718	0.728	0.724	0.716	0.739	0.865	0.0	0.0
CAK 3933	0.990	0.997	1.017	1.017	0.970	0.839	0.739	0.591	0.517	0.508	0.501	0.479	0.609	0.687	0.0
H 4101	0.877	0.781	0.694	0.615	0.493	0.535	0.692	0.822	0.913	0.963	0.994	1.059	1.059	1.027	1.056
CN 4200	0.961	1.010	1.002	0.984	1.003	1.000	0.995	1.003	1.026	0.994	0.971	0.998	1.083	1.121	1.150
G 4305	1.004	1.004	0.997	0.988	0.941	0.904	0.910	0.843	0.756	0.741	0.732	0.783	0.878	0.954	0.922
IS 4430	0.973	0.999	0.999	1.002	1.017	1.026	1.011	1.015	1.028	1.033	1.037	1.007	0.943	0.915	0.999
MGI 5175	1.003	1.010	0.966	0.988	0.972	0.953	0.958	0.916	0.863	0.819	0.725	0.638	0.639	0.733	0.685
NAD 5892	0.956	0.961	0.964	0.987	0.986	0.970	0.975	0.953	0.952	0.928	0.878	0.819	0.690	0.544	0.466
TIO 6180	0.990	0.982	1.021	0.994	0.984	0.989	1.000	0.976	0.977	0.981	0.981	0.966	0.934	0.752	0.636
TIO 7100	1.001	1.014	1.005	1.000	1.002	0.998	0.989	1.012	0.991	0.994	0.991	0.989	0.975	0.805	0.689
NAI 8190	1.048	0.984	1.051	1.000	1.002	0.993	0.993	0.995	0.994	0.998	0.977	0.988	0.943	0.928	0.926
CAII 8542	1.023	1.009	1.012	0.986	0.952	0.900	0.948	0.918	0.924	0.916	0.916	0.914	0.938	0.970	0.927
TIO 8880	1.008	1.057	0.925	0.978	0.884	0.925	0.994	0.992	1.011	1.009	1.036	1.035	1.043	1.013	0.994
CN 9190	0.957	0.933	0.925	0.967	0.948	0.953	0.985	0.992	0.976	1.000	1.007	0.998	1.001	1.014	1.033
U/B	1.237	0.886	0.659	0.475	0.317	0.299	0.355	0.399	0.386	0.319	0.278	0.208	0.189	0.0	0.0
B/V	1.453	1.306	1.256	1.252	1.141	0.983	0.818	0.669	0.557	0.446	0.403	0.321	0.220	0.164	0.156
V/R	1.472	1.414	1.341	1.279	1.196	1.110	0.918	0.864	0.792	0.751	0.722	0.677	0.683	0.309	0.225
V/I	1.929	1.774	1.613	1.443	1.331	1.157	0.934	0.836	0.743	0.689	0.650	0.562	0.357	0.192	0.117
V/J	2.747	2.104	2.024	1.914	1.527	1.303	1.024	0.884	0.784	0.676	0.619	0.506	0.249	0.141	0.080

INDEX	M5-6 V	G0-5 IV	G6-9 IV	K0-3 IV	K0-3 IV SMR	B0-6 III	A5-9 III	F0-5 III	G5-9 III	K0-3 III	K0-3 III SMR	K4-5 III	K4-5 III SMR	M0-2 III	M4-5 III
H 3798	0.0	0.926	0.935	0.937	0.952	0.829	0.774	0.856	0.933	0.986	0.952	0.895	0.929	0.988	0.958
H 3835	0.0	0.756	0.741	0.723	0.843	0.767	0.627	0.711	0.805	0.853	0.823	0.796	0.786	0.878	0.959
CAK 3933	0.0	0.532	0.488	0.457	0.476	1.012	0.791	0.620	0.442	0.422	0.402	0.376	0.384	0.423	0.440
H 4101	1.032	0.971	1.007	1.000	0.904	0.780	0.575	0.758	0.966	0.960	0.874	0.974	0.938	0.990	1.067
CN 4200	1.078	0.986	0.973	0.951	0.835	1.016	0.989	0.984	0.901	0.871	0.764	0.862	0.809	0.913	1.035
G 4305	0.917	0.757	0.723	0.715	0.720	0.996	0.907	0.877	0.724	0.738	0.749	0.796	0.774	0.878	0.930
IS 4430	0.989	1.039	1.038	1.030	1.052	0.999	1.019	1.007	1.017	1.020	1.020	0.994	1.021	0.996	0.970
MGI 5175	0.634	0.852	0.876	0.803	0.754	0.996	0.954	0.949	0.880	0.814	0.728	0.729	0.697	0.477	0.583
NAD 5892	0.407	0.924	0.951	0.931	0.871	0.946	0.965	1.006	0.940	0.911	0.831	0.850	0.792	0.731	0.558
TIO 6180	0.574	0.970	0.976	0.986	0.992	1.014	0.974	0.972	0.984	0.988	0.984	0.945	0.941	0.806	0.523
TIO 7100	0.667	1.006	0.980	0.994	0.999	1.007	1.011	0.982	0.989	0.982	0.967	0.936	0.919	0.820	0.512
NAI 8190	0.966	0.981	0.978	0.962	0.966	1.029	0.987	0.997	0.996	0.968	0.938	1.004	1.001	0.993	1.080
CAII 8542	0.943	0.921	0.922	0.927	0.933	1.024	0.919	0.906	0.902	0.929	0.913	0.890	0.912	0.871	0.795
TIO 8880	0.928	1.016	0.991	1.041	1.039	0.907	0.936	0.996	1.021	1.045	1.067	1.052	1.072	1.039	0.901
CN 9190	1.106	0.966	0.967	0.955	0.928	0.961	0.940	0.961	0.932	0.924	0.896	0.923	0.918	0.935	1.013
U/B	0.0	0.333	0.312	0.247	0.188	0.568	0.283	0.373	0.269	0.266	0.142	0.125	0.107	0.100	0.114
B/V	0.126	0.468	0.411	0.364	0.318	1.299	0.926	0.721	0.417	0.342	0.249	0.190	0.185	0.153	0.178
V/R	0.211	0.744	0.675	0.666	0.628	1.325	1.031	0.834	0.703	0.643	0.601	0.468	0.491	0.383	0.184
V/I	0.102	0.668	0.584	0.573	0.509	1.611	1.051	0.811	0.616	0.560	0.481	0.381	0.346	0.252	0.088
V/J	0.060	0.651	0.555	0.526	0.426	2.029	1.137	0.924	0.565	0.493	0.387	0.301	0.275	0.180	0.055

TABLE B III (continued)

INDEX	M6-8 III	B0-7 I	M I-II	Pop II gi
H 3798	0.950	0.948	0.952	0.990
H 3835	0.920	0.953	0.992	0.881
CAK 3933	0.372	0.980	0.474	0.558
H 4101	1.162	0.916	0.947	1.003
CN 4200	1.144	1.003	0.868	0.989
G 4305	0.938	0.998	0.870	0.838
IS 4430	0.859	0.947	0.887	0.995
MG1 5175	0.658	0.985	0.687	0.945
NAD 5892	0.447	0.957	0.663	0.949
TIO 6180	0.468	0.982	0.693	0.991
TIO 7100	0.399	1.019	0.707	1.046
NAI 8190	1.357	1.003	0.979	1.020
CAII 8542	0.656	1.004	0.823	0.941
TIO 8880	0.705	0.986	1.029	1.039
CN 9190	1.073	0.980	0.857	0.956
U/B	0.132	1.047	0.105	0.255
B/V	0.199	1.252	0.127	0.357
V/R	0.089	1.363	0.310	0.571
V/I	0.027	1.592	0.185	0.458
V/J	0.012	2.086	0.123	0.395

TABLE B IV

INDEX DATA FOR TWO METAL-POOR STARS

Index	HD 6582 (μ Cas)	HD 161817
H 3798	0.98	0.80
H 3835	0.64	0.67
CaK 3933	0.49	0.94
H 4101	0.97	0.59
CN 4200	1.04	0.99
G 4305	0.74	0.93
IS 4430	1.04	1.01
MgI 5175	0.78	0.99
NaD 5892	0.95	0.97
TiO 6180	0.98	0.96
TiO 7100	1.00	0.96
NaI 8190	1.01	1.05
CaII 8542	0.91	0.89
TiO 8880	1.01	1.13
CN 9190	1.14	0.89
U/B	0.43	0.26
B/V	0.50	1.01
V/R	0.74	1.03
V/I	0.62	0.93
V/J	0.65	1.00

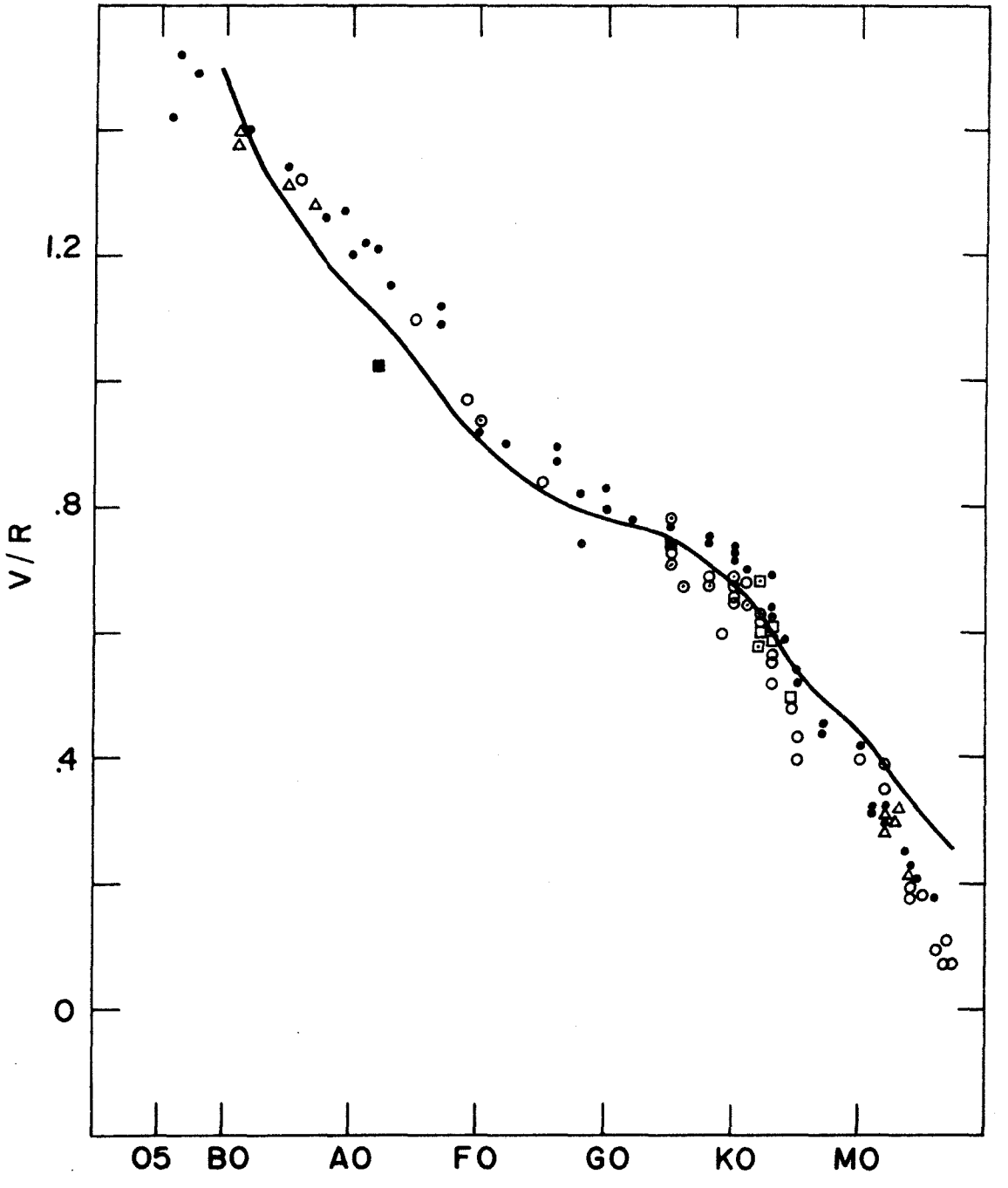

FIGURE B 1

FIGURE B 2

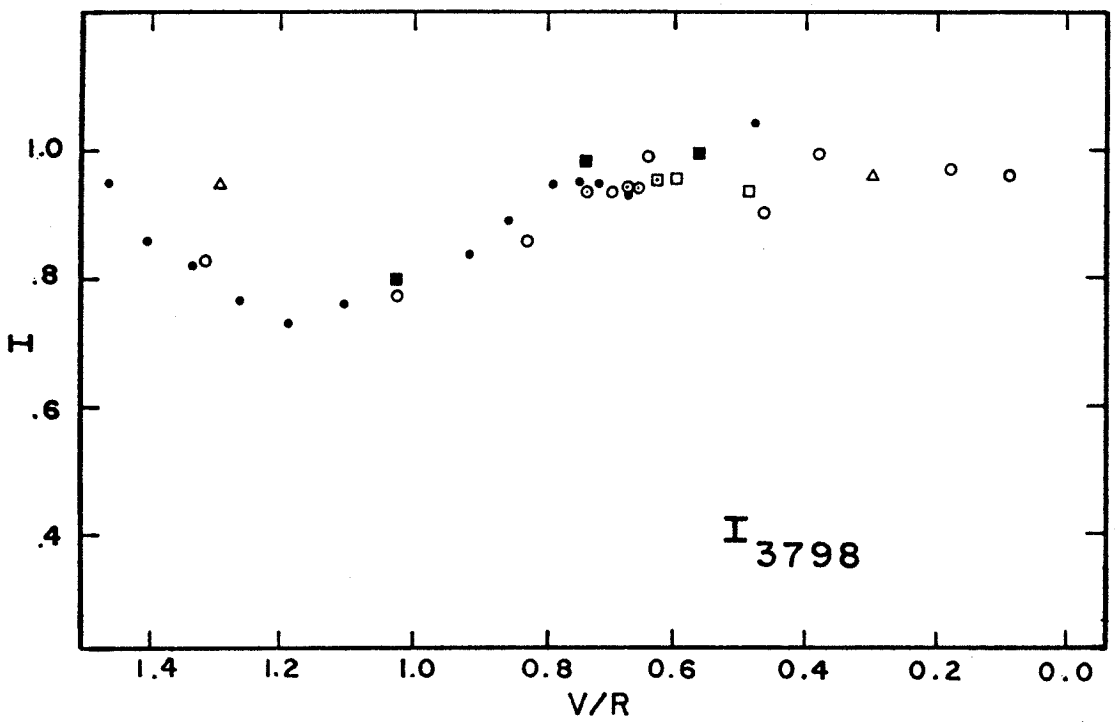

FIGURE B 3

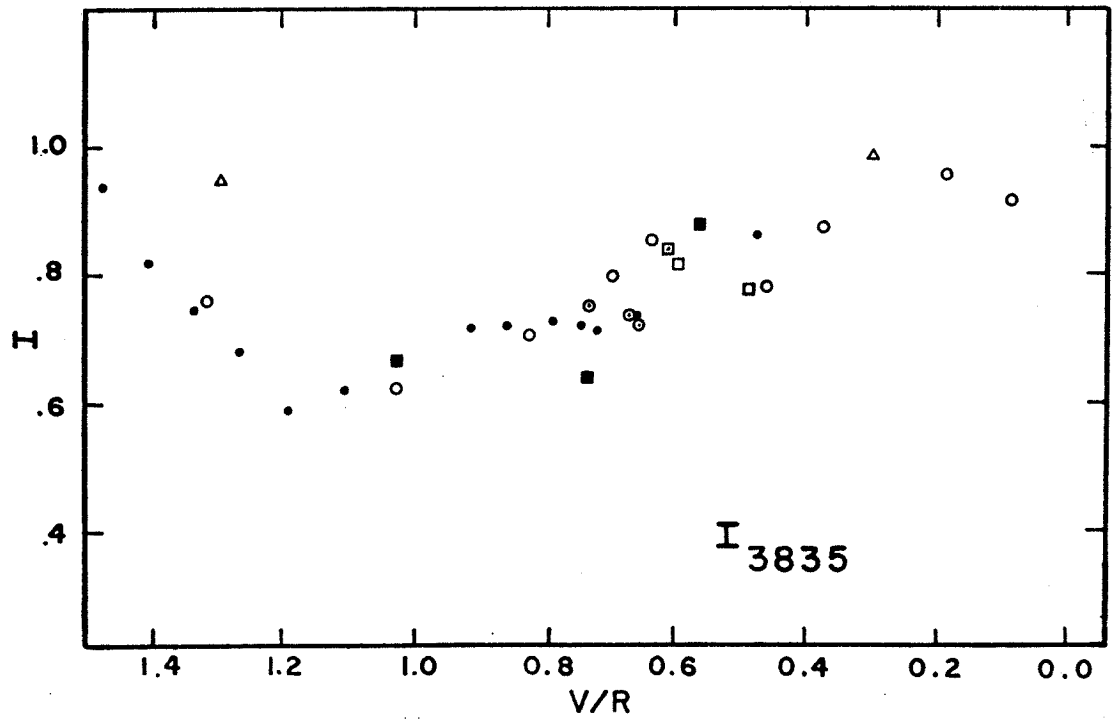

FIGURE B 4

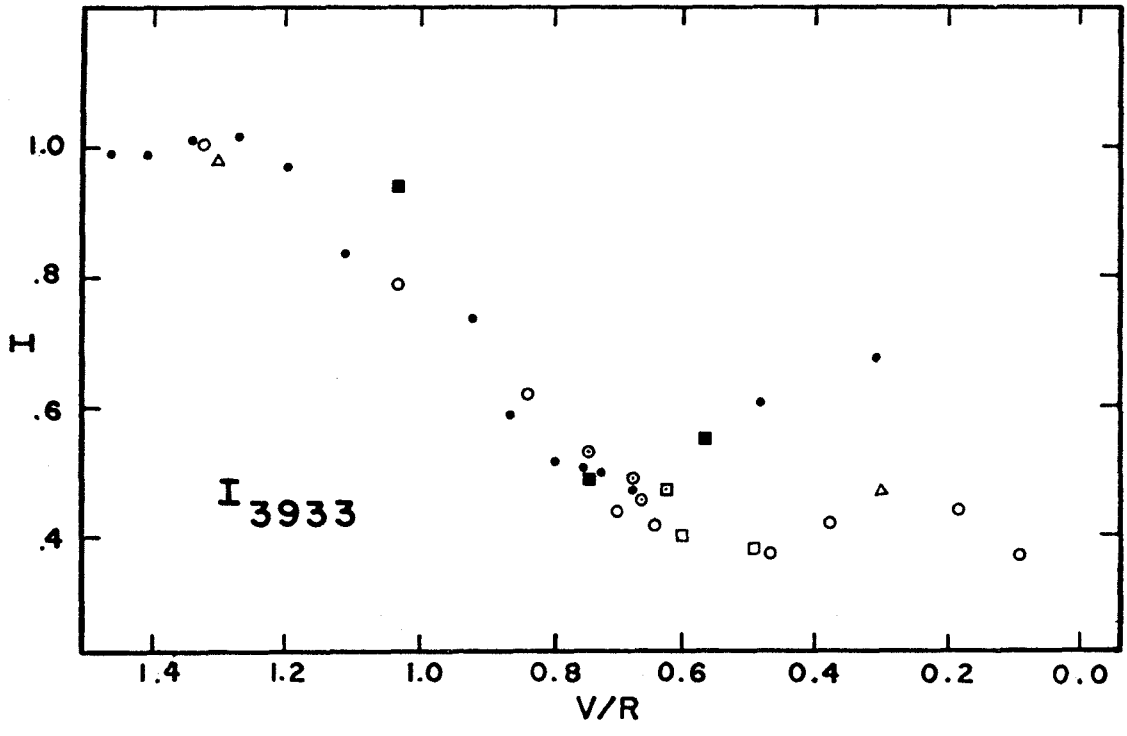

FIGURE B 5

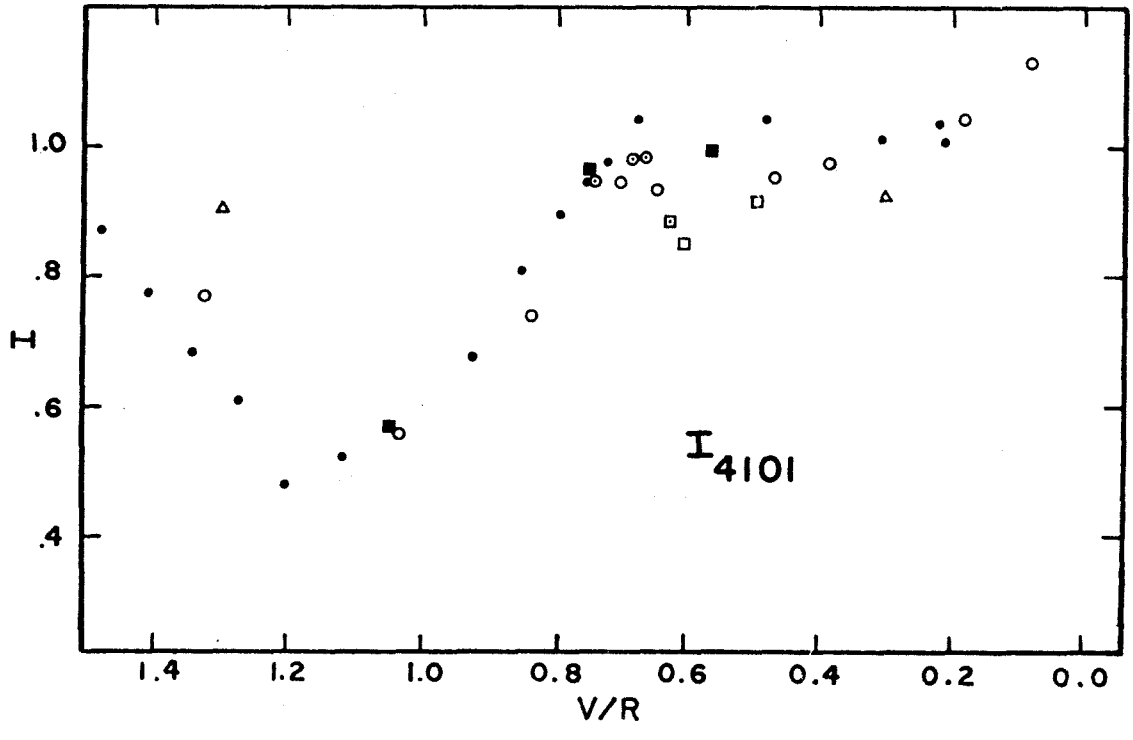

FIGURE B 6

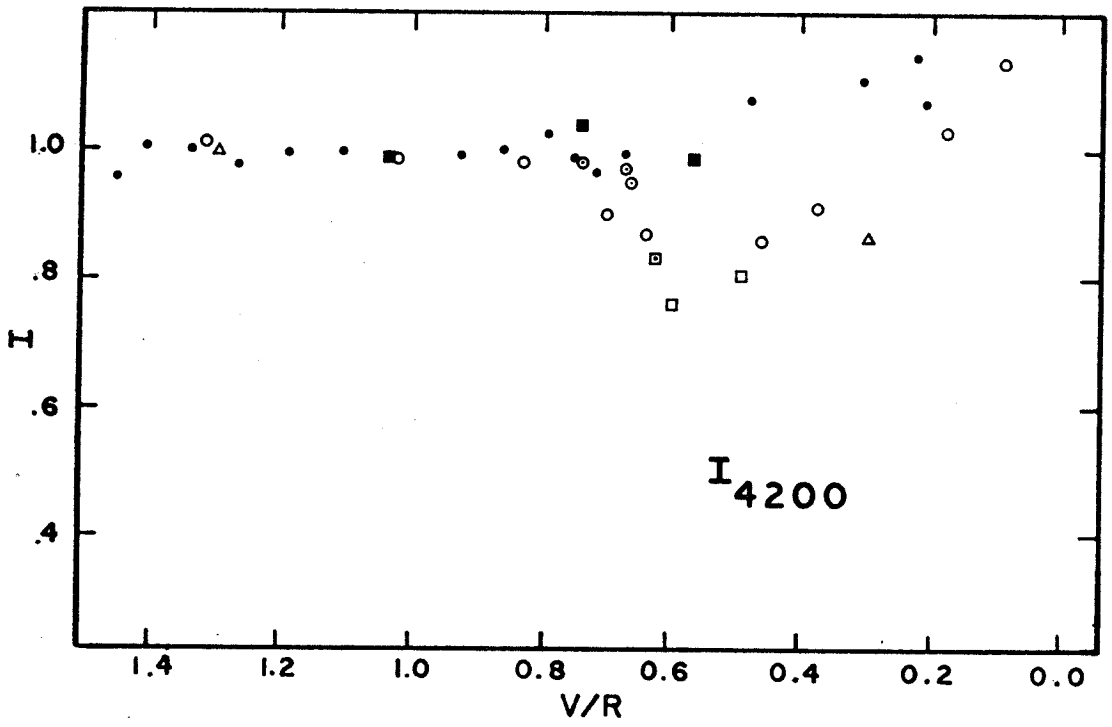

FIGURE B 7

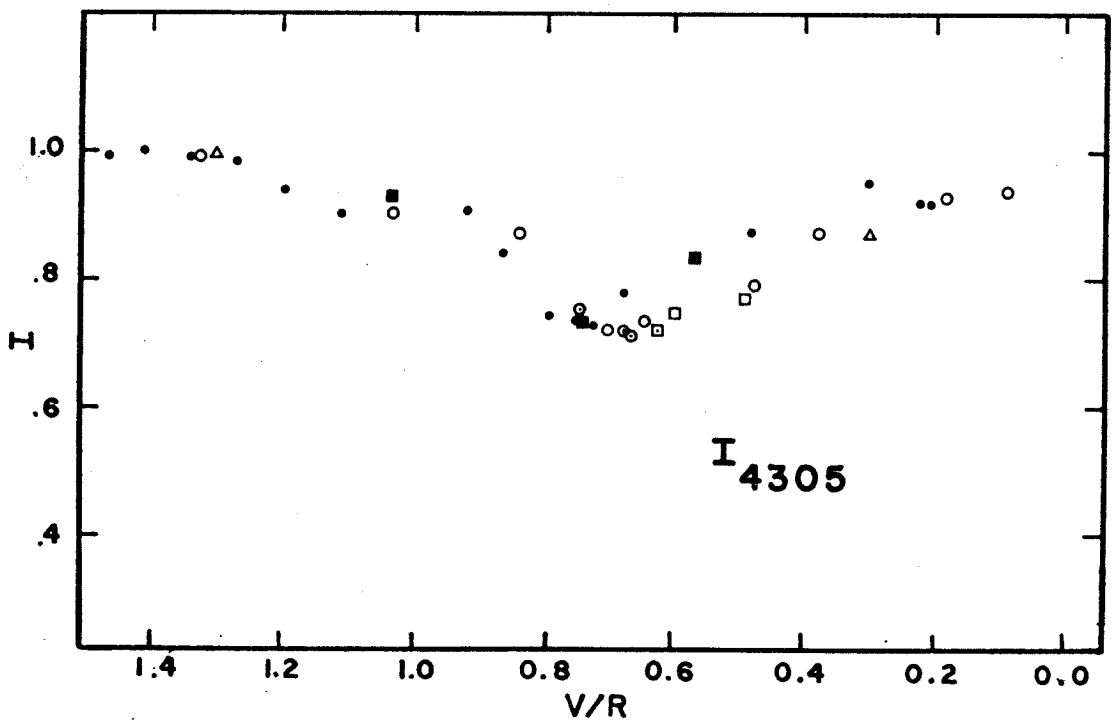

FIGURE B 8

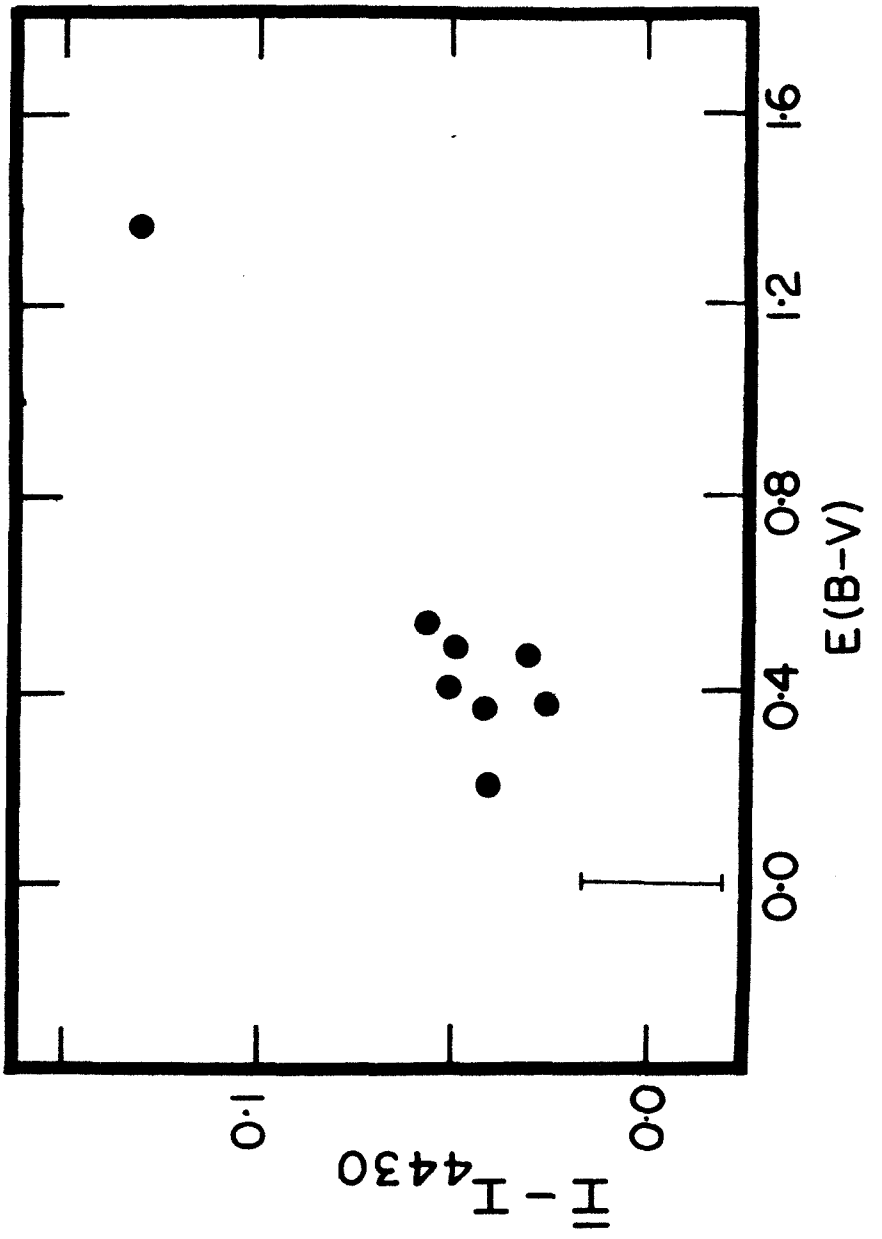

FIGURE B 9

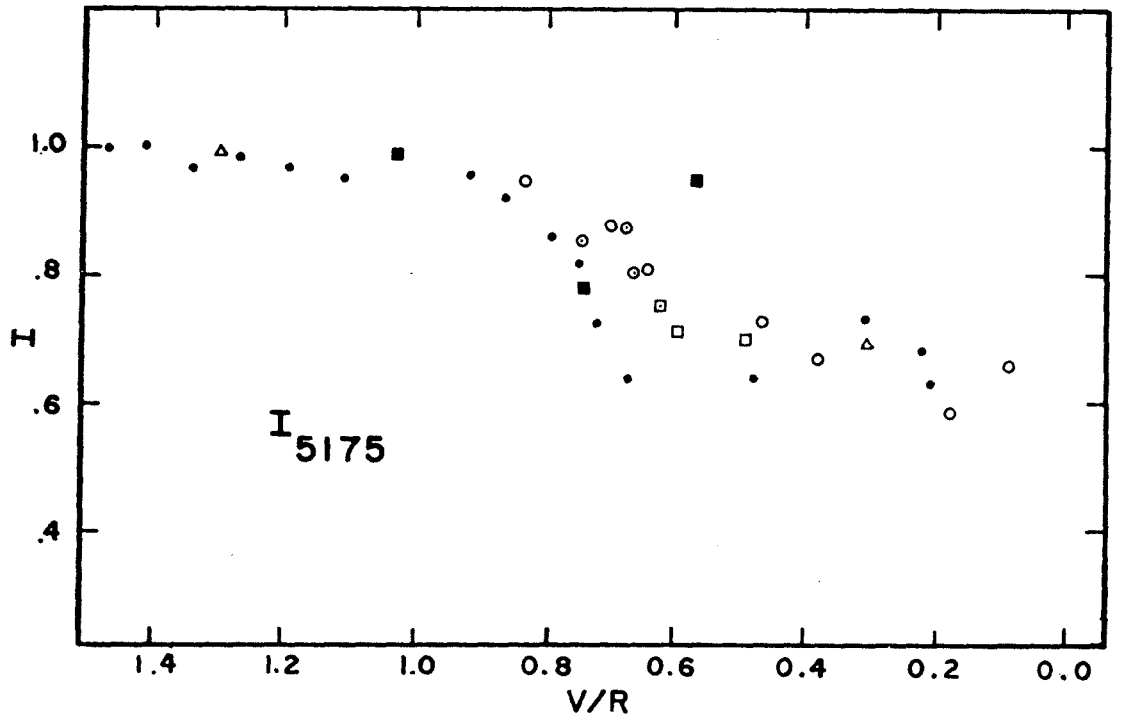

FIGURE B 10

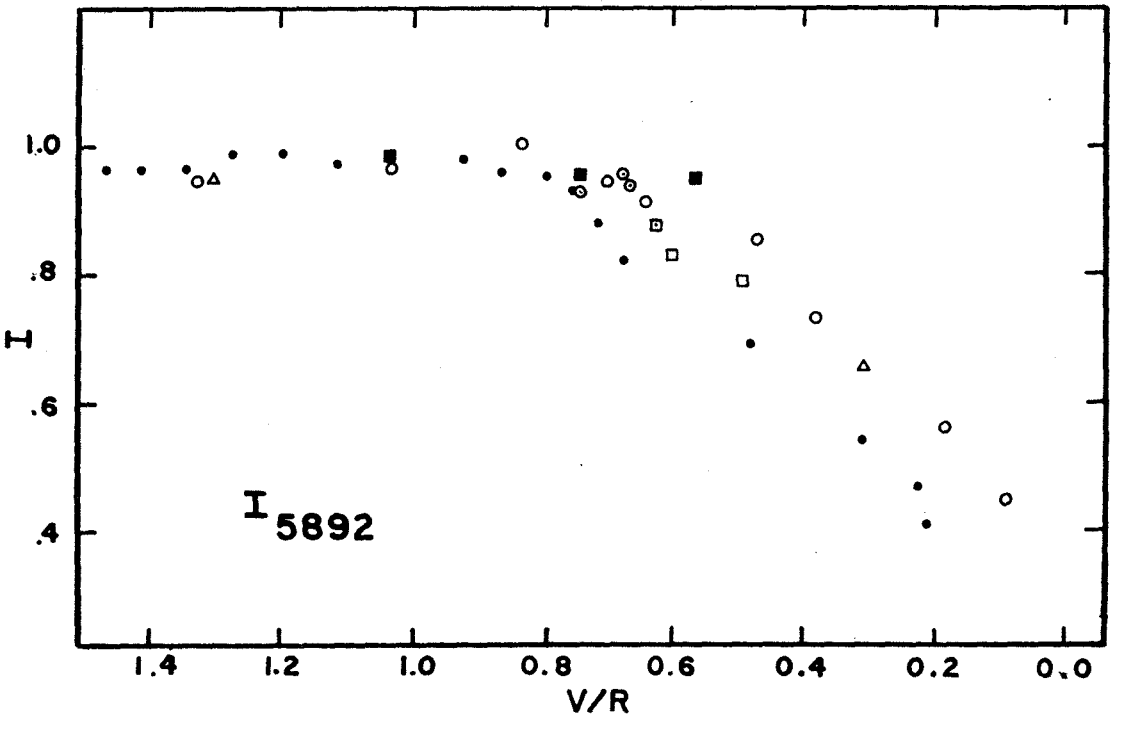

FIGURE B 11

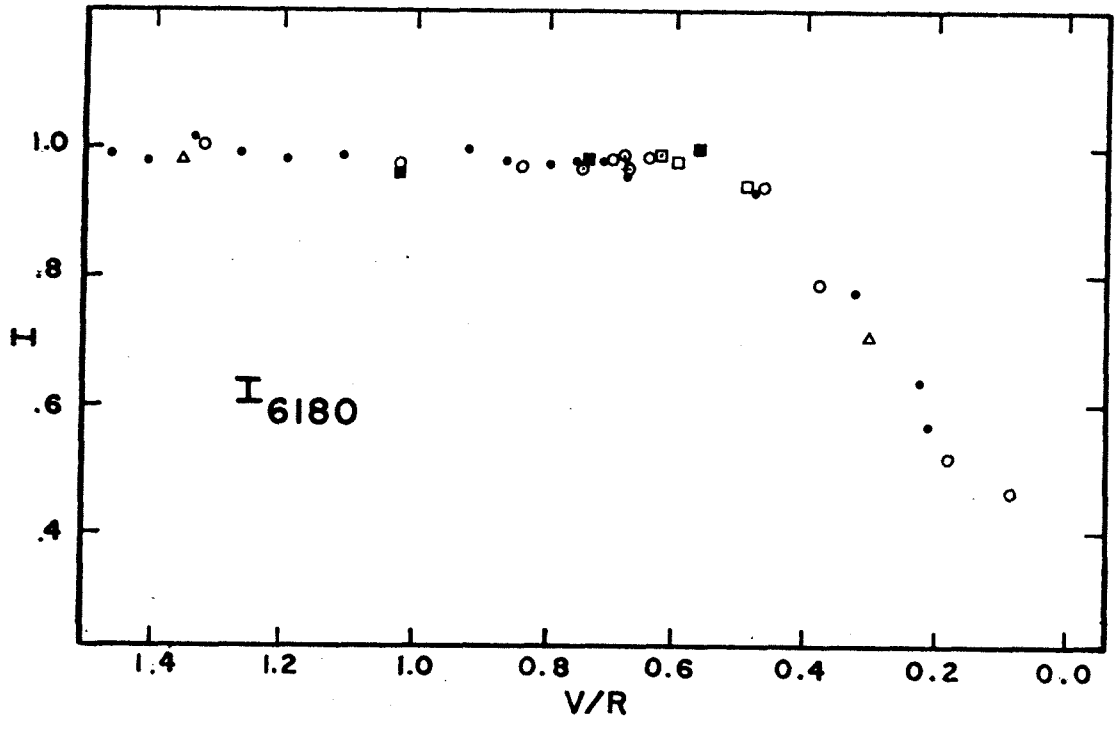

FIGURE B 12

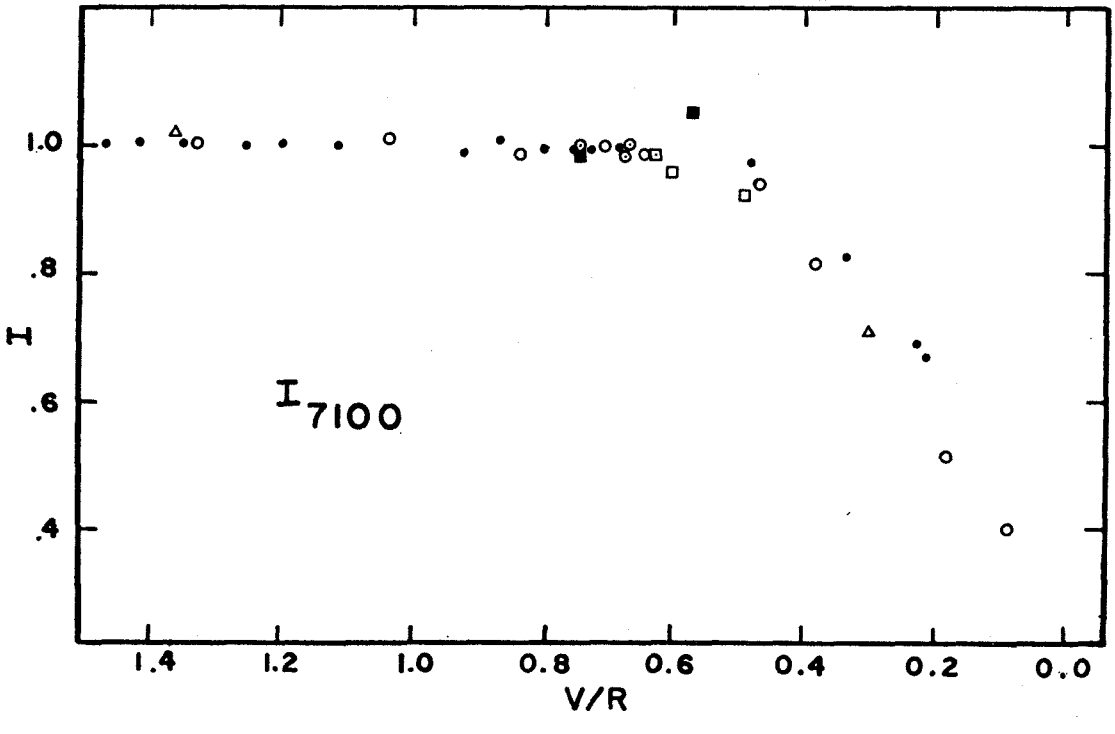

FIGURE B 13

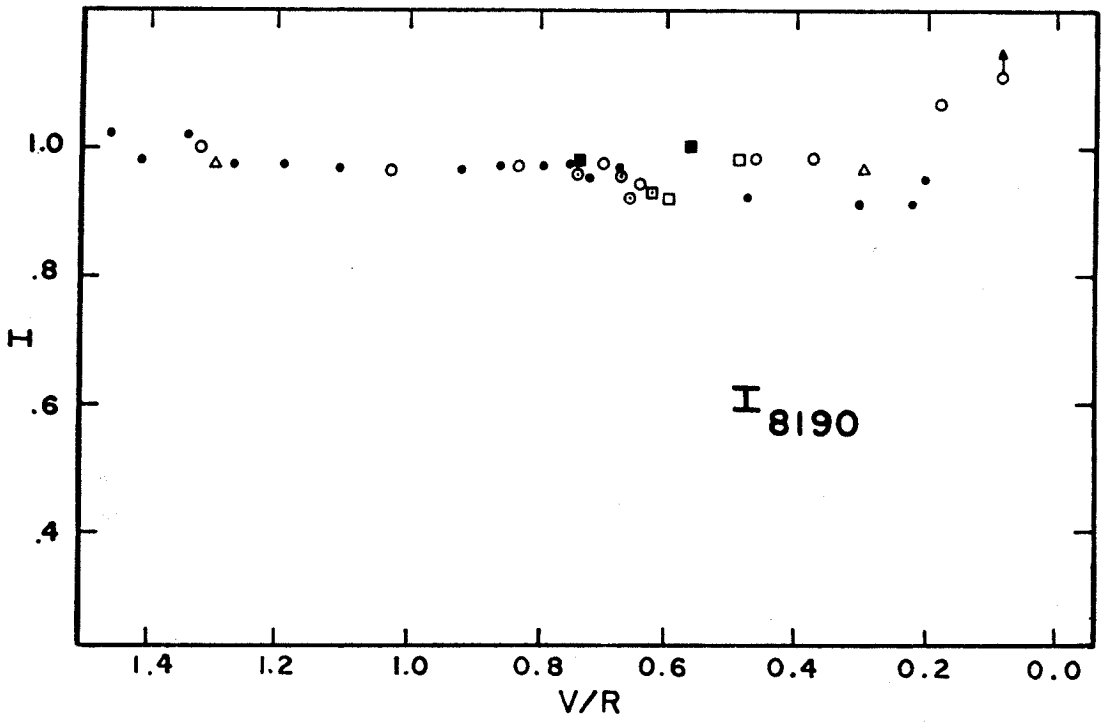

FIGURE B 14

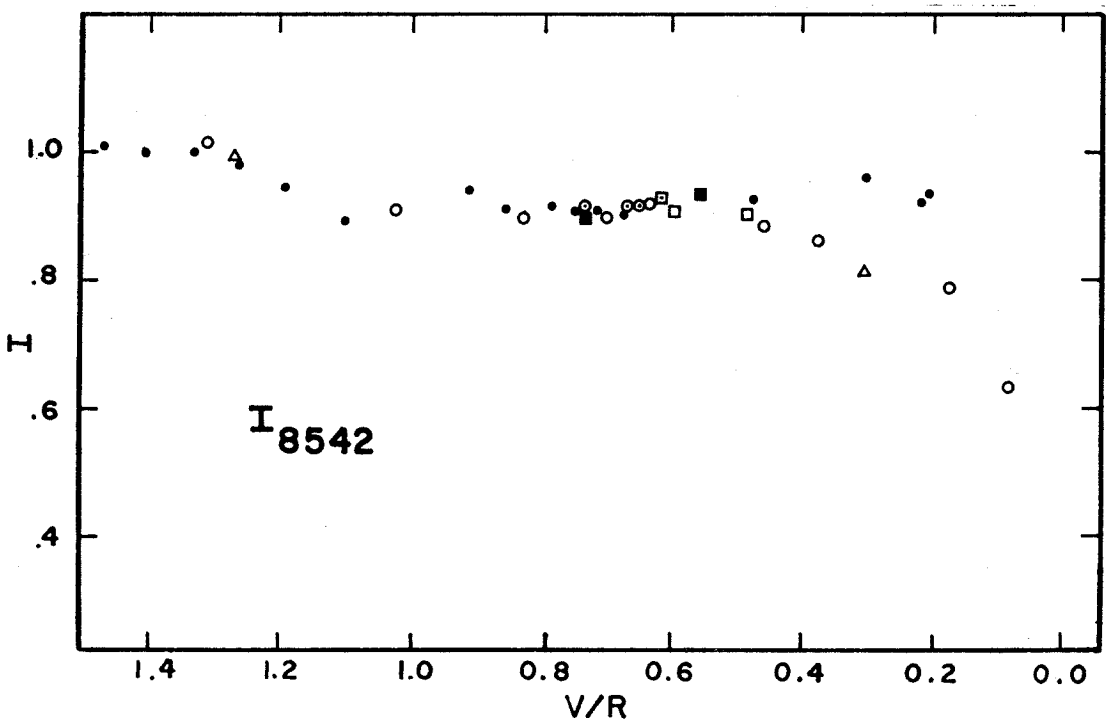

FIGURE B 15

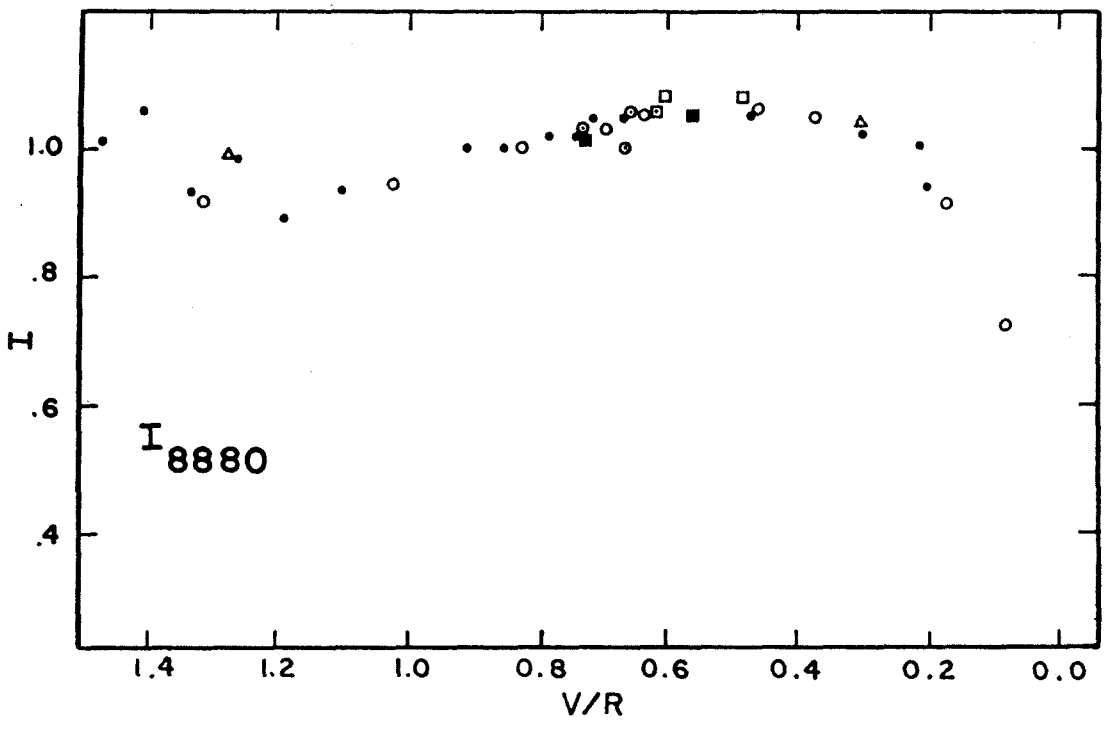

FIGURE B 16

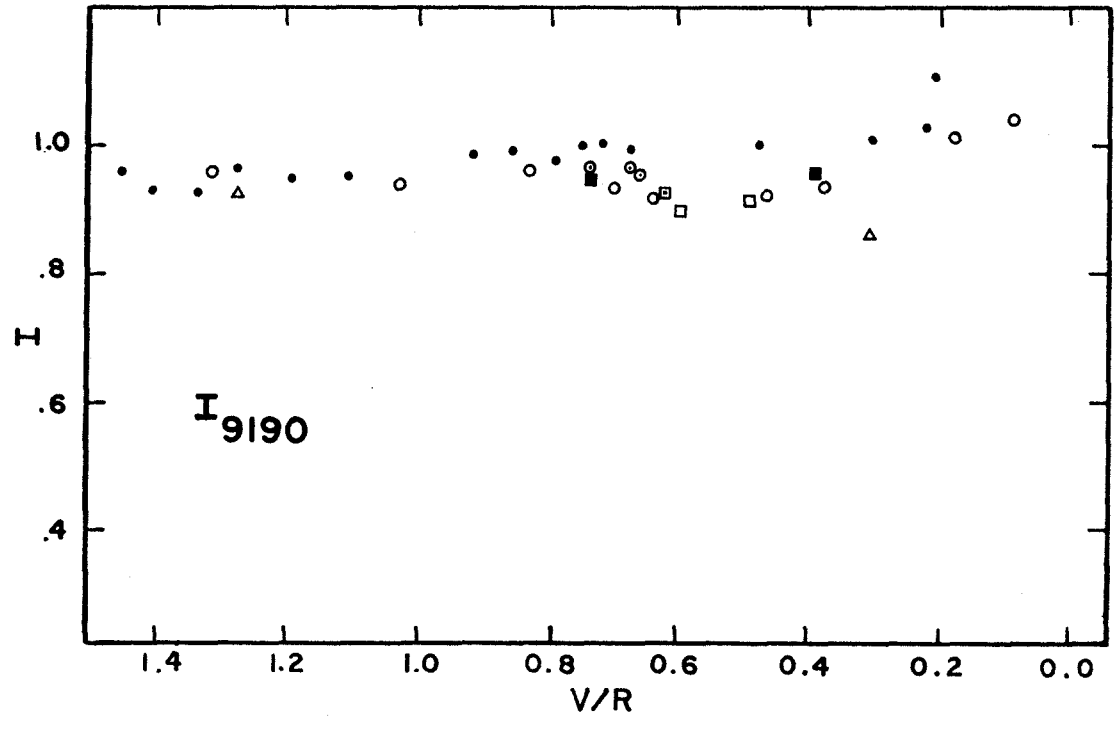

REFERENCES

Ables, H.D., and Christy, J.W. 1966, Pub. A.S.P., 78, 495.

Allen, C.W. 1964, Basic Astrophysical Quantities, (2d ed; London: Athlone Press).

Aller, L.H. 1960, in Stellar Atmospheres, ed. J.L. Greenstein, (Chicago: University of Chicago Press), pp. 156, 232.

------. 1963, Astrophysics, the Atmospheres of the Sun and Stars, (New York: Ronald Press).

Aller, L.H., and Greenstein, J.L. 1960, Ap.J.Suppl., 5, 139.

Ambartsumian, V. 1963, I.A.U. Symposium No. 20, p. 122.

Anderson, C.M. 1968, thesis, California Institute of Technology.

Anderson, K.S. 1968, thesis, California Institute of Technology.

Barbier, D., Chalonge, D., and Morguleff, N. 1941, Ann.d'Ap., 4, 137.

Becker, W. 1963, in Basic Astronomical Data, ed. K.Aa. Strand (Chicago: University of Chicago Press), p. 241.

Bergh,S. van den 1969, Ap.J. (Letters), 156, L19.

Bertola, F., D'Odorico, S., Ford, W.K., and Rubin, V.C. 1969, Ap.J. (Letters), 157, L27.

Blaauw, A. 1965, in Galactic Structure, ed. A. Blaauw and M. Schmidt (Chicago: University of Chicago Press), p. 435.

Blanco, V.M. 1965, in Galactic Structure, ed. A. Blaauw and M. Schmidt (Chicago: University of Chicago Press), p. 241.

Blanco, V.M., Demers, S., Douglass, G.G., and Fitzgerald, M.P. 1968, Pub. U.S. Naval Obs., Ser II, 13.

Bok, B.J. 1966, Ann. Rev. Ast. and Ap., 4, 95.

Burbidge, E.M., and Burbidge, G.R. 1956, Ap.J. 124, 116.

------. 1962, Ap.J. 135, 694.

Burbidge, E.M., Burbidge, G.R., and Prendergast, K.H. 1960, Ap.J., 131, 282.

Burbidge, E.M., Burbidge, G.R., and Rubin, V.C. 1964, Ap.J., 140, 942.

Burbidge, G.R., Burbidge, E.M., and Sandage, A.R. 1963, Rev. Mod. Phys., 35, 947.

Burbidge, G.R., and Hoyle, F. 1968, A.J., 73, 907.

Cayrel, R., and Cayrel de Strobel, G. 1966, Ann. Rev. Astr. and Ap., 4, 1.

Cayrel, R., and Jugaku, J. 1963, Ann.d'ap., 26, 495.

Cohen, J.G. 1968, Ap.J., 154, 179.

Conway, R.G., Kellermann, K., and Long, R.J. 1963, M.N.R.A.S., 125, 261.

Courtes, G., Viton, M., and Veron, P. 1965, in Quasi-Stellar Sources and Gravitational Collapse, ed. I. Robinson, A. Schild, and E.L. Schucking (Chicago: University of Chicago Press), p. 307.

Deeming. T.J. 1960, M.N.R.A.S., 121, 52.

Dent, W.A., and Haddock, F.T. 1966, Ap.J., 144, 568.

Dixon, M.E. 1965, M.N.R.A.S. 129, 51.

------. 1966, M.N.R.A.S., 131, 325.

Duflot, R. 1965, J.des. Observatuers, 48, No. 11.

Eggen, O.J. 1960, M.N.R.A.S., 120, 430.

------. 1965, in Galactic Structure, ed. A. Blaauw and M. Schmidt (Chicago: University of Chicago Press), p. 435.

Elvius, A. 1963, Lowell Obs. Bull., 5, 281.

------. 1964, Nature, 201, 171.

------. 1969, Lowell Obs. Bull., 7, 117.

Elvius, A., and Hall, J.S. 1964, Lowell Obs. Bull., No. 123.

Epstein, E. 1964, A.J. 69, 490.

Fitch, W.S., and Morgan, W.W. 1951, Ap.J., 114, 548.

Fomalont, E. 1968, Ap.J. Suppl., 15, 203.

Gouguenheim, L. 1969, Astr. and Ap., 3, 281.

Greenstein, J.L., and Keenan, P.C. 1958, Ap.J., 127, 172.
Griffin, R.F. 1961, M.N.R.A.S., 122. 181.
------. 1968, A Photometric Atlas of the Spectrum of Arcturas (Cambridge: Cambridge Philosophical Society).
Griffin, R., and Redman, R.O. 1960, M.N.R.A.S., 120, 287.
Gurzadian, G.A. 1963, Soobshch. Byurakansk Obs., 34, 37.
Harris, D.L. III, Strand, K.Aa., and Worley, C.E. 1963, in Basic Astronomical Data, ed. K.Aa. Strand (Chicago: University of Chicago Press), p. 273.
Haro, G. 1956, Bol. Obs. Tonantzintla y. Tacubaya, No. 14.
Helfer, H.L., and Wallerstein, G. 1968, Ap.J. Suppl., 16, 1.
Hiltner, W.A. 1956, Ap. J. Suppl., No. 24.
------. 1960, Ap.J. 131, 164.
Hiltner, W.A., and Iriarte, B. 1958, Ap.J. 128, 443.
Hodge, P.W. 1967, A.J. 72, 129.
------. 1969a, Ap.J., 155, 417.
------. 1969b, Ap.J. 156, 847.
Hoffleit, D. 1964, Catalogue of Bright Stars (New Haven: Yale University Press).
Holmberg, E. 1958, Medd. Lunds Astr. Obs., Ser. II, No. 136.
------. 1964, Arkiv. for Astron., 3, no. 30.
Hoyle, F., and Wickramasinghe, N.C. 1968, Nature, 218, 1126.
Humason, M.L., Mayall, N.U., and Sandage, A.R. 1956, A.J., 61, 97.
Hutchings, J.B. 1964, I.A.U. Symposium No. 24, p. 93.
Johnson, H.L. 1955, Ann.d'ap., 18, 292.
------. 1966a, Ann. Rev. Ast. and Ap., 4, 193.
------. 1966b, Ap.J., 143, 187.
------. 1968, in Nebulae and Interstellar Matter, ed. L. H. Aller and B.M. Middlehurst (Chicago: University of Chicago Press), p. 167.
Johnson, H.L., and Morgan, W.W. 1953, Ap.J. 117, 313.

Jones, D.H.P. 1966, M.N.R.A.S., 139, 189.
Kayser, S. 1967, A.J., 72, 134.
Keenan, P.C. 1963, in Basic Astronomical Data, ed. K. Aa. Strand (Chicago: University of Chicago Press), p. 78.
Kellermann, K., Pauliny-Toth, I.I.K., and Williams, P.J.S. 1969, Ap.J., 157, 1.
Kleinmann, D.E., and Low, F.J. 1969, paper presented at the 129th meeting of the A.A.S..
------. 1970, Ap.J. (Letters), 159, L165.
Lallemand, A., Duchesne, M., and Walker, M.F. 1960, Pub. A.S.P., 72, 76.
Lasker, B.M. 1966, A.J., 71, 862.
------. 1968, A.J., 73, S187.
------. 1970, A.J., 75, 21.
Low, F.J. 1970, Ap.J. (Letters), 159, L173.
Low, F.J., and Kleinmann, D.E. 1968, A.J., 73, 868.
Lynds, C.R., and Sandage, A.R. 1963, Ap.J., 137, 1005.
MacDonald, G.H., Kenderdine, S., and Neville, A.C. 1968, M.N.R.A.S., 138, 259.
Markaryan, B.E. 1963a, Sov. A.J., 6, 808.
------. 1963b, Soobshch. Byurakansk Obs., 34, 19.
Mathis, J.S. 1970, Ap.J., 159, 263.
Mayall, N.U. 1958, I.A.U. Symposium No. 5, p. 23.
------. 1960, Ann.d'ap., 23, 344.
McClure, R.D. 1969, A.J., 74, 50.
McClure, R.D., and van den Bergh, S. 1968, A.J. 73, 313.
McCuskey, S.W. 1965, in Vistas of Astronomy Vol. 7, ed. A. Beer (New York: Permagon Press), p. 141.
Mihalas, D. 1965, Ap.J. Suppl., 9, 321.
Minnaert, M. 1940, A Photometric Atlas of the Solar Spectrum (Amsterdam: Schnabel).

Morgan, W.W. 1958, Pub. A.S.P., 70, 364.
------. 1959a, Pub. A.S.P., 71, 92.
------. 1959b, Pub. A.S.P., 71, 394.
Morgan, W.W., Keenan, P.C., and Kellmann, E. 1943, An Atlas of Stellar Spectra (Chicago: University of Chicago Press).
Morgan, W.W., and Mayall, N.U. 1957, Pub. A.S.P., 69, 291.
------. 1959, Science, 130, 1421.
------. 1962, I.A.U. Symposium No. 15, p.3.
Morgan, W.W., and Osterbrock, D.E. 1969, A.J., 74, 515.
Münch, G. 1968, in Nebulae and Interstellar Matter, ed. L.H. Aller and B.M. Middlehurst (Chicago: University of Chicago Press), p. 365.
Ohman, Y. 1936, Stockholm Obs. Ann., 12, No. 8.
Oke, J.B. 1964, Ap.J., 140, 689.
------. 1965, Ann. Rev. Astr. and Ap., 3, 23.
------. 1969, Pub. A.S.P., 81, 11.
Oke, J.B., and Conti, P.S. 1966, Ap.J. 143, 134.
Oort, J.H. 1965, in Galactic Structure, ed. A. Blaauw and M. Schmidt (Chicago: University of Chicago Press), p. 455.
Pacholczyk, A.G., and Weymann, R.J. 1968, A.J., 73, 870.
Pauliny-Toth, I., and Kellermann, K. 1968, A.J., 73, 953.
Peimbert, M., and Spinrad, H. 1970, Ap.J., in press.
Pengelly, R.M. 1964, M.N.R.A.S., 127, 145.
Peterson, B. 1968, thesis, California Institute of Technology.
Price, M.J. 1966, M.N.R.A.S., 134, 135.
Raff, M.I. 1969, Ap.J. (Letters), 157, L29.
Rees, M.J., Silk, J.I., Werner, M.W., and Wickramasinghe, N.C. 1969, Nature, 223, 788.
Roman, N. 1952, Ap.J., 116, 122.
Routly, P., and Spitzer, L. 1952, Ap.J., 115, 227.
Sandage, A.R. 1961, The Hubble Atlas of Galaxies (Washington: Carneige Institution of Washington).

Sandage, A.R. 1962, in I.A.U. Symposium No. 15, p. 359.
Sandage, A.R., Becklin, E.E., and Neugebauer, G. 1969, Ap.J., 157, 55.
Sandage, A.R., and Miller, W.C. 1964, Science, 144, 405.
Sandage, A.R., and Visvanathan, N. 1969, Ap.J., 157, 1065.
Scargle, J.D. 1969, Ap.J. 156, 401.
Schmidt-Kaler, T. 1965, in Numerical Data and Functional Relationships in Science and Technology Group VI Vol. 1, ed. H.H. Voigt (Berlin: Springer-Verlag), p. 284.
Seaton, M.J. 1960, Rept. Prog. Phys., 23, 313.
Sharpless, S.L. 1956, Ap.J., 124, 342.
Solinger, A.B. 1969a, Ap.J., 155, 403.
------. 1969b, Ap.J. (Letters), 158, L21.
------. 1969c, Ap.J. (Letters), 158, L25.
Spinrad, H. 1962, Ap.J., 135, 715.
------. 1966, Pub. A.S.P., 78, 367.
Spinrad, H., and Taylor, B. 1969, Ap.J., 157, 1279.
------. 1970, in preparation.
Spitzer, L. 1969, Diffuse Matter in Space (New York: Interscience), p. 120.
Starikova, G.A. 1960, Sov. A.J., 4, 451.
Stoeckly, R., and Dressler, K. 1964, Ap.J., 139, 240.
Stothers, R. 1969, Ap.J., 155, 935.
Strom, S., and Strom, K. 1967, Ap.J., 150, 501.
Strömgren, B. 1963, in Basic Astronomical Data, ed. K. Aa. Strand (Chicago: University of Chicago Press), p. 123.
Tammann, G.A., and Sandage, A.R. 1968, Ap.J., 151, 825.
Taylor, B.J. 1969, thesis, University of California, Berkeley.
Thackeray, A.D. 1949, M.N.R.A.S., 109, 436.
Tinsley, B.M. 1967, Pub. Astron. Dept. Univ. of Texas, Ser. II, 1, No. 15.

Tull, R.G. 1963, thesis, University of Michigan.
Vaucouleurs, G. de 1959, Lowell Obs. Bull., No. 97.
------. 1961a, Ap.J., 133, 405.
------. 1961b, Ap.J. Suppl., 5, 233.
------. 1962, I.A.U. Symposium No. 15, p. 3.
------. 1963, Ap.J., 137, 363.
Vaucouleurs, G. de, and Vaucouleurs, A. de 1960, Lowell Obs. Bull, No. 92.
Volders, L., and Hogbom. J. 1961, B.A.N., 15, 307.
Walker, M.F. 1962, Ap.J., 136, 695.
Wallerstein, G., Greenstein, J.L., Parker, R., Helfer, H., and Aller L. 1963, Ap.J. 137, 280.
Wampler, E.J. 1966, Ap.J., 144, 921.
------. 1968, Ap.J. (Letters), 154, L53.
Wehinger, P., and Wyckoff, S. 1966, A.J. 71, 185.
Whitford, A.E. 1958, A.J. 63, 201.
------. 1966, I.A.U. Symposium No. 24, p. 17.
Whiteoak, J.B. 1967, Ap.J., 150, 521.
Wickramasinghe, N.C. 1967, Interstellar Grains (London: Chapman and Hall), p. 52.
Wildey, R.L. 1964, Ap.J. Suppl., No. 84.
Wildey, R.L., Burbidge, E.M., Sandage, A.R., and Burbidge, G.R. 1962, Ap.J., 135, 94.
Wilson, O.C. 1962, Ap.J., 136, 793.
Wing, R.F. 1966, in Colloquium on Late-Type Stars, ed. M. Hack (Trieste: Osservatorio Astronomico di Trieste), p.231.
Wing, R.F., Spinrad, H.S., and Kuhi, L. 1967, Ap.J., 147, 117.
Wood, D.B. 1966, Ap.J., 145, 36.
------. 1969, A.J. 74, 177.
Wooley, R. 1963, Royal Obs. Bull., No. 66.
Wray, J.D., and Heckathorn, H.M. III 1969, Bull. A.A.S., 1, 370.

Addenda to References

Demoulin, M. 1969, Ap.J., 157, 75.

Ebert, R., von Hoerner, S., and Temesvary, S. 1960, Die Entstehung von Sternen durch Kondensation Diffuser Materie (Heidelberg: J. Springer).

Lynden-Bell, D. 1969, Nature, 223, 690.